Newly dated permafrost deposits and their paleo-ecological inventory reveal a much warmer-than-today Eemian in Arctic Siberia

Lutz Schirrmeister[1], Margret C. Fuchs[2], Thomas Opel[3], Andrei Andreev[3], Frank Kienast[4], Andrea Schneider[5], Larisa Nazarova[6], Larisa Frolova[7], Svetlana Kuzmina[8], Tatiana Kuznetsova[9], Vladimir Tumskoy[10], Heidrun Matthes[11], Gerrit Lohmann[12], Guido Grosse[1, 13], Viktor Kunitsky[10], Hanno Meyer[3], Heike H. Zimmermann[14], Ulrike Herzschuh[3, 15], Thomas Böhmer[3], Stuart Umbo[16], Sevi Modestou[16], Sebastian F.M. Breitenbach[16], Anfisa Pismeniuk[17], Georg Schwamborn[18], Stephanie Kusch[19], Sebastian Wetterich[1, 20]

[1]Permafrost Research Section, Alfred Wegener Institute, Helmholtz Center for Polar and Marine Research, Potsdam, Germany

[2]Exploration, Helmholtz Institute for Resource Technology, Freiberg, Germany

[3]Polar Terrestrial Environmental Systems Section, Alfred Wegener Institute, Helmholtz Center for Polar and Marine Research, Potsdam, Germany

[4]Quaternary Paleontology, Senckenberg Research Institute and Natural History Museum, Weimar, Germany

[5]Arctic University of Norway, Tromsø, Norway

[6]Krasnoyarsk Science Center, SB RAS, Krasnoyarsk, Russia

[7]Institute of Archaeology and Ethnography, SB RAS, Novosibirsk, Russia

[8]Boryssyak Paleontological Institute, RAS, Moscow, Russia

[9]Faculty of Geology, Lomonosov Moscow State University, Russia

[10]Mel'nikov Permafrost Institute, SB RAS, Yakutsk, Russia

[11]Atmospheric Physics Section, Alfred Wegener Institute, Helmholtz Center for Polar and Marine Research, Potsdam, Germany

[12]Paleoclimate Dynamics Section, Alfred Wegener Institute, Helmholtz Center for Polar and Marine Research, Bremerhaven, Germany

[13]Institute of Geosciences, University of Potsdam, Germany

[14]Glaciology and Climate Department, Geological Survey of Denmark and Greenland, Copenhagen, Denmark

[15]Institute of Environmental Science and Geography, Institute of Biochemistry and Biology, University of Potsdam, Germany

[16]Geography and Environmental Sciences, Northumbria University, Newcastle, UK

[17] Department of Geosciences, University of Oslo, Oslo, Norway

[18]Eberswalde University for Sustainable Development, Department of Landscape Management and Nature Conservation, Eberswalde, Germany

[19]Institute of Marine Sciences (ISMER), University of Quebec Rimouski, Rimouski, Canada

[20]Current address: Institute of Geography, Technische Universität Dresden, Germany

Correspondence to: Lutz Schirrmeister (lutz.schirrmeister@awi.de)

Keywords: Marine Isotope Stage 5e, luminescence dating, cryolithology, paleo-proxy, model-based climate reconstructions, MTWA, MTCO, MAP, clumped isotopes

Abstract. In this study, we integrate geochronological, cryolithological, paleo-ecological, and modeling data to reconstruct the Last Interglacial (LIG) climate around the New Siberian Islands, revealing significantly warmer conditions compared to today. New luminescence dating of the lacustrine deposits mostly preserved in ice-wedge pseudomorphs of 1-3 m thickness along the Dmitry Laptev Strait indicates ages consistent with the LIG (MIS 5e). Analysis of plant macrofossils, pollen and faunal records (beetles and chironomids) from these deposits suggests mean temperatures of the warmest month (MTWA) of 10.3 to 12.9°C, 9.0±3.0°C, 8 to 10.5°C and 9.4 to 15.3°C for Bol'shoy Lyakhovsky and of 12.7 to 15.3°C, 9.7±2.9°C, 8 to 14°C and 12.0-13.8°C for Oyogos Yar. The fossil beetle-based mutual climate range for mean temperatures of the coldest month is –34 to –26°C for Bol'shoy Lyakhovsky and –38 to –26°C for Oyogos Yar. Our chironomid-based reconstructions of water table depth suggest 1.7 to 5.6m for Bol'shoy Lyakhovsky, while previous analysis suggested 1.1 to 3.3m for Oyogos Yar. Pollen-based reconstruction of mean annual precipitation for Bol'shoy Lyakhovsky suggests 271±56mm, for Oyogos Yar 229±22mm. The first-time application of clumped isotopes to permafrost-preserved biogenic calcite of ostracods and bivalves for Oyogos Yar reconstructed near-surface water temperature of 10.3±3.0°C and bottom water temperatures of 5.3±1.5°C in thermokarst lakes during summers. In summary, the analyzed proxies suggest summers warmer than today by 5.5 to 12.8°C for Bol'shoy Lyakhovsky and by 0.2 to 7.5°C for Oyogos Yar, and winters warmer than today by up to 7.1°C and 8.4°C, respectively. Modern mean annual precipitation values are within the uncertainty range of the reconstructions. Climate model simulations for the LIG from the PMIP project suggest MTWAs warmer than today for Bol'shoy Lyakhovsky (4.4±1.0 °C compared to 2.5 °C) and colder than today for Oyogos Yar (4.5±1.2 °C compared to 7.8°C), underestimating the Eemian warming reconstructed from our multiple paleoecological proxies. The LIG warming mainly affected summer conditions, whereas modern and future warming will rather impact winter conditions. As the LIG annual mean temperature is often used as an analog for the future climate in the High Arctic, the proxy-model mismatch highlights the urgent need for more systematic quantitative proxy-based temperature reconstructions in the Arctic and more sophisticated Earth system models capable of capturing Arctic paleoenvironmental conditions.

1   Introduction

The climate control on permafrost dynamics during the late Quaternary is reflected in large-scale permafrost aggradation during glacial periods and extensive thaw in interglacial periods (Shur and Jorgenson, 2007; Jones et al., 2023; Opel et al., 2024). These broader climate-driven dynamics were superimposed local factors, including topography, hydrology, and vegetation cover, as well as natural disturbances causing localized rapid thaw such as thermokarst lakes or wildfires. During warm periods, rising air temperatures and, consequently, rising ground temperatures and active-layer thickening promoted ground-ice melting, surface subsidence, and the formation of thermokarst lakes and basins in areas underlain by ice-rich permafrost (Czudek and Demek, 1970; Grosse et al., 2013; Brosius et al., 2021). Shallow thermokarst lakes might develop that can preserve traces of landscape evolution, paleoclimate, and paleoecology in lacustrine sediments (Murton, 1996; Lenz et al., 2016; Bouchard et al., 2017). Thawing ice-wedge polygons below the lake-water level form ice-wedge casts (pseudomorphs), which may also preserve laminated lacustrine deposits (Farquharson et al., 2016). Lake drainage or desiccation over time promotes the formation of typically palustrine (peaty) deposits above the lacustrine sequences in thermokarst basins (e.g., Morgenstern et al., 2013). However, permafrost aggradation and degradation are not restricted to

glacial and interglacial periods, respectively. On the local to regional scale, permafrost formation is also reported for interglacial times such as associated with pingo formation (Wetterich et al., 2018) or peat growth during the Holocene (Kaplina, 2011a, 2011b; Wetterich et al., 2009), and permafrost degradation occurred during interstadial stages of glacial periods (Vaks et al., 2020, 2013).

The globally warmer-than-today Last Interglacial (LIG, ca. 130-115 ka) (e.g., Past Interglacials Working Group of PAGES, 2016; Fischer et al., 2018; Snyder, 2018; Wilcox et al., 2020) is commonly seen as a potential analog for future climate warming (Burke et al., 2018; Gulev et al., 2021; Otto-Bliesner et al., 2013). Due to summer insolation higher than today and additional feedback effects such as the retreat of ice sheets, reduction of summer sea ice, and expansion of boreal forests, the LIG warming in the Arctic was amplified compared to the Northern Hemisphere as a whole (CAPE-LIG Project Members, 2006). Recent studies combining proxy evidence across the Arctic (mainly from terrestrial and lacustrine pollen and plant macrofossils and Greenland ice cores) and paleoclimate modeling largely agree on 4-5 °C higher summer temperatures than today and a nearly sea-ice free Arctic Ocean during summers (Guarino et al., 2020; Sime et al., 2023; Vermassen et al., 2023), accompanied by a High Arctic greening (Crump et al., 2021). For a reduced Greenland Ice Sheet, up to +5 °C, regional warming is modeled for the LIG (Pfeiffer and Lohmann, 2016). However, the warmer than today conditions during the LIG were predominantly driven by increased summer solar insolation, unlike modern Arctic warming, which is most pronounced in winter due to anthropogenic forcing. Despite this difference, many of the consequences of summer warming in the LIG – such as ice sheet retreat, reduction of sea ice, and permafrost degradation – are observable in the changing Arctic today. That supports the continued relevance of the LIG as an analog setting. There are only limited quantitative paleoclimate data on the terrestrial interglacial MIS 5e conditions in the Arctic (e.g., CAPE-LIG Project Members, 2006; Sime et al., 2023), with sparse sites that are widely spaced and which often have only single or few selected paleoproxies and rather poor temporal constraints. Many terrestrial records of the LIG in the Arctic are found in fluvial deposits exposed in river bluffs or artificial placer mining cuts in Alaska (Hamilton & Brigham-Grette, 1991; Edwards et al., 2003; Jensen et al., 2013), Siberia (Velichko et al., 2008), or NW Canada (Reyes et al., 2010). Because interglacial climate conditions degraded pre-existing ice-rich permafrost deposits and also promoted the formation of thermokarst basins and lakes, the interglacial legacy in permafrost regions is also commonly represented by thaw unconformities and lacustrine and palustrine deposits. Some of these sites attributed to the LIG are known from eastern Siberia in the Yana-Indigirka Lowland (site Achagy-Allaikha, Kaplina, 1980, 1981) and the Kolyma Lowland (site Duvanny Yar; Kaplina, 2011a). Furthermore, the world's currently largest permafrost degradation feature, the Batagay megaslump in the Yana Upland in eastern Siberia, exposes a distinct woody debris layer below an erosional disconformity of Marine Isotope Stage (MIS) 5e age, i.e., the LIG, that is overlain by MIS 4 to MIS 2 Yedoma Ice Complex deposits (Ashastina et al., 2017; Murton et al., 2022).

Extensive late Pleistocene paleoecological studies on ice-wedge pseudomorphs and other lacustrine sequences were conducted on coastal exposures at both coasts of the Dmitry Laptev Strait that connects the Laptev and the East Siberian seas (Figure 1). Both the southern coast of Bol'shoy Lyakhovsky Island near the Zimov'e River mouth and the Oyogos Yar mainland coast near the Kondrat'eva River mouth have been studied for LIG pollen, plant macrofossils, fossil insect remains including beetles and chironomids, lacustrine invertebrates such as ostracods, cladocera, and mollusks, and testate amoebae and sedimentary ancient DNA (Andreev et al., 2004, 2011; Ilyashuk et al., 2006; Kienast et al., 2008, 2011; Wetterich et al., 2009; Schneider, 2010; Zimmermann et al., 2017). However, only scarce chronological control is available (Andreev et al., 2004; Opel et al., 2017) for

lacustrine deposits, which are locally named the Krest-Yuryakh stratum (Tumskoy and Kuznetsova, 2022) and commonly interpreted as deposits of the LIG, i.e., MIS 5e (Eemian). Mammal bones belonging to the late Pleistocene mammoth fauna in Krest-Yuryakh deposits are very rare and poorly dated (Kuznetsova et al., 2022).

Ancient thermokarst deposits and their paleoenvironmental inventory can provide interesting analogs for modern and (near-)future warming and its impact on periglacial landscapes and ecosystems. During the Lateglacial to Holocene transition, thermokarst processes re-shaped vast areas of the Beringian periglacial landscapes by thawing the MIS 4 to MIS 2 Yedoma Ice Complex deposits (Jones et al., 2022; Walther Anthony et al., 2014, Morgenstern et al., 2013), and paleoecological records from past warming episodes such as the Lateglacial Interstadials (e.g., Allerød) and the early Holocene with rapid permafrost degradation are fairly well characterized, helping to understand interactions between climate, permafrost, and ecosystem dynamics. For example, previous paleobotanical studies associated with thermokarst deposits from NE Siberia revealed quantitative estimates of the Lateglacial-early Holocene warming with a pollen-based mean temperature of the warmest month (MTWA) of 8-12 °C (Andreev et al., 2009, 2011). Likewise, the LIG climate warming led to the degradation of previously aggraded ice-rich permafrost deposits by thermokarst processes. A LIG (MIS 5e) macrofossil-based reconstruction of MTWA reached >12.5 °C (Kienast et al., 2008, 2011), suggesting the potential for more intense warming during MIS 5e, which in turn could be considered – at least in the amplitude – a representative analog for stronger modern warming in the Arctic than during the Lateglacial or early Holocene.
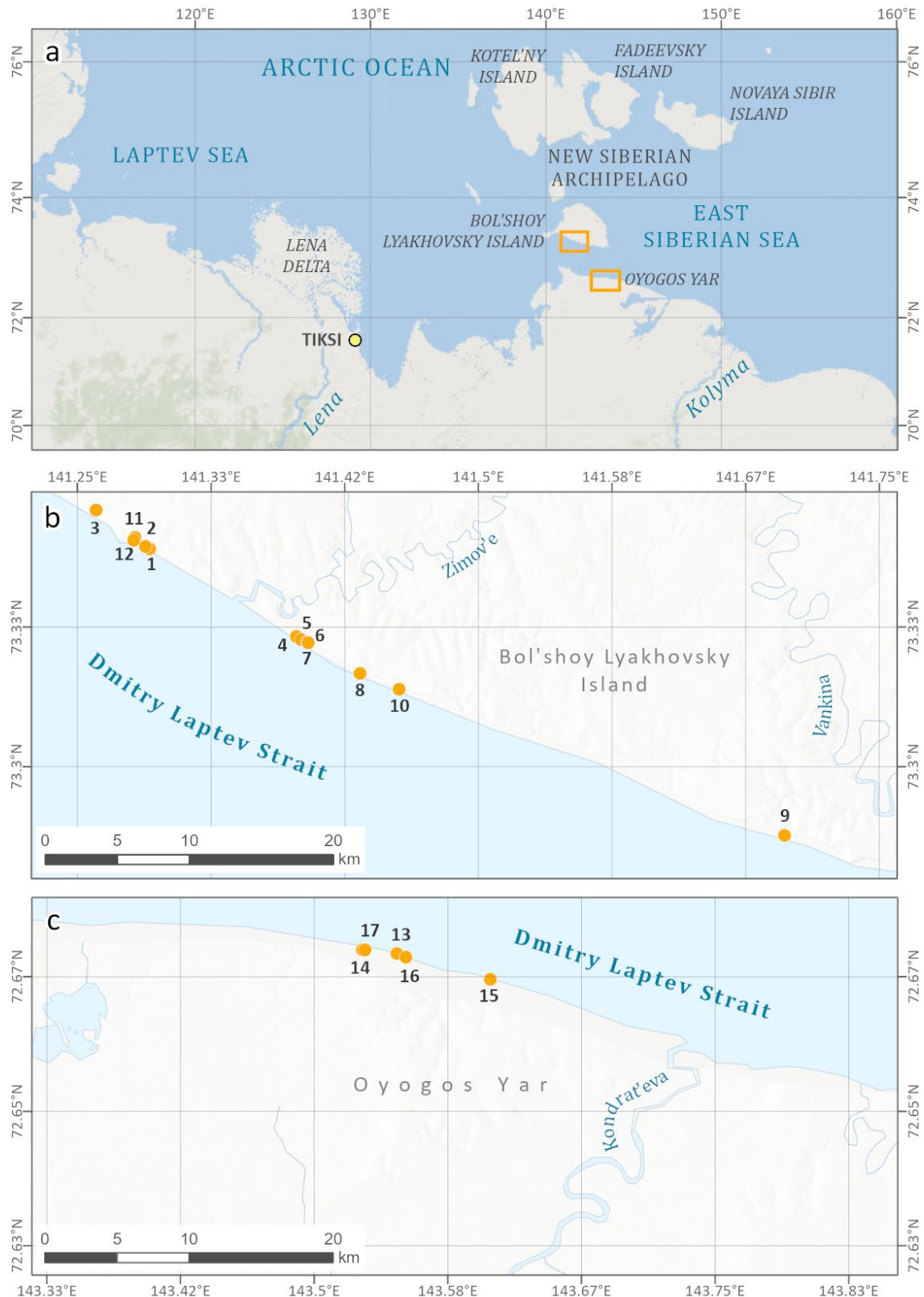
Figure 1. Study area (a) in northeastern Siberia along the Dmitry Laptev Strait, (b) at the southern coast of Bol'shoy
Lyakhovsky Island, and (c) the opposite mainland coast of Oyogos Yar. The locations of sampling profiles of LIG
deposits are also indicated in Table A1 and Figure 2. The maps were compiled by Sebastian Laboor, AWI Potsdam,
using World Imagery (Credits: Esri, Maxar, GeoEye, Earthstar Geographics, CNES/Airbus DS, USDA, USGS,
AeroGRID, IGN, and the GIS User Community) and World Ocean Base (Credits: Esri, Garmin, GEBCO, NOAA
NGDC, and other contributors).

According to Rovere et al. (2016), the global sea level of MIS 5e might have reached levels 5 to 9.4 m higher than today. For north-eastern Siberia, especially for the Laptev Sea and the East Siberian Sea coastal regions, only scarce information on the MIS 5e coastline is available and outlined below. According to Ivanenko (1998), a distinctive feature of the Fadeevsky and Novaya Sibir islands (especially at their northern coasts; Figure 1) are widely distributed marine deposits (called the Kanarchak Formation), which are overlain by terrestrial Yedoma Ice Complex or, rarely, by terrestrial Holocene deposits. A smooth boundary between the marine and terrestrial strata is striking, indicating a continuous sedimentation regime and uninterrupted transition from marine to terrestrial conditions. According to Alekseev et al. (1991a, 2001), the lower part of the sections consists of marine terrace deposits, assumed to have formed during the LIG (Kazantsevo period in Russian). The sandy series corresponding to the Kazantsevo transgression overlays the marine terrace deposits, which are today situated at 8-10 m above sea level (a.s.l.). Remnants of the marine terrace deposits with mollusk fauna are widely distributed and well expressed on the Novaya Sibir, Fadeevsky, and Kotel'ny islands, mainly in the estuarine parts of river valleys. Later studies on Novaya Sibir and Fadeevsky islands were undertaken by Basilyan et al. (2010), Tumskoy (2012), and Nikolskiy et al. (2017), including first detailed investigations of the Kanarchak Formation that contains a prominent massive ground ice body. These studies recognized the massive ground ice as a relic of a late mid-Pleistocene (MIS 6) glaciation, and the upper part of the Kanarchak Formation was assigned to the LIG (Basilyan et al., 2010). We conclude that the northern coast of the Fadeevsky and Novaya Sibir islands is characterized by marine and coastal deposits of the LIG, which delineate the approximate position of the coastline during MIS 5e.

Linking the paleoecologic records from the different locations in order to understand the regional context requires a robust geochronological framework. While Lateglacial and early Holocene thermokarst deposits are commonly well-constrained via radiocarbon dating (Wetterich et al., 2009), the chronostratigraphy of MIS 5 deposits attributed to the LIG suffers from large dating uncertainties of the available dating methods that include radioisotope disequilibria (^{230}Th/U) of peat (Schirrmeister et al., 2002; Wetterich et al., 2016) and optically stimulated luminescence of quartz (OSL) or infrared stimulated luminescence of feldspar (IRSL) (Andreev et al., 2004; Opel et al., 2017). Therefore, the highly variable millennial climate dynamics from about 130 to 80 ka during MIS 5 (expressed as MIS 5 sub-stages 5e to 5a; Shackleton et al., 2003) are not yet resolved in terrestrial permafrost records and hinder the paleoclimatic interpretation of permafrost-preserved fossil proxy records.

Our study summarizes previously published and newly obtained data from coastal permafrost exposures at both coasts of the Dmitry Laptev Strait to (1) provide new luminescence dates that constrain the timing of the LIG and thus to resolve regional MIS 5e climate variability better; (2) summarize cryolithological and geochemical characteristics of LIG deposits that capture depositional processes and preservation conditions; (3) deduce the ecological response and quantify the paleoclimatic parameters linked to LIG warming as reflected by fossil proxy data of vegetation, terrestrial and aquatic invertebrates, and compare them with results of climate model simulations; and (4) discuss LIG climate-ecology-permafrost dynamics and their potential as analogs for the ongoing and future climate warming in the terrestrial Siberian Arctic.

2   Study sites

The study sites stretch along the Dmitry Laptev Strait at the southern coast of Bol'shoy Lyakhovsky Island and the opposite mainland coast of Oyogos Yar (Figure 1). Various coastal outcrops, thaw slumps, and drill sites were

1 studied along an approximately 16.5 km long section west and east of the Zimov'e River mouth on Bol'shoy
2 Lyakhovsky (Figure 1b; Figure 2a) and along a 5.5 km long section west of the Kondrat'eva River mouth at the
3 Oyogos Yar mainland coast (Figure 1c; Figure 2b). A recent review of the permafrost research history of the
4 Dmitry Laptev Strait shores is provided in Tumskoy and Kuznetsova (2022).

5   The modern climate of the study area is characterized by short, cold summers with a mean July
6 temperature (MTWA) of 2.5 to 2.8 °C (WMO stations 216470, 216360). Long, harsh winters of eight months are
7 characterized by low light availability and low temperatures, with a mean January temperature (mean temperature
8 of the coldest month, MTCO) of −34.4 to −33.1°C. The annual precipitation varies from 243 to 262 mm, yet
9 overall conditions are humid due to low evaporation rates and poor drainage of the wet active layer during summer
10 (Hersbach et al., 2020, ERA5, 1990-2019). The area belongs to the Arctic tundra subzone (Chernov and Makarova,
11 2008), more specifically, the moist to dry tundra vegetation zone with open to continuous plant cover (G2) on
12 Bol'shoy Lyakhovsky Island and sedge/grass, moss wetland (W1) on the Oyogos Yar coast (CAVM Team, 2003).

13   The region is underlain by continuous permafrost with a thickness of 400-600 m, and the mean annual
14 ground temperature is about −14 to −12 °C (Yershov, 1989). The mean thickness of the active layer is about 30-
15 40 cm (Schwamborn and Wetterich, 2015).

16   In its western, central, and eastern parts, Bol'shoy Lyakhovsky Island is shaped by hills reaching
17 elevations of about 100 to 300 m a.s.l. In the central part and the coastal region, Yedoma uplands up to 40 m a.s.l.
18 are present and dissected by large thermokarst basins (alases), wide and flat thermo-erosional valleys (logs), gullies
19 or ravines (ovrags). The southern coast of Bol'shoy Lyakhovsky Island is characterized by vast retrogressive thaw
20 slumps (thermo-cirques), the mouth of the Zimov'e River, and numerous smaller streams. Widespread thermokarst
21 characterizes the Oyogos Yar mainland coast (Günther et al., 2013), covered by polygonal peatlands, shallow
22 thermokarst lakes, and erosional remnants of Yedoma uplands. The general stratigraphy of both coastal sections
23 with deposits between MIS 7 and MIS 1 is presented in Figure 2.
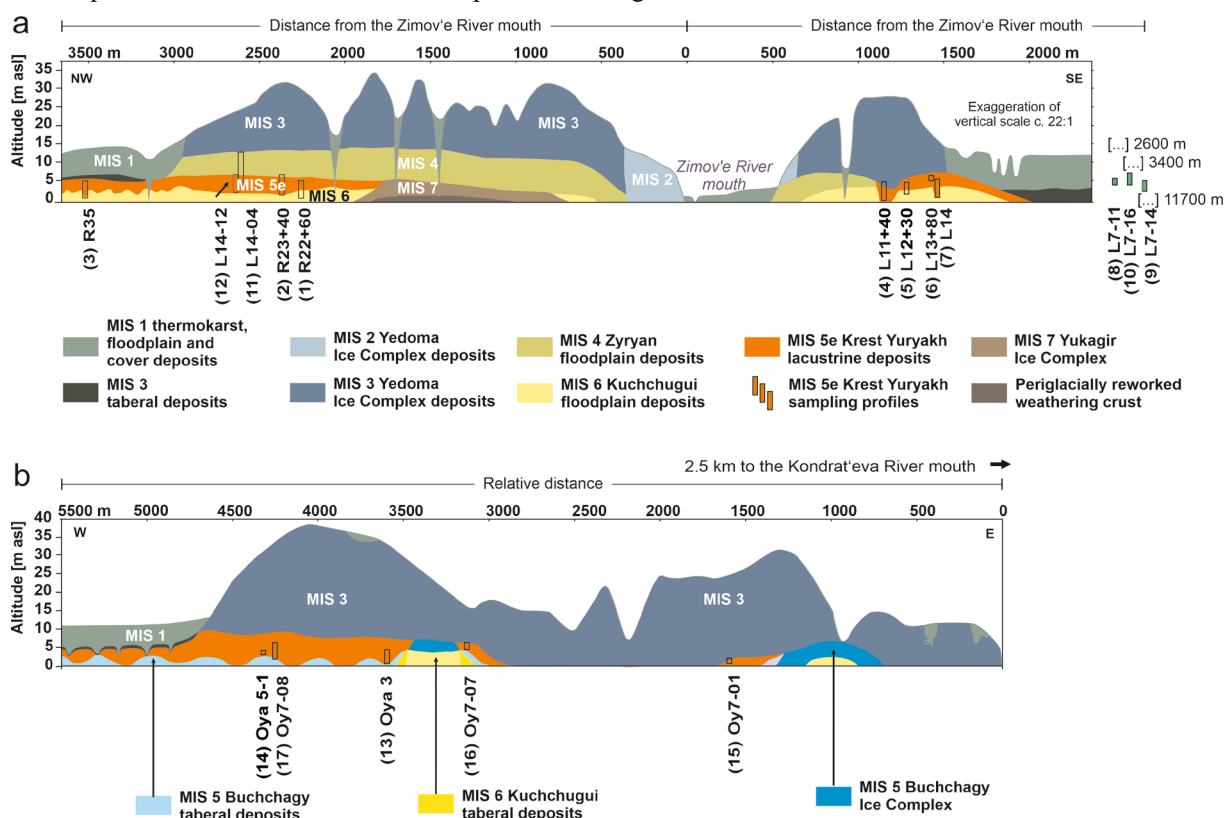
Figure 2. Cryostratigraphic schematics of both coasts of the Dmitry Laptev Strait with LIG (Krest-Yuryakh) profile locations: (a) Bol'shoy Lyakhovsky Island (re-drawn from Andreev et al., 2009 and Wetterich et al., 2021), (b) Oyogos Yar coast (re-drawn from Tumskoy and Kuznetsova, 2022). Taberal deposits mean thawed and refrozen permafrost deposits. The numbers in parentheses in front of the profile IDs correspond to the numbers in Figure 1.

3 Material and methods

3.1 Fieldwork

Field studies on both sides of the Laptev Strait were conducted in the summers of 1999, 2002, 2007, and 2014, as well as in spring of 2014 (Schirrmeister et al., 2000, 2003; Boike et al., 2008; Schwamborn and Wetterich, 2015). After an initial survey, selected coastal exposures (Figure 2) were sampled in detail. Vertical profiles were cleaned with spades and hoes to remove the outermost thawed material. The exposed sequences were surveyed, described, photographed, and sketched to document sediment structures, cryostructures, color, and visible organic content. The frozen deposits were sampled for further studies using hammers and small axes. In spring 2014, a Russian drill rig (KMB3-15M) mounted on an all-terrain vehicle was used to retrieve permafrost cores on Bol'shoy Lyakhovsky Island using a rotary mechanism in dry holes.

Sections of Krest-Yuryakh deposits sampled at the southern coast of Bol'shoy Lyakhovsky Island included the profiles R35, R22+60, R23+40, L11+40, L12+30, L13+80 and L14 in 1999; the profiles L7-14, L7-11 and L7-16 in 2007; and the profile L14-12 and the permafrost core L14-04 in 2014 (Figure 2; Table A1). On the Oyogos Yar coast, the profiles Oya-3-10, Oya-3-11, and Oya 5-1 were obtained in 2002, and the profiles Oy7-01, Oy7-07, and Oy7-08 A-C in 2007 (Figure 2; Table A1).

Except for the permafrost core, the ice content of all permafrost samples was determined in the field in closed aluminum boxes. The samples were weighed while still frozen, dried in a field oven, and weighed again. The absolute gravimetric ice content is the ratio of the ice mass in a sample to the dry sample mass, expressed as a percentage (van Everdingen, 2005).

In 1999, screening for rodent remains using a woody screen box with a metallic screen (1mm mesh) and a motor pump was carried out. Although no rodents were found, the screened sediment was used to extract insects. In addition, insects were collected by screening the thawed sediment with a 0.4 mm mesh. Plant macrofossils were excavated from insect samples and large (up to 2 kg) bulk samples. Large mammal bones were collected from the section and below at the seashore. Some small rodent teeth were picked up from mineral and plant debris below the section.

3.2 Luminescence dating

Previous luminescence sampling in 1999 on Bol'shoy Lyakhovsky is described in Andreev et al. (2004, 2009) and on Oyogos Yar in Opel et al. (2017). In 2014, Krest-Yuryakh deposits were sampled atone site on the southern coast of Bol'shoy Lyakhovsky Island for luminescence dating (profile L14-12, 73.34055°N, 141.28498°E; Figure 1). After cleaning and cryolithological description, the ca. 7 m high steep exposure was sampled for luminescence dating at heights of 4.5 m a.s.l. (L14-12-OSL1) and 2.7 m a.s.l. (L14-12-OSL3) (Table A1, Figure S1). We used a HILTI TE6 - A36 cordless rotary hammer to obtain frozen cores protected from sunlight that were packed dark, stored in an ice cellar next to the camp at –4 °C, and kept frozen until arrival in the laboratory.

The luminescence samples were processed and analyzed at the luminescence laboratory at the Institute of Applied Physics, TU Bergakademie Freiberg. Sample preparation targeted K-feldspar extracts at grain sizes of

1 40–63 μm for IRSL dating from both samples, L14-12-OSL1 and L14-12-OSL3. Additionally, the coarser grain-

2 size fraction 63–90 μm yielded sufficient material for sample L14-12-OSL1. Coarser material (>100 μm) did not

3 provide enough material for further analysis. Pure mineral extracts were obtained via carbonate and organic

4 removal (10% HCl and 30% H_2O_2, respectively), feldspar flotation (0.2% HF, pH 2.4–2.7, dodecylamine) for

5 efficient separation from quartz, density separation to enrich K feldspars (2.53–2.58 g cm^{-3}) and 5 min final

6 etching in 10% HF. Extracted feldspars were prepared for measurement assets of homogenous subsamples

7 (aliquots) by fixing grain monolayers on aluminum discs within a 2 mm diameter. Measurements and analyses

8 for age estimation were based on 20 aliquots, while four aliquots per sample and grain size fraction were used for

9 quality tests. For L14-12-OSL3, five additional aliquots were used in equivalent dose screening sequences to

10 optimize the regenerative dose points. The IRSL signals of feldspars were measured using a TL/OSL DA-20 reader

11 (Bøtter-Jensen et al., 2003) equipped with a ^{90}Sr beta irradiation source (4.95 Gy min^{-1}). Signals were stimulated

12 at 870 nm (IR diodes, 125°C for 100 s) and detected through a 410 nm optical interference filter (Krbetschek et

13 al., 1997).

14 The measurement sequence followed the single-aliquot regenerative dose (SAR) protocol according to

15 Murray and Wintle (2000), including cycles to record recycling ratios and recuperation and to correct for sensitivity

16 changes. Preheat (before each IRSL stimulation) and cut-heat temperatures (before each test dose stimulation)

17 were set to 230 °C and 160 °C, respectively, according to preheat tests. Emitted signals were recorded for 100 s to

18 ensure the acquisition of pure background signals at the end of each measurement cycle. Dose-recovery tests

19 (Murray and Wintle, 2003) confirmed suitable luminescence properties under the chosen conditions with

20 coefficients of variations of 3.8% and 5.3%. The data processing was performed using the R package

21 "Luminescence" (Kreutzer et al., 2012), version 0.9.20.

22 The datasets (n = 20 to 25) revealed equivalent dose distributions of low skewness (below 0.8%) and low

23 standard deviations (below 5%). No evidence of insufficient bleaching or significant post-depositional mixing was

24 found, and hence, paleodose estimates were based on the Central Age Model (CAM) (Galbraith et al., 1999). The

25 CAM-based paleodose was then processed together with all sample-specific dose rates (sediment-internal,

26 mineral-internal, cosmic) and correction (grain sizes, water content, sediment cover, etc.) parameters using the

27 online DRAC calculator (Durcan et al., 2015). For the mineral-internal dose rate of the K feldspars, a potassium

28 content of 12.5 ± 0.5% was assumed (Huntley and Baril, 1997).

30 **3.3   Sediment analyses**

31 In the laboratory, the sediment samples were freeze-dried, carefully manually homogenized, and split into sub-

32 samples for sedimentological, geochemical, and paleo-ecological analyses. Grain-size distribution was analyzed

33 using a laser-particle analyzer (Beckmann Coulter LS 200) and computed with GRADISTAT 4.0 software (Blott

34 and Pye, 2001). The mass-specific magnetic susceptibility (MS) was measured using a Bartington MS2 instrument

35 (MS2B sensor), and values are given in SI units (Le Système International d'Unités; 10^{-8} m^3 kg^{-1}). The total

36 Carbon (TC), total organic carbon (TOC), and total nitrogen (TN) contents were measured by a carbon-nitrogen-

37 sulfur (CNS) analyzer (Elementar Vario EL III), and the total organic carbon to total nitrogen ratio was calculated

38 as TOC/TN ratio. The difference between TC and TOC calculated the total inorganic carbon (TIC). TIC values

39 were used to estimate carbonate contents stoichiometrically. Stable carbon isotopes (δ^{13}C) of TOC were measured

40 until 2014 with a Finnigan DELTA S mass spectrometer coupled to a FLASH element analyzer and a CONFLO

1	III gas mixing system after the removal of carbonates with 10% HCl in Ag-cups and combustion to CO_2. The
2	accuracy of the measurements was determined by parallel analysis of internal and international standard reference
3	material. The analyses were accurate to ±0.2 ‰. Later, the measurement was undertaken using a Thermo Scientific
4	Delta V Advantage isotope ratio MS equipped with a Flash 2000 organic elemental analyzer using helium as a
5	carrier gas. The accuracy was better than ±0.15 ‰. The $\delta^{13}C$ values are expressed in delta per mil notation (δ, ‰)
6	relative to the Vienna Pee Dee Belemnite (VPDB) standard.
7	Values are given as per mil (‰) difference from the Vienna Pee Dee Belemnite (VPDB) standard for
8	$\delta^{13}C$ and from nitrogen in ambient air (AIR) for $\delta^{15}N$. The accuracy was better than ±0.15 ‰ for $\delta^{13}C$ and ±0.2 ‰
9	for $\delta^{15}N$.
10	

3.4 Paleo-ecological analyses and paleoclimate reconstructions

Pollen data are available (Table A1) from Bol'shoy Lyakhovsky Island from Krest-Yuryakh deposits in profiles R22+60, L11+40, L12+30 and L14 (Andreev et al., 2004), R23+40 (Andreev et al., 2009), R35 (Ilyashuk et al., 2006), L7-14 (Wetterich et al., 2009), and in the drill core and hand pieces of the permafrost core L14-04 (Zimmermann et al., 2017). On Oyogos Yar, pollen data were obtained from profiles Oy7-08 (Wetterich et al., 2009) and Oya 5-1 (Kienast et al., 2011). The pollen sample preparation followed standard methods (e.g., Andreev et al., 2004).

Pollen-based climate reconstructions were based on a northern hemispheric modern pollen training dataset comprising 15,379 sites in Eurasia and North America (Herzschuh et al., 2023). Only terrestrial pollen taxa (including Cyperaceae) were used for reconstructions, while aquatic pollen taxa, as well as spores from mosses, ferns, fungi, and algae, were excluded. Woody taxa, as well as some very common herbaceous taxa (e.g., *Artemisia*, *Thalictrum*, or *Rumex*), were harmonized to the genus level, and all other herbaceous taxa were harmonized to the family level (Herzschuh et al., 2022). Site-specific mean July temperatures (T_{July}) and annual precipitation (P_{ann}) were derived from WorldClim 2 version 2.1 (https://www.worldclim.org; Fick and Hijmans, 2017) by extracting the climate data at the location of the modern samples. The pollen taxa in the fossil pollen samples noted above were harmonized in the same way as the taxa in the modern training dataset. For each location, we calculated the geographic distance between each sampling site in the modern training dataset and the fossil pollen record. The dissimilarity analysis shows very high quality of analogs. All samples are below the 5% threshold, which corresponds to "good analogs"; the majority of the samples even have "close analogs" (threshold < 1%). (Figure S2). Climate reconstructions were performed using the modern analog technique (MAT, Overpeck et al., 1985) by applying the MAT function from the rioja package (version 0.9-21, Juggins, 2019) for R (R Core Team, 2020) to the pollen percentages of the selected fossil pollen taxa, looking for seven analogs between the pollen data and the calibration dataset. The dissimilarity between the fossil samples and the modern pollen assemblages was determined by the squared-chord distance of the percentage data (Cao et al., 2014; Simpson, 2012).

Plant macrofossils were examined (Table A1) in profiles R22+60, L12+30, R35 (Kienast et al., 2008), and L7-11 (Schneider, 2010) on Bol'shoy Lyakhovsky Island and in profile Oya 5-1 on Oyogos Yar (Kienast et al., 2011). Sample preparation followed standard methods (e.g., Kienast et al., 2008). The MTWA tolerances of plant species identified by macrofossils were calculated by correlating their modern distribution in Yakutia, pooled in the online database. The Global Biodiversity Information Facility - GBIF (2023), which comprises geocoded

distribution data from maps published in the Flora of Siberia (Artemov and Egorova, 2021), permanently updated iNaturalist research-grade observations (iNaturalist, 2023) and records from literature on local floras of Russia (Bochkov and Seregin, 2022) with monthly mean temperatures from the updated database of Leemans and Cramer (1991). We considered only the Yakutian distribution of recovered plant species because of the relative climatic stability of Yakutia throughout the late Quaternary and the related conservative genetic configuration of plant populations in Yakutia with a low percentage of polyploidy and a narrower ecological tolerance in comparison with more western populations. The temperature range of a certain species was determined by the correlation of the species occurrences within Yakutia published in GBIF (2023), with the mean July temperature as MTWA at the t grid point closest to the respective occurrence with a resolution of 0.5° longitude/latitude (Leemans and Cramer, 1991). The temperature extremes within the Yakutian distribution range, e.g., the northernmost occurrence as the minimum and the presence in the Central Yakutian Plain with an MTWA of up to 18.4 °C as the possible maximum, reveal the temperature range of a species. The minimum requirement for MTWA of the most thermophilous species, together with the maximum MTWA tolerance of the most cold-adapted plant within a paleo-flora, reveal the temperature interval (or mutual climatic range, MCR) for the coexistence of all species. We focused on species with particularly high (boreal) and low (arctic) temperature demands (Table S1).

Sedimentary ancient DNA (sedaDNA) refers to the desoxyribonucleic acid (DNA) preserved in sedimentary deposits that stem from biological material such as plants, animals, and microorganisms that live in or near the depositional environment. In permafrost, sedaDNA is predominantly local in origin (Alsos et al., 2018), and its source can be derived from preserved plant tissues, from extracellular DNA bound to mineral particles, and from feces, and only to a lesser degree from pollen (Crump, 2021). That allows for the reconstruction of past community composition, diversity, and temporal dynamics up to geological timescales (Courtin et al., 2022; Kjær et al., 2022). We used DNA metabarcoding to amplify and sequence a short plant-specific genetic marker (see details in Zimmermann et al., 2017). DNA metabarcoding was successfully applied (Table A1) to seven samples of the permafrost core L14-04, three samples from profile L14-04-B, and seven samples of profile L14-04-C (Zimmermann et al., 2017).

Lipid biomarkers were analyzed in permafrost core L14-04. A total of 10 samples were processed, and microbial ether lipids (branched and isoprenoid glycerol dialkyl glycerol tetraethers; brGDGTs, isoGDGTs) were analyzed as described by Kusch et al. (2019). The methylation index of 5-methyl branched tetraethers (MBT'_{5ME}) was calculated using $MBT'_{5ME} = (Ia + Ib + Ic)/(Ia + Ib + Ic + IIa + IIb + IIc + IIIa)$ (de Jonge et al., 2014). The Isomer Ratio (IR) of penta- and hexamethylated brGDGTs was calculated as $IR = (IIa' + IIIa')/(IIa + IIIa + IIa' + IIIa')$ (Yang et al., 2015). We use the MBT'_{5ME}-based Air Growing Season Temperature (Air GST, April to October) calibration (calibration D; Air GST $= -3.82 + 22.71 * MBT'_{5ME} + 8.78 * IR$) recently developed by de Jonge et al. (2024) since it is the only calibration available that accounts for seasonal production bias by including soils frozen during part of the year and corrects for the influence of pH on MBT'_{5ME}. This calibration has a residual square mean error of 2.2°C. The branched and isoprenoid tetraether index (BIT; Hopmans et al., 2004) was calculated following $BIT = (Ia + IIa + IIIa + IIa' + IIIa')/(Ia + IIa + IIIa + IIa' + IIIa' + crenarchaeol)$, and the ratio of isoGDGTs to brGDGTs (Ri/b; Xie et al., 2012) was calculated using $Ri/b = \Sigma isoGDGTs/\Sigma brGDGTs$. For details about the chemical structures and nomenclature of GDGTs, we refer to Kusch et al. (2019).

Terrestrial insect remains (mostly beetles) were studied (Table A1) in four samples from Bol'shoy Lyakhovsky Island (L-11-B17, L-11-B19, L-12+30-B-18, R-22-B15, R-22-B16; Andreev et al., 2004, 2009;

Kuzmina, 2015b) and one sample from Oyogos Yar (Oya 5-1; Kienast et al., 2011). Sample preparation for terrestrial insect fossils followed standard methods (Kuzmina, 2015b). The MCR method described above for plant macrofossils allows reconstructing the MTWA and MTCO of the year by overlapping coexistence intervals of several species of insects (or any other taxa) in single samples (Atkinson et al., 1987). The MCR method is widely used on fossil beetle remains in Europe mainly because of the continuous research project and database BugsCEP (Buckland, 2007, 2014). The method has been adapted for North America (Elias, 2000, 2001) for the study of the late Quaternary beetle fauna of East Beringia. To evaluate the LIG warming in the Dmitry Laptev Strait region, two sources of thermal requirements are used, which are a West Beringian list (including phytophagous species; Alfimov et al., 2003) and a Transberingian list (excluding phytophagous species; Elias, 2000), both based on museum collections.

Chironomids were studied (Table A1) in profile R35 (Ilyashuk et al., 2006) on Bol'shoy Lyakhovsky Island and profile Oya 5-1 on Oyogos Yar (Kienast et al., 2011). Chironomid sample preparation followed standard methods (Brooks et al., 2007). For the paleotemperature reconstruction from chironomid data, we inferred the T_{July} (MWTA) by using a North Russian (NR) chironomid-based temperature inference model (WA-PLS, 2 component; r^2 boot = 0.81; RMSEP boot=1.43°C) based on a modern calibration data set of 193 lakes and 162 taxa from northern Russia (spanning from 61 to 75°N, and 50 to 140 °E, T_{July} range 1.8 to 18.8 °C; Nazarova et al., 2015). Water depths (WD) were reconstructed using a modern chironomid-based calibration dataset from East Siberia that includes 147 lakes (WD range 0.1 to 17.1 m). The one-component WA-PLS model had the best performance: r^2 boot = 0.62, RMSEP boot = 0.35 m for WD reconstructions (Nazarova et al., 2011). Both the T_{July} NR and the WD East Siberia models were previously applied for paleoclimatic inferences in East Siberia and the Russian Far East and demonstrated high reliability of the reconstructed parameters (Syrykh et al., 2017; Nazarova et al., 2017a, 2017b; Wetterich et al., 2018). Chironomid-based reconstructions were performed in C2 version 1.7.7 (Juggins, 2007). The data were square-rooted to stabilize species variance. Information on the ecology of chironomid taxa was taken from Brooks et al. (2007), Moller Pilot (2009), and Nazarova et al. (2008, 2011, 2015, 2017a).

Cladocera were newly studied (Table A1) in profile L7-11 on Bol'shoy Lyakhovsky Island, in profiles Oya-3-11, Oy7-01, Oy7-08, and in profile Oya 5-1 (Kienast et al., 2011) on Oyogos Yar. The cladocera sample preparation followed the standard methods (e.g., Kienast et al., 2011).

Mollusk fossil remains were obtained from samples BL-R-M1 (taken 1.8 m a.s.l. at profile R 41+50 m in 1999) and BL-R-M4 (taken at profile R32 in 1999) on Bol'shoy Lyakhovsky Island (E.E. Taldenkova, T.A. Yanina, unpublished data (Table A1), and from sample Oya 5-1 on Oyogos Yar (Kienast et al., 2011). The mollusk sample preparation followed standard methods (e.g., Kienast et al., 2011).

Ostracod valves from Bol'shoy Lyakhovsky Island were studied in profiles R23+40, L11+40 (S. Wetterich, unpublished, Table A1), L7-14 (Wetterich et al., 2009) and L7-11 (Schneider, 2010), and on Oyogos Yar in profiles Oy7-08 (Wetterich et al., 2009), Oy7-01 (Schneider, 2010) and Oya 5-1 (Kienast et al., 2011). The ostracod sample preparation followed standard methods (e.g., Wetterich et al., 2009).

3.5   Clumped isotope derived lake water temperature and δ¹⁸O signatures

An emerging method to derive quantitative paleotemperature estimates from ostracods is clumped isotope thermometry (Song et al., 2022). The advantage of this method is its independence of the temperature estimate from the δ¹⁸O signal of the water from which the ostracod and mollusk carbonate formed (Eiler, 2007). Two

ostracod species (*Cytherissa lacustris*, *Candona candida*) and a bivalve mollusk (*Pisidium casertanum*) were selected from sample Oya 5-1 for clumped isotope analysis based on their relatively high abundance providing sufficient sample material. Complete adult valves, with no visual evidence of dissolution or degradation, were selected and cleaned. We manually removed sediment contamination under a binocular microscope with a paintbrush and deionized water prior to the homogenization of the carbonate with a clean agate pestle and mortar.

Clumped isotope analysis was conducted in the NICEST laboratory at Northumbria University on a Nu Instruments Perspective IRMS coupled with a NuCarb dual inlet prep system. Powdered samples of 325 ± 25 µg were loaded into sample vials, evacuated, and reacted with concentrated orthophosphoric acid at 70 °C. Analyte gas was dehydrated and cleaned following established methodologies (e.g., Bernasconi et al., 2018; Eiler and Schauble, 2004; Petersen et al., 2015). Briefly, CO_2 was cryofocused and then dehydrated at –70 °C in two liquid nitrogen-cooled traps (coldfingers) and scrubbed of contaminants by passing through a static cryotrap filled with PorapakTM Q absorbent (Waters Corporation) cooled to –30 °C. Traps were baked at 150 °C after each measurement to avoid cross-contamination. The sample preparation system was baked out at 80 °C after each measurement to avoid cross-contamination. A minimum of 17 replicate measurements was made of each sample, sufficient to achieve standard errors ≤ 0.01 ‰ (i.e., 95% confidence interval < 0.02 ‰). Long-term instrument performance was monitored with an internal laboratory standard, POL-2, giving a long-term Δ_{47} external standard deviation of 0.032 ‰.

Isotopic outliers (stable and clumped) and samples with elevated Δ_{48} values, indicative of sample contamination, were discarded before final Δ_{47} values were calculated in the free software Easotope (www.easotope.org; John and Bowen, 2016) using the IUPAC parameters for ^{17}O correction and calculation of isotopic ratios for VPDB and VSMOW (Bernasconi et al., 2018; Brand et al., 2010; Daëron et al., 2016). Internal Δ_{47} values were projected onto the carbon dioxide equilibrium space (ICDES-90) using standards ETH1, ETH2, and ETH3 (ETH Zurich, Bernasconi et al., 2018), following the methods of Dennis et al. (2011), using ICDES Δ_{47} values (Bernasconi et al., 2021). Clumped isotope-based carbonate precipitation temperatures ($T\Delta_{47}$) were calculated using the composite calibration of Anderson et al. (2021), which has recently been shown to produce reliable temperature estimates for ostracods (Marchegiano et al., 2024).

We determined the $\delta^{18}O$ of the water in which ostracod carbonates formed using $T\Delta_{47}$ values and the $\delta^{18}O$ values of fossil ostracod and bivalve carbonate (measured during clumped isotope analysis). A constant $\delta^{18}O$ vital offset +2.2 ‰ to *Candona candida*, +1.2 ‰ to *Cytherissa lacustris*, and +0.86 ‰ to *Pisidium casertanum* (von Grafenstein et al., 1999) was applied before $\delta^{18}O$ of the formation waters were calculated using the calibration of Coplen (2007) to describe the temperature-dependent water-calcite oxygen isotope fractionation.

3.6   Paleoclimate modeling data

Within the framework of the 6th phase of the IPCC Climate Model Intercomparison Project (CMIP6, Eyringt et al., 2016), the PaleoMIP intercomparison project was endorsed, leading to the identification of several past time periods for paleo-climate simulations to focus on, following a standardized modeling protocol (Kageyama et al., 2018). One of these time periods is the LIG, with a center on the time slice around 127,000 years ago, which led to modeling experiments summarized under the acronym lig127k (Otto-Bliesner et al., 2017). Monthly mean air temperature and precipitation are available from 12 different global coupled climate models in the ligk127 experiment, provided by 13 different modeling groups worldwide, and providing between 100 and 700 years of

simulated climatic values for the LIG for the calculation of long-term averages (climatological means). In order to provide a reference for these simulations, all models also provided simulations of the pre-industrial period (PIcontrol). Commonly, model results are presented as anomalies to this reference period to reduce the impact of systematic model biases in the results (delta change method, e.g., Maraun and Widmann, 2018). The horizontal resolution of the models varies between 100 km and 500 km (Table S8). Monthly mean temperatures of MTWA and MTCO were calculated from each model on the model's native grid, first finding the maximum and minimum monthly values for each year and then averaging over all years the model provided, both for the lig127k simulations and the pre-industrial simulations. To obtain the anomalies, the resulting values were subtracted from each other (lig127k minus PIcontrol). Mean annual precipitation (MAP) was calculated on each model's native grid, summing up monthly precipitation values. Then, climatological means were calculated, averaging the years the model provided for both the lig127 and the PIcontrol simulations. Anomalies were again obtained by subtracting both averages (lig127k minus PIcontrol). Estimates and uncertainties for the sample sites Bol'shoy Lyakhovsky and Oyogos Yar, as well as a generic reference point, were computed from the multi-model ensemble mean anomalies and of the grid cell values the sites fall in, without spatial interpolation. To visualize temperature and precipitation patterns of the Laptev Sea area, temporal averages of all models were regridded to a common 1° x 1° grid.

In order to compare the modeled anomalies with the absolute values determined from the proxies, it is necessary to calculate absolute values from the PMIP climate change signals. This can be achieved by adding the PMIP climate change signal to observed values for the pre-industrial period (lig127k minus PIcontrol plus PIobs). This requires observed data for the pre-industrial period for data availability defined as 1850-1900 (Allen et al., 2018). For temperature, we retrieved data from NOAA GlobTemp V6, the most comprehensive gridded observational data record covering both present-day and pre-industrial climates (Huang et al., 2024). However, for similar reasons, climate models usually present their data as anomalies to a reference period; the NOAA GlobTemp data set presents temperatures as anomalies relative to the average over 1991-2020. In order to derive absolute values for the pre-industrial period, we need to add the anomalies provided by NOAA GlobTemp to an observed mean value for the same period, which we derived from the ERA5 reanalysis, the latest reanalysis product of the European Center for Medium-Range Weather Forecast (Hersbach et al., 2020). This method is in accordance with Allen et al. (2018) and Capron et al. (2014); the final formula for calculating the absolute values for the lig127k can be found in equation S1. For pre-industrial precipitation, no equivalent data set to NOAA GlobTemp exists. Therefore, it was not possible to obtain absolute values for MAP from the PMIP model anomalies. Instead, we use the multi-model ensemble mean. All models contributing to this experiment use a present-day land-sea mask and sea level (Figure S3) that does not conform to the suggested land-sea mask of the area during the LIG. The warmest temperatures and mean annual precipitation are influenced by a site's proximity to the coast. In the models, the horizontal resolution influences the position of the coastline and its distance to the sample sites. The model grid layout also influences the partitioning between the water and land of the grid cells in which the sample sites are located. To estimate the impact of the differences in coastlines among the models as well as between the models and the conditions of the LIG, an additional reference point was chosen for computation of MTWA, MTCO, and MAP that is situated within a land grid cell in every model and as close to the sample sites as possible, referred to as LandPoint, situated at 71.2°N, 142°E (Figure S3).

As a reference for the present day, monthly mean air temperatures and precipitation ERA5 were used to calculate MTWA, MTCO, and MAP. Values were calculated on the ERA5's native equal-area grid (nominal resolution about 35 km) and then interpolated onto a regular grid for plotting maps. Climatological means are

calculated over the period 1990-2019 (WMO present-day climate reference period). Values for the sample sites and the reference point were taken from respective grid cell values without spatial interpolation. Note also, that we use the modern calendar instead of an adjusted angular calendar that would account for shifts in solstice and the related seasons during the lig127 period caused by the high eccentricity of Earth's orbit around the sun. While studies like Shi et al. (2022) and Xu et al. (2024) demonstrate the profound impacts of using the classical calendar in particular in autumn, we expect the impacts on MTWA and MTCO calculations to be negligible because shifts in the position of a single month are small, especially winter and summer. We do not predefine which month of the year is considered warmest or coldest; rather, we determine them for each year individually.

4 Results

4.1 Field observations

Ice-wedge pseudomorphs of 1-3 m thickness of the Krest-Yuryakh stratum are exposed between 0.5-10 m a.s.l. in places along the southern coast of Bol'shoy Lyakhovsky Island (Figure 2a, Figure 3a). Such ice-wedge pseudomorphs are filled with alternating beds of peaty brownish plant detritus layers, partly with twig and wood fragments up to 5-8 cm in diameter and gray clay-rich silt layers. The thickness of individual layers varies from a few millimeters to 1-2 cm. Ripple bedding (ripples 1-2 cm high, 2-5 cm distance), finely laminated layers (each lamina 5-10 mm thick), and small-scale syn-sedimentary slumping structures are common (Figure 3b). Several layers contain 5-10 mm large mussel fragments. Larger twig fragments and peat inclusions of 2-3 cm are present. The cryostructure is dominantly massive, i.e., without visible ice structures. Only single thin ice veins (< 1 mm thick) are observed in places parallel to the sedimentary bedding. Besides ice-wedge pseudomorphs, there are also lacustrine deposits with horizontally alternating layers of well-laminated silty sand and peat.

Figure 3. LIG (Krest-Yuryakh) deposits exposed at the southern coast of Bol'shoy Lyakhovsky Island (Figure 2a): (a) ice-wedge pseudomorph (profile L7-11) with well-bedded lacustrine deposits and (b) laminated lacustrine deposits (profile L7-14 A-C) with alternate bedding of peaty and silty sand layers, and a slumping structure (next to the hoe).

Ice wedge pseudomorphs like those on Bol'shoy Lyakhovsky Island have been studied at various locations along the Oyogos Yar coast (Figure 4a). In addition, exposure of lacustrine gray silty fine sand (partly stratified) deposits was studied over a length of about 110 m at 1–3 m a.s.l. with two-meter-thick deposits (profile Oy7-01; Figure 4b). About 50 m toward the east, the profile is characterized by alternating beds of grayish-brown silty material and dark plant detritus, and mollusk shells.
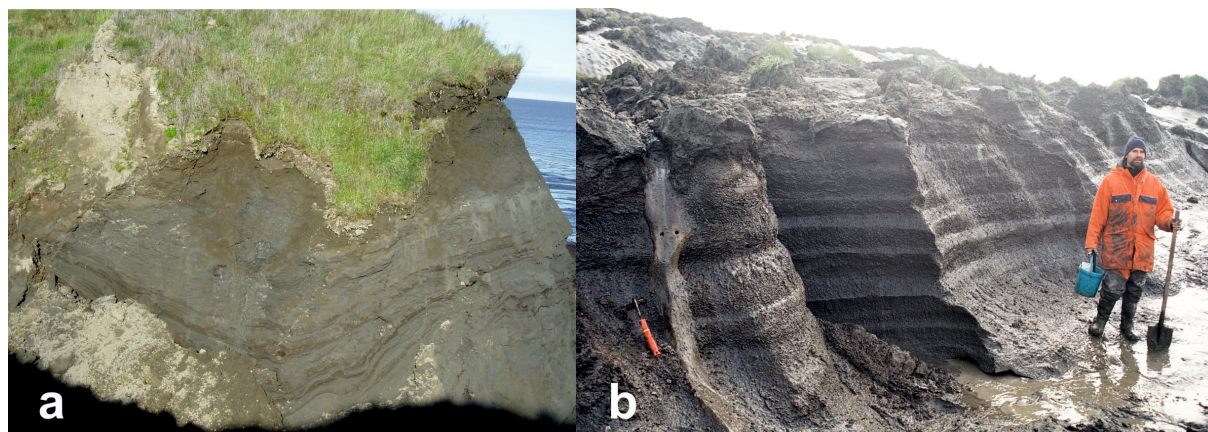
Figure 4. LIG (Krest-Yuryakh) deposits at the Oyogos Yar coast (Figure 2b): (a) ice-wedge pseudomorph of alternately bedded peat and silty sand layers (ca. one meter high from the bottom to the grass cover); (b) stratified lacustrine deposits (profile Oy7-01) above the beach.

4.2 Luminescence dating

After preparation, two samples from stratified lacustrine Krest-Yuryakh deposits (profile L14-12) revealed sufficient material for IRSL dating of one sub-sample in the coarse silt fraction (40-63 μm) and two sub-samples in the fine sand fraction (63-90 μm). The obtained ages range from 127.3±6.1 ka to 117.6±6.0 ka (Table 1). The three ages agree within errors, nevertheless the luminescence signal dispersion corresponding to the oldest age shows a slightly higher skewness and hence, indicates a slight overestimation.

Table 1: IRSL sample characteristics, including paleodose and dose rate parameters.

Sample ID (Grain size fraction)		L14-12-OSL3 (63-90 μm)	L14-12-OSL1 (63-90 μm)	L14-12-OSL1 (40-63 μm)
Paleodose parameters				
n		25	20	20
Mean	[Gy]	295.1±1.2	287.5±2.7	271.9±0.6
Standard deviation	[%]	5.8	4.2	2.8
Skewness		0.2	0.8	0.4
Coefficient of variation	[%]	5.1	3.8	5.3
CAM	[Gy]	295.2±3.5	287.2±3.14	271.8±2.9

Dose rate parameters				
^{238}U-series	[Bq kg^{-1}]	28.11±0.90	20.96±0.72	20.96±0.72
^{232}Th-series	[Bq kg^{-1}]	31.14±1.40	24.22±1.07	24.22±1.07
^{40}K	[Bq kg^{-1}]	475.32±1.82	481.98±1.66	481.98±1.66
Water content	[%]	35±5	35±5	35±5
Height	[m a.s.l.]	2.7	4.5	4.5
Cover thickness	[m]	30	28	28
Total dose rate	[Gy ka^{-1}]	2.6±0.1	2.4±0.1	2.4±0.1
Age	**[ka]**	**117.6±6.0**	**127.3±6.1**	**117.8±6.8**

2   4.3   Sedimentology and biogeochemistry

3   Krest-Yuryakh deposits on Bol'shoy Lyakhovsky Island are characterized by low ice contents (20-33 wt%) and no

4   wedge ice at all. The magnetic susceptibility (MS) values vary between 22 and 55 10^{-8} m^{3}kg^{-1}, differing from

5   outcrop to outcrop, while within single profiles, the differences are much smaller (Figure 5a). The TOC contents

6   range widely from 0.6 to 15.3 wt%. High TOC values (> 5 wt%) are related to plant detritus, peat, and woody

7   remains. The TOC/TN ratio, which reflects the degree of organic matter decomposition, is between 1.8 and 26.2.

8   Low TOC/TN ratios indicate high decomposition (Carter and Gregorich, 2008; White, 2005). The δ^{13}C values

9   range from –30.1 ‰ to –25.8 ‰. Differences of 3-4‰ occur within individual profiles. The carbonate contents

10   derived from the TIC values range from 0.2 to 6.7 wt% . High values are linked to the higher presence of mollusk

11   remains. The arithmetic mean grain size ranges between 15 and 78 μm, and the grain-size distribution curves are

12   characterized by a three-modal shape, with peaks in the fine silt, fine sand, and medium sand fractions (Figure 5b).
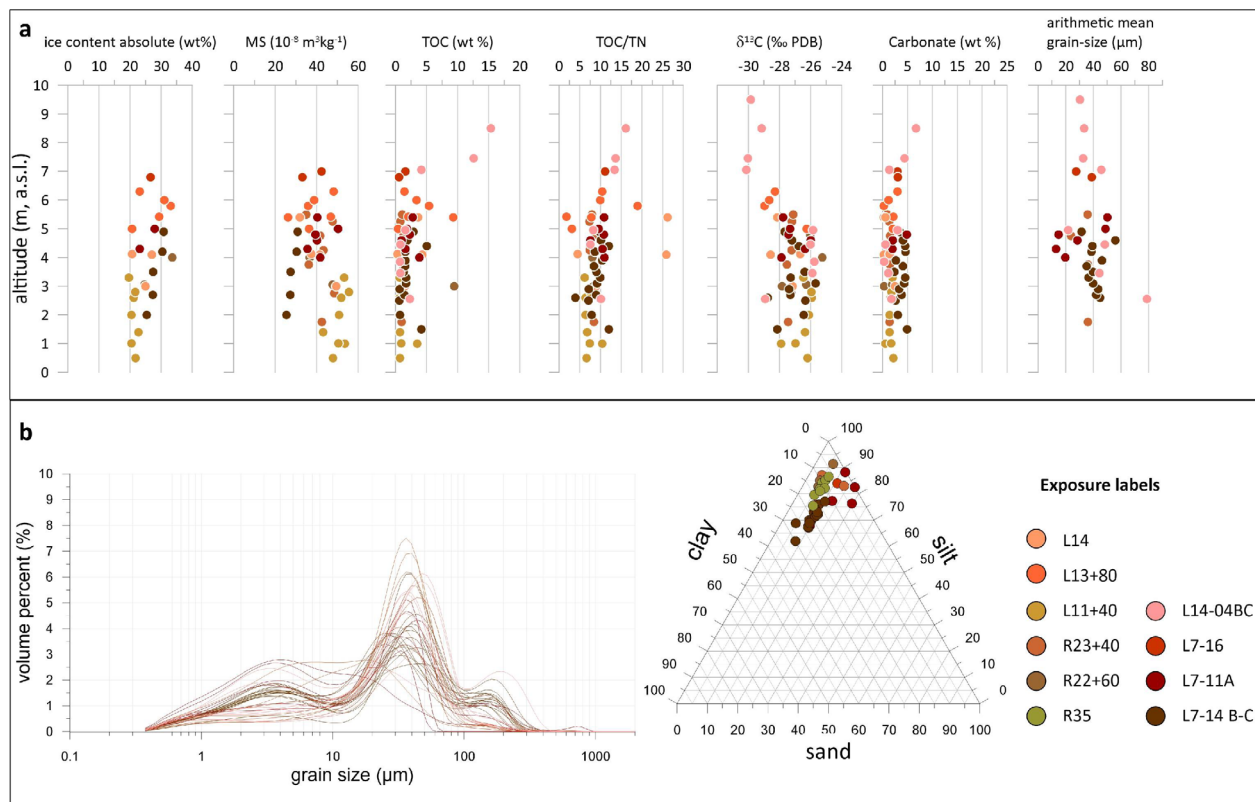
Figure 5. Sediment data of LIG (Krest-Yuryakh) profiles on Bol'shoy Lyakhovsky Island: (a) absolute gravimetric ice content, mass-specific magnetic susceptibility (MS), TOC content, TOC/TN ratio, δ¹³C, carbonate content, arithmetic grain-size mean; (b) grain-size distribution curves and sand-silt-clay percentages.

The cryolithological characteristics of Krest-Yuryakh deposits from the Oyogos Yar coast are similar to those of Bol'shoy Lyakhovsky Island (Figure 6a). The absolute ice contents range from 18 to 34 wt%. The MS varies between 12 and 45 10^{-8} m^{3}kg^{-1}. Within individual profiles, the differences are rather low, but there are stronger differences in MS values between the profiles. The TOC contents range from 0.6 to 21.3 wt%. The TOC/TN ratio is between 3.5 and 18.7. The δ¹³C values range from –30.8 ‰ to –26 ‰. The carbonate contents range from 1.4 to 22.4 wt%. The arithmetic mean grain sizes are between 15 and 59 µm, and the grain-size distribution curves are three-modal (Figure 6b).
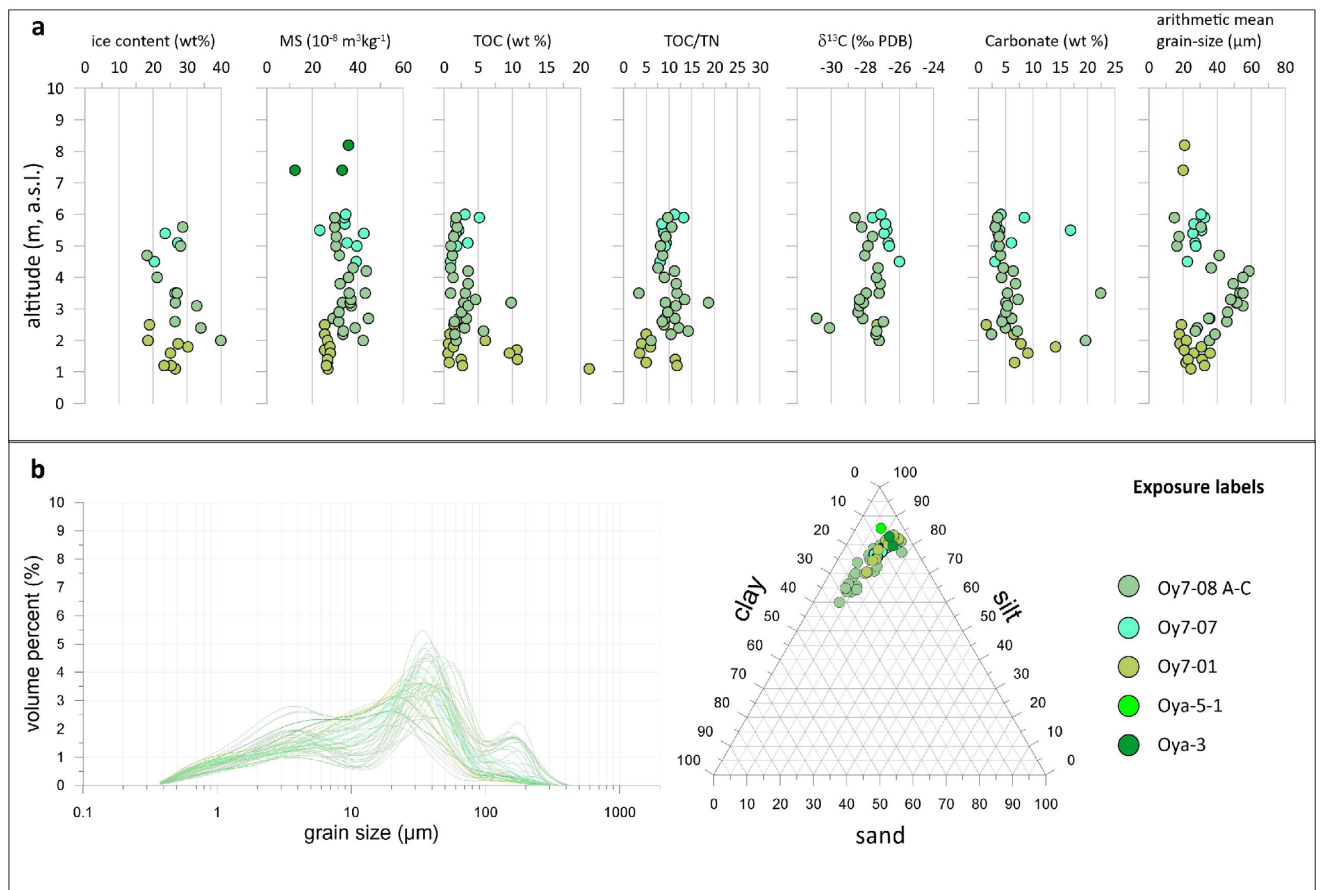
Figure 6. Sediment data of LIG (Krest-Yuryakh) profiles on Oyogos Yar: (a) absolute gravimetric ice content, mass-specific magnetic susceptibility (MS), TOC content, TOC/TN ratio, δ¹³C, carbonate content, arithmetic grain-size mean; (b) grain-size distribution curves and sand-silt-clay percentages.

4.4 Pollen-spores-based vegetation and paleoclimate reconstructions

The pollen assemblages of the bottom sections of ice-wedge pseudomorphs of Krest-Yuryakh deposits on Bol'shoy Lyakhovsky Island indicate that open steppe or tundra-steppe habitats with Poaceae and *Artemisia* dominated the vegetation at the beginning of the LIG (Andreev et al., 2004; Ilyashuk et al., 2006). However, relatively high abundances of *Alnus fruticosa*, *Salix*, and *Betula* sect. *nana* pollen indicate shrub presence in more protected places such as thermokarst basins and river valleys. The large amounts of coprophilous Sordariaceae fungal spores indirectly point to the presence of grazing herds of the late Pleistocene mammoth fauna (Andreev et al., 2011). The early to middle LIG pollen spectra are dominated by Poaceae, Cyperaceae, *Betula*, and *Alnus* (Andreev et al., 2004; Ilyashuk et al., 2006; Wetterich et al., 2009), reflecting a shrub-tundra vegetation. Relatively high concentrations of herb pollen taxa (*Artemisia,* Brassicaceae, Caryophyllaceae, Asteraceae) indicate that open habitats were also common. Relatively high amounts of *Glomus* fungal spores suggest that the local vegetation was frequently disturbed, probably due to active erosion processes connected with melting ice wedges and the formation of thermokarst lakes.

Pollen assemblages of the middle LIG from the Oyogos Yar coastal sections are dominated by Poaceae, Cyperaceae, *Larix*, *Alnus fruticosa*, and *Betula* sect. *nana* and spores of *Equisetum*, dung-inhabiting Sordariaceae, and *Glomus* (Wetterich et al., 2009; Andreev et al., 2011). Based on the quite high percentage of *Larix* pollen, we may infer that larch forest or forest-tundra with shrub alder and dwarf birch stands dominated the vegetation in the

Oyogos Yar area and document that the treeline was at least 270 km north of its current position during the LIG optimum.

Based on seven Krest Yuryakh profiles with 69 samples from Bol'shoy Lyakhovsky and one profile with 25 samples from Oyogos Yar, the reconstructed mean MTWA was 9.0±3.0 °C for Bol'shoy Lyakhovsky (median 9.7±3.1 °C) and 9.7±2.9 °C at Oyogos Yar (median 9.6±2.8 °C). The MAP was 271±56 mm (median 264±52 mm) on Bol'shoy Lyakhovsky and 229±22 mm (median 230±23 mm) at Oyogos Yar, implying that the summer climate conditions on Bol'shoy Lyakhovsky were a bit colder and moister than on Oyogos Yar.

4.5   Plant macrofossil-based vegetation and paleoclimate reconstructions

Plant macrofossil assemblages from Krest-Yuryakh deposits at both sides of the Dmitry Laptev Strait are exceptionally well preserved and frequently allowed for identification at the species level, giving a detailed picture of local vegetation and habitat conditions at the time of deposition (Table S2). On Bol'shoy Lyakhovsky Island, assemblages are composed of remains of 100 vascular plant taxa, including aquatic macrophytes living in the thermokarst lakes (Table A1). The detected species reflect a wide range of plant communities comprising open subarctic shrub tundra with the tall shrubs *Alnus alnobetula* ssp. *fruticosa* and *Betula fruticosa,* as well as dwarf shrubs like *Betula nana* s.l., *Vaccinium vitis-idaea*, *Rhododendron tomentosum*, and *Empetrum nigrum* interspersed with patches of dry grasslands with *Carex* (formerly *Kobresia*) *myosuroides*, *Potentilla* spp., *Artemisia* sp., *Androsace septentrionalis,* several steppe sedge species, and *Ranunculus pedatifidus* ssp. *affinis* suggesting the existence of arid habitats during MIS 5e. Arid conditions are confirmed by the halophytes (*Puccinellia, Tripleurospermum hookeri, Stellaria crassifolia, Rumex maritimus*) characteristic of salt marsh and saline meadow vegetation near lake shores with fluctuating water levels. The salt accumulation in the upper soil layer results from the capillary rise of solutes due to high evaporation under arid continental climates. The lakes formed habitats of aquatic macrophytes like *Callitriche hermaphroditica, Stuckenia vaginata, Myriophyllum spicatum*, *Batrachium* sp., *Nitella* sp., *Hippuris vulgaris, Sparganium hyperboreum* and *S. minimum*, species absent in the study area today. Constantly wet habitats were occupied by littoral and tundra wetland vegetation with *Eriophorum* spp., *Carex aquatilis*, *C.* sect. *Phacocystis*, *Juncus biglumis, Chrysosplenium alternifolium*, *Comarum palustre, Caltha palustris, Parnassia palustris*, *Ranunculus hyperboreus, R. lapponicus* and *Gastrolychnis violascens*. The estimated LIG MTWA on Bol'shoy Lyakhovsky Island is based on the MCR of 15 selected taxa (Table 2) and ranges from 10.3 °C to 12.9 °C.

The plant remains at the mainland coast of Oyogos Yar reflect a LIG vegetation similar to Bol'shoy Lyakhovsky Island consisting of open shrub tundra and forest tundra interspersed with patches of steppe and meadow grassland. In contrast to modern larch-dominated forest-tundra, the LIG woodland was dominated by birches, as shown by the abundance of birch remains from both trees and shrubs. In addition to tall and dwarf shrubs already recovered from Bol'shoy Lyakhovsky Island, extralimital Ericaceae taxa (*Arctostaphylos uva-ursi, Andromeda polifolia, Chamaedaphne calyculata*) and forbs (*Moehringia laterifolia, Stellaria longifolia*, *Chamaenerion angustifolium*) occurred at Oyogos Yar. Characteristics of the undergrowth of modern boreal forests likewise indicate a relatively long and warm growing season during MIS 5e.

Analogous to Bol'shoy Lyakhovsky Island, the reconstructed wooded tundra at Oyogos Yar was rather open as suggested by abundant remains of tundra-steppe plants like *Carex myosuroides, Dryas octopetala* s.l., *Rhododendron* sp., *Potentilla stipularis, P. nivea, Ranunculus pedatifidus* ssp. *affinis* and meadow steppe species,

1   such as *Odontarrhena obovata*, *Allium* sp., *Artemisia* sp., *Carex duriuscula*, *C. supina* s.l., *Eritrichium sericeum*,

2   *Rumex acetosella* s.l.. These meadow steppes merged into productive alkali grass meadows indicated by abundant

3   remains of *Puccinellia*. *Puccinellia* sp. and other halophilic taxa, like *Chenopodium* sp. and *Spergularia salina*,

4   have an affinity to brackish conditions, which suggests high evaporation and low lake levels in response to seasonal

5   aridity at Oyogos Yar during the LIG, similar to Bol'shoy Lyakhovsky Island.

6   The inventory of water plants at Oyogos Yar resembles that of the Bol'shoy Lyakhovsky assemblage and

7   was supplemented by abundant extralimital, i.e., thermophilous, aquatic macrophytes like *Stuckenia filiformis* and

8   *Potamogeton perfoliatus*. The estimated LIG MTWA at Oyogos Yar is based on the MCR of 17 selected taxa

9   (Table 2) and ranges from 12.7 °C to 15.3 °C.

10   **Table 2: MTWA requirements and updated coexistence interval of selected vascular plant species that were identified**
11   **in LIG (Krest-Yuryakh) deposits on Bol'shoy Lyakhovsky Island and the Oyogos Yar mainland coast. Determining**
12   **values of the coexistence intervals are highlighted in bold.**

Taxon	MTWA$_{Min}$ [°C]	MTWA$_{Max}$ [°C]	Bol'shoy Lyakhovsky Island	Oyogos Yar
Alnus hirsuta	**12.7**	18.4		X
Alnus alnobetula subsp. *fruticosa*	7.5	18.4	X	X
Betula nana s.l.	5.2	18.0	X	X
Betula fruticosa	9.1	18.4	X	X
Potamogeton perfoliatus	10.3	18.4		X
Myriophyllum spicatum / M. sibiricum	**10.3**	18.4	X	X
Larix gmelinii	8.0	18.4		X
Betula divaricata	7.6	18.4		X
Arctostaphylos uva-ursi	10.6	18.4		X
Moehringia lateriflora	9.9	18.4	X	X
Callitriche hermaphroditica	8.1	18.4	X	X
Menyanthes trifoliata	5.2	18.1	X	
Sparganium hyperboreum	8.1	18.1	X	X
Sparganium minimum	10.3	18	X	X
Cherleria arctica	3.3	13.3	X	
Coptidium lapponicum	3.5	16.9	X	X
Silene involucrata	3.3	15.7	X	X
Ranunculus pedatifidus ssp. *affinis*	5.6	17.6	X	X
Sagina nivalis	2.6	**12.9**	X	
Potentilla hyparctica	2.6	14.6	X	
Ranunculus nivalis	1.6	**15.3**		X
Coexistence interval MTWA [°C]			**10.3 to 12.9**	**12.7 to 15.3**

14   **4.6   *Sed*aDNA-based vegetation reconstruction**

15   The Krest-Yuryakh deposits on Bol'shoy Lyakhovsky Island exhibit rich vegetation with *sed*aDNA derived from

16   several woody taxa, including trees, shrubs, and sub-shrubs, suggesting interglacial, warmer-than-present

17   conditions (Figure 7). The proportions of sequences assigned to woody taxa (trees < 1% and shrubs 6-87%), forbs

18   (8-91%), and grasses (2-39%) were highest, while the proportions of sedges (< 1%), cryptogams (< 1%), and

aquatic forbs (up to 1.6%) were very low. Among woody taxa, we detected *Larix*, *Picea*, *Populus, Alnus, Betula*, *Ribes*, *Saliceae,* and *Cornus,* as well as sub-shrubs such as arctic-alpine *Dryas* and Ericaceae, including *Arctous*, *Pyrola* spp., *Vaccinium uliginosum*, and *Vaccinium vitis-idaea* (Zimmermann et al., 2017) which are typical components of the understory in boreal forests but also of subarctic tundra habitats. The forbs contain mainly taxa adapted to dry steppe conditions (*Artemisia gmelinii,* including halophilic *Puccinellia*), arctic-alpine tundra (*Braya*, *Draba*, and *Dryas*), or pioneer plants (*Papaver* and *Oxyria digyna*). Other forbs such as *Geum*, *Myosotis alpestris*, and *Bistorta* are typical components of forest margins or meadows. The Krest-Yuryakh deposits formed in a shallow lake in which aquatic and riparian forbs included *Menyanthes trifoliata*, *Stuckenia*, *Potamogenton*, *Hippuris*, and *Caltha palustris*. Nevertheless, sedges in the lower part of the core L14-04 were composed of two distinct *Kobresia* variants (same barcode shared between *K. filifolia* and *K. simpliciuscula* and between *K. sibirica* and *K.myosuroides* (now *Carex myosuroides*) typical of dry to wet habitats while the upper section of the profile also contained the sedges *Carex* and *Eriophorum* that are typical for wet habitats but also steppe. This shift between 8 and 12 m a.s.l. is accompanied by high proportions (up to 33%) of cryptogams and graminoids (*Eriophorum*, Bryophytes). At the same time, woody taxa were only represented by *Salix*, overall suggesting a transition to cooler and more moist conditions.

We refrain from paleoclimatic inferences as *sed*aDNA (compared to traditional proxies like pollen assemblages) provides only qualitative or semi-quantitative assemblage information, is rather local in the origin of the signals and the lack of taxonomic resolution to species level in many taxa hampers the accurate inference of past temperatures. However, the northern distribution limit of *Larix* is clearly spatially linked to the 10–12.5°C isotherm (based on its modern ecology (MacDonald et al. 2008)) and the co-occurrence of *Picea* (likely *P. obovata*) suggests an active layer depth of at least 1.5–2 m (Tchebakova et al. 2009). Thus, our results align with other proxy reconstructions presented in this study, supporting the interpretation of warmer-than-present temperatures during the Last Interglacial (LIG).
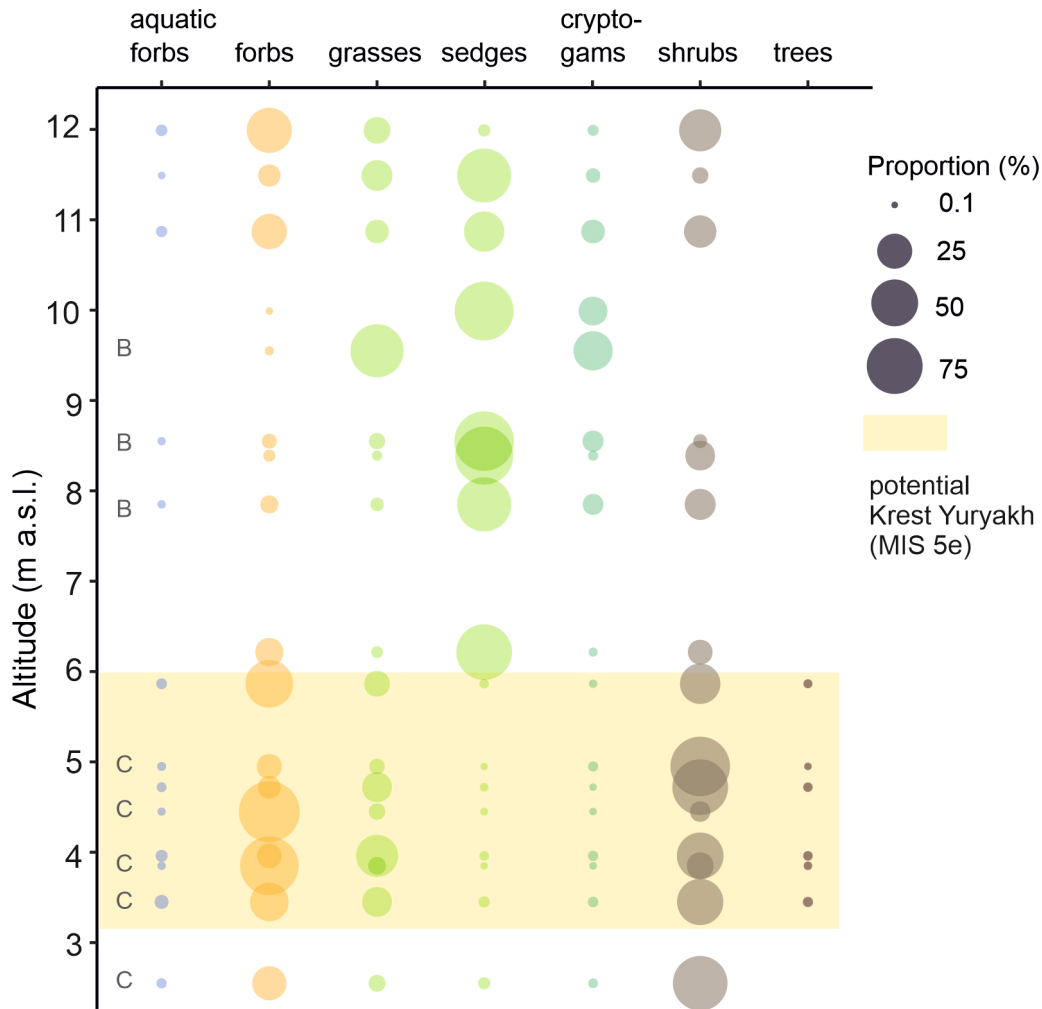
Figure 7. Composition of plant functional groups in the *sed*aDNA metabarcoding record of combined LIG (Krest-Yuryakh) samples from core L14-04 and profiles L14-04-B (indicated by B) and L14-04-C (indicated by C) from Bol'shoy Lyakhovsky Island. Figure 7 was generated using ggplot2 v. 3.4.2 (Wickham, 2016) in R v. 4.1.3 (R Core Team, 2022). For detailed stratigraphic co-occurrences of all taxa at the highest feasible taxonomic resolution, see Zimmermann et al. (2017).

4.7 Biomarker-based paleoclimate reconstruction

Samples from core L14-04 analyzed for GDGTs (Table S3) include those from the MIS 5e (Krest-Yuryakh stratum (n = 3) as well as deposits from younger MIS 5d-a horizons (n = 6) and MIS 1 (active layer; n = 1). BrGDGT distributions globally have a near-universal relationship with temperature irrespective of sample type (Raberg et al., 2022), yet their producers are ubiquitous in nature. Since the Krest-Yuryakh stratum is composed of both lacustrine deposits and peaty plant detritus layers, we tested the potential influence of in-situ production by benthic bacteria in sediments using $\#rings_{tetra}$ (Sinninghe Damsté, 2016). The $\#rings_{tetra}$ values throughout core L14-04 range from 0.04 to 0.25, with values from 0.12 to 0.15 in the LIG deposits. These values indicate that brGDGTs are not produced by benthic bacteria ($\#rings_{tetra}$ >0.7) but instead mostly derive from soil/peat and, thus, record Air Growing Season Temperature (GST). Reconstructed Air GST is 0.9 °C for the active layer, 2.8±0.3 °C for the MIS 5e deposits, and 1.3±0.9 °C for the MIS 5d-a deposits (Figure 8).

Although brGDGT distributional changes have been observed as a direct physiological response to temperature (as well as pH and O_2 concentrations) in acidobacterial cultures (Halamka et al., 2021, 2023), various confounding factors such as soil chemical properties (pH, cation availability) and bacterial community composition (e.g., Halffman et al., 2021; de Jonge et al., 2024) can also affect brGDGT distributions. For example,

1   the BIT and Ri/b indices in soils show a relationship with mean annual precipitation/soil moisture. At lower soil

2   moisture, the BIT index decreases, and the Ri/b increases (Xie et al., 2012; de Jonge et al., 2024). For core L14-

3   04, Ri/b values are substantially higher in the Krest-Yuryakh stratum (Figure 8), suggesting more arid conditions

4   during MIS 5e compared to MIS 5d-a and MIS1. The (isoGDGT-1 + isoGDGT-3)/(isoGDGT-1 + crenarchaeol)

5   values, which seem to correlate with mean monthly precipitation (de Jonge et al., 2024) also follow this overall

6   trend. Absolute crenarchaeol concentrations do not correlate with Air GST (Pearson correlation coefficient r =

7   0.058, *p* = 0.87), suggesting the observed trends are indeed controlled by soil moisture/precipitation rather than

8   temperature. Yet, no calibration exists that would allow us to calculate mean annual precipitation; thus, we only

9   use this information qualitatively.
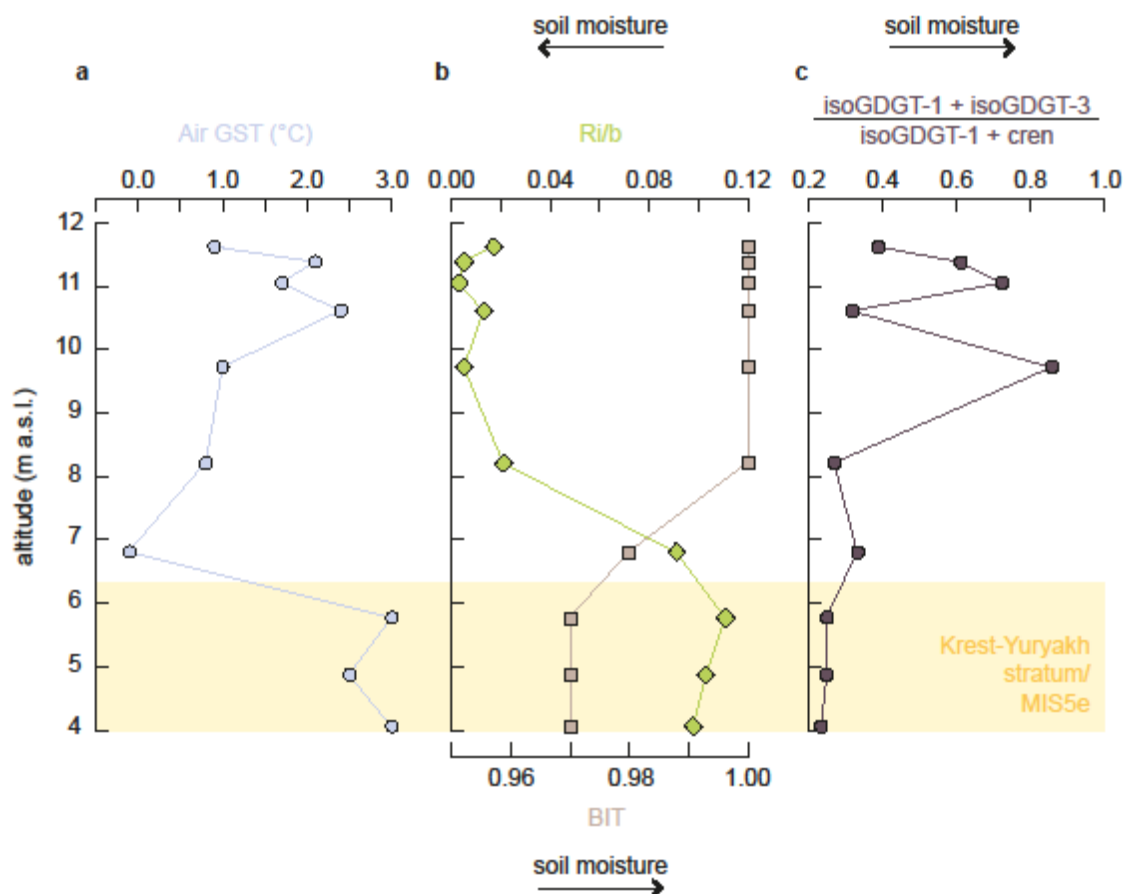
11 **Figure 8. BrGDGT-based proxies in core L14-04: (a) MBT'₅ME-based Air Growing Season Temperature (Air GST)**

12 **following de Jonge et al. (2024); (b) branched and isoprenoid tetraether index (BIT) and ratio of isoGDGTs to brGDGTs**

13 **(Ri/b); (c) ratio (isoGDGT-1 + isoGDGT-3)/(isoGDGT-1 + crenarchaeol).**

15 **4.8   Beetle-based faunal habitat and paleoclimate reconstructions**

16 The fossil insect assemblages of the LIG on Bol'shoy Lyakhovsky Island and on Oyogos Yar are rich in species,

17 and the concentration of remains is very high in comparison to other stratigraphic units in the study area (Kuzmina,

18 2015a, 2015b, Table S4). Insect remains are well preserved. The fossil insect fauna shows a high amount of steppe

19 species (Table S5). The share of *Morychus viridis* reaches up to 15%. Several identified thermophilous steppe

20 species (*Cymindis arctica*, *Chrysolina brunnicornis bermani*, *Stephanocleonus eruditus*, *S. fossulatus*) are absent

21 in other Pleistocene samples (Andreev et al., 2004, 2009; Kiselev and Nazarov, 2009), Arctic species (*Chrysolina*

22 *subsulcata, Ch. bungei*) present only 3 % of the entire association. The weevil *Dorytomus imbecillus* indicates

shrub vegetation. Several species prefer habitats in and on plant litter (*Cyrtodactylus irregularis*, *Eucnecosum tenue*, *Lathrobium* sp., *Philonthus* sp., *Quedius* sp.). A number of riparian and aquatic insects (*Colymbetes dolabratus*, *Aegialia kamtschatica*, *Agonum impressum*, *Sericoda quadripunctata*, *Scymnus* sp., *Notaris bimaculatus*) identified in the Interglacial samples are not recorded on the island today. The predaceous diving beetle *Colymbetes dolabratus* lives in the north of boreal forest and tundra zones up to Baffin Island and Greenland. In Eurasia, the species is common in the north but is not found today in the high Arctic. Other species are nowadays distributed mostly in the forest zone, but their life cycle is not connected directly to the trees. The ground beetle *Sericoda quadripunctata* is known as post forest-fire species but can also occur in any open disturbed habitats. A brief comparison of representative insects from older and younger stratigraphic horizons is summarized in a separate text as Text S1 and a possible periglacial landscape is presented in Figure S4.

To evaluate the LIG climate conditions in the Dmitry Laptev Strait region, two sources of thermal requirements are used, which are a West Beringian list (including phytophagous species; Alfimov et al., 2003) and a Transberingian list (excluding phytophagous species; Elias, 2000), both based on museum collections. In these datasets, several species have slightly different temperature ranges in East and West Beringia (Table S6). The overlap in coexistence intervals for West Beringian species is shown in Figure S5. The combined results are presented in Table 3. Including phytophagous beetles provides important environmental information. The weevils *Stephanocleonus eruditus* and *S. fossulatus* need high soil temperature (>12 °C) for the larvae to grow. Larvae of these weevils are root eaters and live in the soil horizon. They are active in warm seasons only. Winter temperature is not critical (Berman et al., 2011). The coexistence of thermophilous weevils and cold-adapted leaf beetles (MTWA range of *Chrysolina subsulcata* is 2 to 10 °C; Table S6) in one fossil assemblage highlights where the coexistence intervals do not overlap (Alfimov et al., 2003) as also observed in samples R-22-B15 and L-11-B19 (Table 3).

The thermal coexistence intervals of all considered beetle species, i.e., their MCR is 8 to 10.5 °C for MTWA and –34 to –26 °C for MTCO on Bol'shoy Lyakhovsky, and 8 to 14 °C for MTWA and –38 to –26 °C for MTCO on Oyogos Yar.

Table 3: MTWA and MTCO requirements and coexistence intervals of beetles from LIG (Krest-Yuryakh) samples based on modern reference data in Alfimov et al. (2003) and Elias (2000) applying the MCR method. Determining values of the coexistence intervals are highlighted in bold.

Sample ID	MTWA$_{Min}$ [C°]	MTWA$_{Max}$ [C°]	MTCO$_{Min}$ [C°]	MTCO$_{Max}$ [C°]
Bol'shoy Lyakhovsky Island				
L-11-B17	**8**	13	–37	**–26**
L-11-B19	4	**10.5**	–38	–24
R-22-B15	4	18	**–34**	–26
R-22-B16	8	14	–35	–26
Oyogos Yar				
Oya 5-1	**8**	**14**	–38	**–26**

1 **4.9 Chironomid-based habitat and paleoclimate reconstructions**

2 In profile R35 (Bol`shoy Lyakhovsky Island, Figure 2), 33 chironomid taxa were identified. The assemblage from

3 the lowermost sample (1.2 m a.s.l.) includes a relatively high share of semi-terrestrial taxa *Metriocnemus-*

4 *Thienemannia, Smittia,* and *Limnophyes-Paralimnophyes* indicative of low and variable water level. Between 1.4

5 and 2.2 m a.s.l., we find a high relative abundance of the taxa typical of warm and more eutrophic conditions

6 (*Chironomus plumosus*-type, *Cricotopus-Orthocladius, Procladius*). Here, taxa characteristic for shallow water,

7 semi-terrestrial conditions, or temporary waters (*Limnophyes-Paralimnophyes, Georthocladius, Hydrobaenus*)

8 and taxa that can tolerate acidic conditions (*Tanytarsus, Psectrocladius sordidellus*-type) are less abundant.

9 Between 2.2 and 5.2 m a.s.l., a high share of eutrophic taxa (*Chironomus plumosus*-type, *C. anthracinus*-type,

10 *Procladius*) and those indicative of cooler and more acidic conditions (*Sergentia coracina*-type) are present.

11 The chironomid-inferred MTWA of R35 varies between 3.4 °C and 15.3 °C (Table 4). The median

12 MTWA is 12.7 °C for the middle part of the section (1.6–3.2 m a.s.l) and 13.9 °C for the upper part (3.6–5.2 m

13 a.s.l.). The highest error of prediction (SE of ± 4.8 °C) occurs in the lowermost sample (at 1.2 m a.s.l.). That can

14 be explained by the dominance of semi-terrestrial taxa, especially *Metriocnemus,* which is also often found in lake

15 sediments but has still debated ecological requirements (Moller Pillot, 2009 and reference therein). In the NR

16 dataset, *Metriocnemus* appears with a broad range of ecological conditions with a high-temperature tolerance of

17 9.3±4.6 °C (Nazarova et al., 2015), which leads to a high error in the temperature reconstruction. Therefore, these

18 data from the lowermost sample of profile R35 (at 1.2 m a.s.l.) are not considered in further paleoclimatic

19 interpretation. For all other samples, the errors of prediction remain at the average level of the transfer function

20 (1.4–1.5 °C; Nazarova et al., 2015). The inferred WD reflects a period of shallow water (WD of 1.7–2.4 m) during

21 deposition of the strata between 1.2 and 2 m a.s.l., rising water level (WD 4.5–5.6 m) between 2.4 and 3.2 m a.s.l.,

22 and decreasing water level (mean WD of 3.8±0.5 m) between 3.6 and 5.2 m a.s.l. (Table 4).

24 **Table 4: Mean air temperature of the warmest month of the year (MTWA) and water depth (WD) and the errors of**
25 **prediction (SE) reconstructed from the chironomid communities of LIG (Krest-Yuryakh) deposits of Bol'shoy**
26 **Lyakhovsky Island (profile R35; Ilyashuk et al., 2006) and Oyogos Yar (profile Oya 5-1; Kienast et al., 2011). Data in**
27 **brackets are not considered for paleoclimatic interpretation.**

Sampling height [m a.s.l.]	MTWA ± SE [°C]	WD ± SE [m]
Bol`shoy Lyakhovsky Island, profile R35		
5.2	13.7 ± 1.4	3.3 ± 1.0
4.8	13.2 ± 1.5	3.8 ± 1.0
4.4	**15.3 ± 1.5**	4.1 ± 1.1
4.0	13.9 ± 1.5	3.9 ± 1.1
3.6	13.9 ± 1.4	2.7 ± 0.9
3.2	12.7 ± 1.4	**5.6 ± 1.0**
2.8	13.7 ± 1.5	4.5 ± 1.0
2.4	**9.4 ± 1.7**	5.4 ± 1.0
2.0	15.1 ± 1.5	**1.7 ± 0.9**

1.6	10.3 ± 2.0	2.4 ± 1.0
(1.2)	(3.4 ± 4.8)	(2.4 ± 1.2)
Oyogos Yar, sample Oya5-1		
3.5	**12.9 ± 0.9**	**2.2 ± 1.1**

The chironomid assemblage in sample Oya 5-1 is diverse and includes 16 taxa. The semi-terrestrial *Limnophyes, Smittia,* and the acidophilic *Psectrocladius sordidellus*-type dominate it. Phytophilic taxa indicative for temperate shallow lakes or littoral conditions are less abundant (*Cricotopus laricomalis*-type, *Tanytarsus pallidicornis*-type, *Endochoronomus albipennis*-type). The inferred MTWA from the chironomid community of the Oyogos Yar sample (Oya 5-1) is 12.9±0.9 °C and WD 2.2±1.1 m (Table 4).

4.10 Cladocera-based habitat reconstruction

The fossil cladocera remains of LIG deposits on Bol'shoy Lyakhovsky Island and Oyogos Yar are exceptionally well preserved. The overall cladocera record comprises 13 taxa, of which six were identified at the species level, four to groups or taxa, and three at the genus level (Table S7). The most common species that occur in at least four of the five profiles are *Chydorus* cf. *sphaericus*, *Bosmina* sp., and *Daphnia pulex* gr. The cladocera communities are dominated by littoral shallow-water taxa, such as *Ch.* cf. *sphaericus* and *Alona guttata*/*Coronatella rectangula* representing 79 % of the total number of individuals, while the proportion of plaktonic taxa (*Bosmina* sp., *D. pulex* gr.) amounts to 21 %.

Profile L7-11 on Bol'shoy Lyakhovsky shows very low concentrations of 1-2 specimens per gram of dry sediment. In total, only 11 individuals of *Ch.* cf. *sphaericus*, *Bosmina* sp., and *D. pulex* gr. are found (Table S7). Of those, *Ch.* cf. *sphaericus* is the most common species, a widely distributed, eurytopic, phytophilous pioneer species inhabiting the littoral (Bledzki and Rybak, 2016). This taxon is highly adaptive, resistant to adverse environmental conditions and low temperatures, and often migrates further north than other cladocera species (e.g. Luoto et al., 2011; Frolova et al., 2014).

The cladoceran records on Oyogos Yar are more diverse and had much higher concentrations than those on Bol'shoy Lyakhovsky. Exemplarily, the Oya 5-1 record (Kienast et al., 2011) revealed the most numerous record comprising >150 specimens per sample, representing a total of nine species, most of which belong to the family Chydoridae (seven species). The assemblage is dominated by *Ch.* cf. *sphaericus* (37%), *A. guttata*/*C. rectangula* (29%), and *Bosmina* sp. (29 %). Littoral species that inhabit macrophytes or detritus-rich silty lake margins, mainly *Ch.* cf. *sphaericus* and *A. guttata*/*C. rectangula*, represent two-thirds of the assemblage, while one-third is planktonic (mainly *Bosmina* sp. and *D. pulex* gr.) (Kienast et al., 2011).

Cladocera remains are also well represented in profile Oy7-08, where the high species richness (9 taxa in sample Oy7-08-19) and the highest concentration of remains in sediments (39 specimens per gram of dry sediment in Oy7-08-19) are noted (Table S7). Most remains belong to littoral species often associated with macrophytes (*Ch.* cf. *sphaericus, Acroperus harpae, Alonella excisa, Eurycercus* sp., *Sida crystallina*). Besides typical northern or Arctic species such as *A. harpae, Ch.* cf. *sphaericus*, and *Alona affinis* taxa indicative of higher water temperatures are observed, such as *Leydigia leidigi* and *S. crystallina* that were not found in modern bottom sediments of >30 water bodies on the coast of the Laptev Sea (L. Frolova, unpublished data). The cladoceran

assemblages of Oyogos Yar indicate habitats with a well-developed vegetated shallow littoral zone and pelagic open-water zones.

4.11 Mollusk-based habitat reconstruction

LIG deposits on Bol'shoy Lyakhovsky Island contain *Sphaerium corneum* with ten complete valves and fragments, *Valvata piscinalis* with ten complete shells and fragments, *Lymnaea* cf. *peregra* with one shell, and *Pisidium* sp. with six valves (E.E. Taldenkova, T.A. Yanina, unpublished data).

At Oyogos Yar, mollusks were identified by A. Kossler (Kienast et al., 2011). There, two freshwater gastropod taxa of the genera *Radix* and *Gyraulus* are represented only by a few juvenile shell fragments impeding species identification and deduction of precise environmental implications (Kienast et al., 2011). The distribution of *Radix* further to the north than today can be interpreted as an indication of warmer than present climate conditions. Additional identified shell fragments include *Valvata* cf. *piscinalis* and *Lymnea* cf. *stagnalis* (E.E. Taldenkova, T.A. Yanina, unpublished data). Furthermore, five bivalve species have been identified (Kienast et al., 2011): *Pisidium casertanum*, *P. subtruncatum*, *P.* cf. *lilljeborgii*, *P. obtusale* f. *lapponicum*, and *P. stewarti* of which the most frequent (*P. casertanum* and *P. subtruncatum*) are eurytopic and widely distributed, while the rare *P. obtusale* f. *lapponicum* inhabits typically arctic and subarctic regions. The stenoecious species *P. lilljeborgii* indicates oxygen-rich, oligotrophic, and stagnant water bodies. *P. stewarti* is only known from the Tibetan Plateau and the Siberian Irtysh region (Kuiper, 1962, 1968). Additionally, the species *Sphaerium* cf. *corneum* has been found (E.E. Taldenkova, T.A. Yanina, unpublished data).

4.12 Ostracod-based habitat reconstruction

The LIG ostracod record obtained at both shores of the Dmitry Laptev Strait comprises 23 taxa, of which 20 were identified at the species level, two at the genus level, and one taxon comprises juvenile Candoninae (Table S8). The most common species that have occurrences in at least four of the five studied profiles are *Candona candida*, *Fabaeformiscandona harmsworthi*, *F. levanderi*, *F. rawsoni*, *F. tricicatricosa*, *Eucypris dulcifons*, *Ilyocypris lacustris*, *Cytherissa lacustris,* and *Limnocytherina sanctipatricii*. The Oya 5-1 record (Kienast et al., 2011), which had the densest fossil occurrences, comprising >1000 specimens per sample belonging to a total of 11 species, is dominated by *C. candida* (34 %), *Cy. lacustris* (26 %), and *F. rawsoni* (15 %).

The species *Cy. lacustris*, *F. tricicatricosa,* and *L. sanctipatricii* are adapted to cool water temperatures (Meisch, 2000), and *T.* cf. *glacialis*, *F. rawsoni,* and *F. harmsworthi* are cold-stenothermic (Wetterich et al., 2008a, 2008b). Increased salinity in the water is tolerated by *L. sanctipatricii* (0.5-5 ‰), *C. lacustris* (up to 1.5 ‰), and *F. levanderi* (up to 6 ‰; Meisch, 2000).

4.13 Clumped isotope temperature and thermokarst lake $\delta^{18}O$ reconstructions from ostracod and bivalve calcite

Clumped isotope Δ_{47} values range between 0.641 and 0.658 ‰, with standard errors between 0.005 and 0.011 ‰ (95% confidence intervals between 0.01 and 0.022 ‰). Of the 54 sample replicates, three erroneous replicates (with stable or clumped isotope values greater than $\bar{x} \pm 2\sigma$), and one contaminated replicate ($\Delta_{48} > 1$ ‰) were

removed from the final Δ_{47} calculations. The final values suggest carbonate precipitation temperatures (TΔ_{47})

between 5.3 and 10.3°C. The raw data is presented in Table S9 and results are summarized in Table 5.

Fossil carbonate $\delta^{18}O$ values range from -14.65 ± 0.02 ‰ to -14.12 ± 0.02 ‰ VPDB, resulting in reconstructed

water $\delta^{18}O$ estimates ($\delta^{18}O_w$) between -18.9 ± 0.3 ‰ and -17.8 ± 0.6 ‰ VSMOW.

Table 5: Clumped isotope results from fossil biogenic carbonates from profile Oya 5-1. N = number of replicate measurements used to calculate Δ_{47} with the number of rejected samples in parenthesis. Δ_{47} and $\delta^{18}O$ of carbonate ($\delta^{18}O_{cc}$) uncertainties are given as external standard errors over multiple replicates. $\delta^{18}O_w$ is the estimated $\delta^{18}O$ of water from which the carbonate formed, with uncertainty estimated through the propagation of temperature and isotope uncertainties.

Sample	N	Δ_{47} [‰ ICDES]	TΔ_{47} [°C]	$\delta^{18}O_{cc}$ measured [‰ VPDB]	$\delta^{18}O_W$ [‰ VSMOW]
Candona candida	18 (1)	0.641 ± 0.011	10.2±3.2	−14.12±0.02	−18.6±0.7
Cytherissa lacustris	21 (1)	0.641±0.010	10.3±3.0	−14.31±0.02	−17.8±0.6
Pisidium casertanum	15 (2)	0.658±0.005	5.3±1.5	−14.65±0.02	−18.9±0.3

4.14   Paleoclimate modeling data

Using the PMIP lig127k model simulations (Otto-Bliesner et al., 2021; Kageyama et al., 2021, Table S10) together with the NOAA GlobTempV6 ERA5 data, we derived maps of climatological means of MTWA, MTCO, and MAP for the Bol'shoy Lyakhovsky and Oyogos Yar region according to the methodology described above. These maps cover the Laptev Sea to the west and north, the Eastern Siberian Sea to the east, and a small part of continental Siberia to the south and provide regional patterns of these climate variables in addition to values for the sample sites (Figure 9). Climate change signals for both the warmest and coldest months, as well as their ensemble spreads, are in agreement with the seasonal signals shown in Otto-Bliesner et al. (2021), where warmer than present winters occur over the Arctic Ocean, albeit with a high inter-model spread. Warmer than present summers are evident dominantly over the continents and less pronounced over the Arctic Ocean, associated with low inter-model spread. Note that due to the lack of a reference data set for pre-industrial precipitation, MAP values are PMIP lig127k ensemble means.

The MTCOs for the LIG derived from modeled anomalies are between –40 and –26 °C, with a distinct north-south gradient and colder temperatures over grid cells that include land (Figure 9). The modern MTCO is higher than modeled temperatures for the LIG with larger differences over the sea than over land. The model agreement is highest over grid cells on the continent distal to the coastline, lower over the ocean, and lowest along the coastline, which indicates that a significant fraction of the uncertainty is related to the different land-sea masks in the different models. This is reflected in the values calculated for the sample sites and the generic LandPoint (see Table 6), with the highest MTCO for Bol'shoy Lyakhovsky and lowest MTCO for the generic LandPoint in both the PMIP multi-model ensemble mean and ERA5, and a higher uncertainty for the sample points than for the generic LandPoint.

LIG MTWA estimates from the PMIP multi-model ensemble mean range from 0°C over the sea to 18°C over the south-western land area. Model temperatures are consistently higher than present-day temperatures from the ERA5 reanalysis. At the same time, the general spatial patterns are very similar (lowest temperatures over the northeastern sea corner of the plotted area, highest temperatures over the southwestern land area). The agreement

between the PaleoMIP models is higher than for the MTCO, with good agreement in all areas except the coastlines, again indicating that higher uncertainties are related to the different land-sea masks in the different models. MTWA values of the sample points and the generic LandPoint reflect the north-south gradient shown in the map (Figure 9), with the lowest MTWA values for Bol'shoy Lyakhovsky and the highest MTWA for the LandPoint. Both the LandPoint and Bol'shoy Lyakhovsky are located in grid cells that are considered land by most models, leading to an uncertainty only half as high as for Oyogos Yar, which is situated in a grid cell with varying land content.

MAP from the PMIP multi-model ensemble mean is between 250 and 450 mm, showing lower values over the sea and higher values over the continental land area. This general pattern is similar to that of the present-day reanalysis results, where precipitation is lower than those modeled for the LIG. The PMIP models show the highest agreement with each other over the sea and the lowest agreement over the continental grid cells.
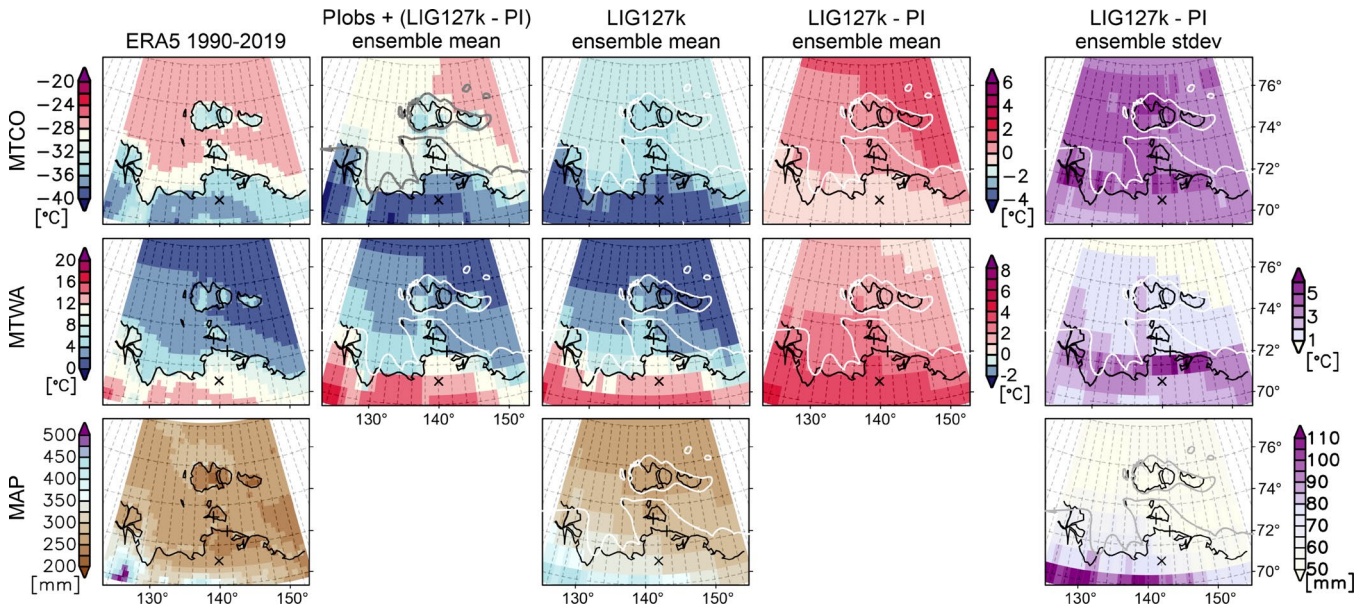
Figure 9. Climatological means of monthly mean temperature of the coldest (MTCO, top row) and the warmest month (MTWA, middle row) and of mean annual precipitation (MAP, bottom row) from the ERA5 reanalysis (left column), PaleoMIP multi-model anomaly added to observed PI values (PIobs+(lig127k-PI) for temperatures and PaleoMIP multi-model ensemble mean (lig127k ensemble mean) for precipitation, PaleoMIP ensemble mean anomaly with respect to modeled PI (lig127k-PI ensemble mean) and PMIP multi-model anomaly standard deviation (ensemble stdev). The plus signs denote the position of the sample sites, and the x signs denote the position of the generic LandPoint. Black lines mark today's coastlines, the white resp. gray lines mark the coastlines of the lig127 (after Alekseev et al., 1991b)

Table 6: Evaluation of MTWA and MTCO from the PIobs+(lig127k-PI) multi-model ensemble mean and MAP from the PMIP lig127k multi-model ensemble mean, uncertainty values are given as ± one standard deviation. Values in parentheses refer to the present-day reference from ERA5 (1990-2019).

Site	MTWA [°C]	MTCO [°C]	MAP [mm]
Bol'shoy Lyakhovsky Island	4.4±1.0 (2.7)	−31.1±1.4 (-32.7)	278±50 (262)
Oyogos Yar	4.5±1.2 (7.5)	−31.6±1.4 (-34.1)	285±55 (243)
LandPoint	13.6±0.9 (11.0)	−38.7±1.0 (−36.3)	328±70 (259)

5 Discussion

5.1 Cryolithology of LIG thermokarst deposits

The cryolithological parameters of the LIG deposits are shown in Figure 10, each in comparison to the stratigraphically younger Yedoma Ice Complex (mostly MIS 3) and Holocene (MIS 1) thermokarst deposits according to Schirrmeister et al. (2011b) and Wetterich et al. (2009) respectively.

The absolute ice contents of the LIG deposits are very similar for Bol'shoy Lyakhovsky Island and the Oyogos Yar coast and up to half as low as those of the Yedoma Ice Complex and Holocene deposits at both sites. Thus, the freezing and thawing processes and moisture content of LIG thermokarst lake sediments are similar but clearly different from those of the younger horizons. The MS for the LIG deposits is similar at both sites, showing comparably high contents of magnetic minerals. These contents are up to twice as high as those of the Yedoma Ice Complex and Holocene horizons. This could mean that the source material in the LIG was different.

The TOC contents show slight differences for both sites, with a mean of 2.4 wt% at Bol'shoy Lyakhovsky and 3.5 wt% at Oyogos Yar. In contrast, Yedoma Ice Complex and Holocene deposits show higher TOC values on Bol'shoy Lyakhovsky with 3.2 and 7.8 wt%, respectively, if compared to Oyogos Yar with 2.7 and 6.2 wt%, respectively. Different environmental conditions could play an important role and influence the preservation of organic matter. Regardless, the Holocene deposits contain two to three times higher wt% of organic matter. The TOC/TN ratio as an indicator for the source of/degree of decomposition of the organic matter in the LIG deposits is very similar on Bol'shoy Lyakhovsky and on Oyogos Yar. The values for the younger deposits are in a similar range (Figure 10), indicating a similar degree of decomposition of organic matter.

The mean carbonate content in LIG (2.3 wt%), Yedoma Ice Complex (0.5 wt%), and Holocene (1.6 wt%) deposits on Bol'shoy Lyakhovsky Island is much lower if compared to the respective horizons on Oyogos Yar with 6.4, 3.9, and 3.5 wt%, respectively. This reflects a higher share of shells of mussels, gastropods, and ostracods in the Oyogos Yar deposits. At each site, the Krest-Yuryakh deposits have the highest carbonate content.
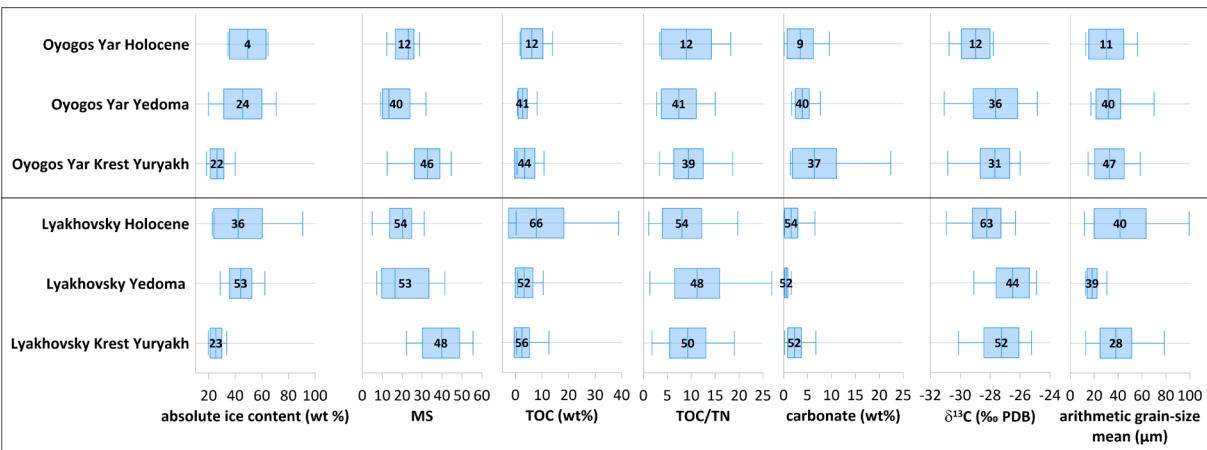
Figure 10. Boxplots of sediment data from both study sites, including the LIG (Krest-Yuryakh) horizon and the stratigraphic younger late Pleistocene Yedoma Ice Complex (mostly MIS 3) and Holocene thermokarst (MIS 1) horizons. The boxplots show the standard deviation, the arithmetic mean, and the IQR (interquartile range). The numbers correspond to the respective number of samples included (Schirrmeister et al., 2011a, 2011b; Wetterich et al., 2009).

The mean $\delta^{13}C$ values of TOC for the LIG deposits are almost identical, with –27.3‰ on Bol'shoy Lyakhovsky and –27.7‰ on Oyogos Yar. The respective values from Yedoma Ice Complex deposits are –26.5‰ and –27.6‰, and from Holocene thermokarst deposits are lower with –28.3‰ and –29.0‰. The relationship between TOC/TN and $\delta^{13}C$ indicates a mixture of organic matter derived from C3-type terrestrial plants and lacustrine algae. A large number of data points plot along the mixing line between both endmembers (Figure S6). The arithmetic mean grain size for the LIG deposits is 38.2 µm on Bol'shoy Lyakhovsky and 32.8 µm on Oyogos Yar. The Yedoma deposits of Bol'shoy Lyakhovsky have a much smaller mean grain size of 18.2 µm, while the Holocene deposits are coarser, with a mean of 41.6 µm (Figure 10). The younger Yedoma and Holocene deposits of Oyogos Yar have a similar arithmetic mean grain size as the LIG sediments with 31.7 and 30.0 µm. This shows that the deposition conditions in the thermokarst lakes were similar in both areas during the LIG. On Bol'shoy Lyakhovsky, the deposition conditions and/or the sources of material in the stratigraphically younger units have changed more than at Oyogos Yar.

5.2 Luminescence dating results of Last Interglacial deposits

Different geochronological results are available for determing the timescale of Arctic permafrost dynamic and corresponding feedbacks within periglacial landscapes and with climate changes. Of core importance are radiocarbon dating (e.g. Wetterich et al., 2014), tephrachronology (e.g. Froese et al., 2009), optically- and infrared-stimulated luminescence (OSL and IRSL; e.g., Murton et al., 2022), radioisotope disequilibria ($^{230}Th/^{234}U$) of frozen peat (e.g. Wetterich et al., 2016), uranium isotope ($^{234}U/^{238}U$) series (Ewing et al., 2015), and $^{36}Cl/Cl$ radionuclide ratios of ground ice (e.g. Blinov et al., 2009). However, dating methods ranging beyond radiocarbon maximum finite ages show specific challenges when applied to frozen material. Additionally, when fusing the dating results into one single multi-method chronology, a careful interpretation is required because individual methods use different components of permafrost deposits, including organic, mineral, or ice components. Uncertainties also arise from unknown influences of freezing and thawing dynamics on chemical and physical parameters, which are important to many age-determination techniques.

The chronostratigraphy of the LIG and its MIS 5 context relies on a few luminescence ages available from Bol'shoy Lyakhovsky Island and the Oyogos Yar coast. The stratigraphic position at studied sites still outlines challenges, especially from vertical discontinuities and hiatus. Currently, available age information of MIS 5-related deposits is summarized in Figure 11. Sediments, which are stratigraphically older than Krest Yuryakh, were found along the Laptev Strait coast as Buchchagy Ice Complex dated using $^{230}Th/U$ to MIS 5e - MIS 5b (126 +16/-13 ka to 89 ± 5 ka, Wetterich et al., 2019, Opel at al., 2017). The large variation of $^{230}Th/U$-ages impedes highly resolved, millennial paleo-climate interpretations.

Stadial conditions are recorded in floodplain sediments locally named the Kuchchugui stratum, which has been cryostratigraphically aligned with the MIS 6 (Tumskoy and Kuznetsova, 2022),- IRSL ages from Bol'shoy Lyakhovsky of 102±16 and 99±15 ka suggest the deposition of these sediments during MIS 5c, a period younger than the LIG. Nevertheless, corresponding deposits associated with the Kuchchugui stratum were dated by IRSL to slightly older ages (112.5 +9.6 -102.4±9.7 ka) at the mainland coast of Oyogos Yar (Opel et al., 2017). In this context, the newly IRSL-dated Krest Yuryakh thermokarst deposits provide, for the first time, robust age control for the LIG based on three consistent ages from two samples and two grain size fractions and with smaller

1 age uncertainties compared to previous luminescence dating results., with ages of 127.3±6.1, 117.8±6.8, and

2 117.6±6.0 ka (Table 1; Figure 11).

3   The observed luminescence properties confirm a reliable luminescence - dose correlation for successful

4 curve fitting and age modeling. The coefficients of variation below 6 % testify suitable measurement conditions

5 and reproducible signals. The low standard deviation below 6 % and corresponding low skewness below 0.8

6 document sufficient signal reset and call for the application of the central age model (CAM). The typical challenges

7 in dating permafrost samples related to sediment mixing are not indicated in our samples nor in the sampled

8 sediment section. The estimates of the paleo-water content were primarily based on the measured in-situ water

9 content. Although slight variations may have occurred over time, we assume that the sampled layers remained

10 frozen and hence, have kept the measured water content relatively constant. Nevertheless, uncertainties remain

11 due to the fact that the water was present not in its liquid but in its frozen form with potential effects on the

12 penetration depth of ionizing radiation. To account for the potential variations in the past plus uncertainties from

13 radiation field modeling based on water instead of ice, we included an overall water content uncertainty of 5 %.

14 Site-specific uncertainties may also arise from the unknown evolution (esp. with respect to timing) of the

15 overburden and its effects on the cosmogenic dose rate due to permafrost formation with sediment aggradation

16 and permafrost degradation with thaw subsidence. We evaluated the influence of an early reduction of overburden

17 thickness by comparing the full thickness of 35 m to 29 m, which would be more comparable to modern thickness

18 assumptions. As both overburden thicknesses are already strongly attenuating the incoming cosmic radiation, the

19 effect on ages is less than 1 %.
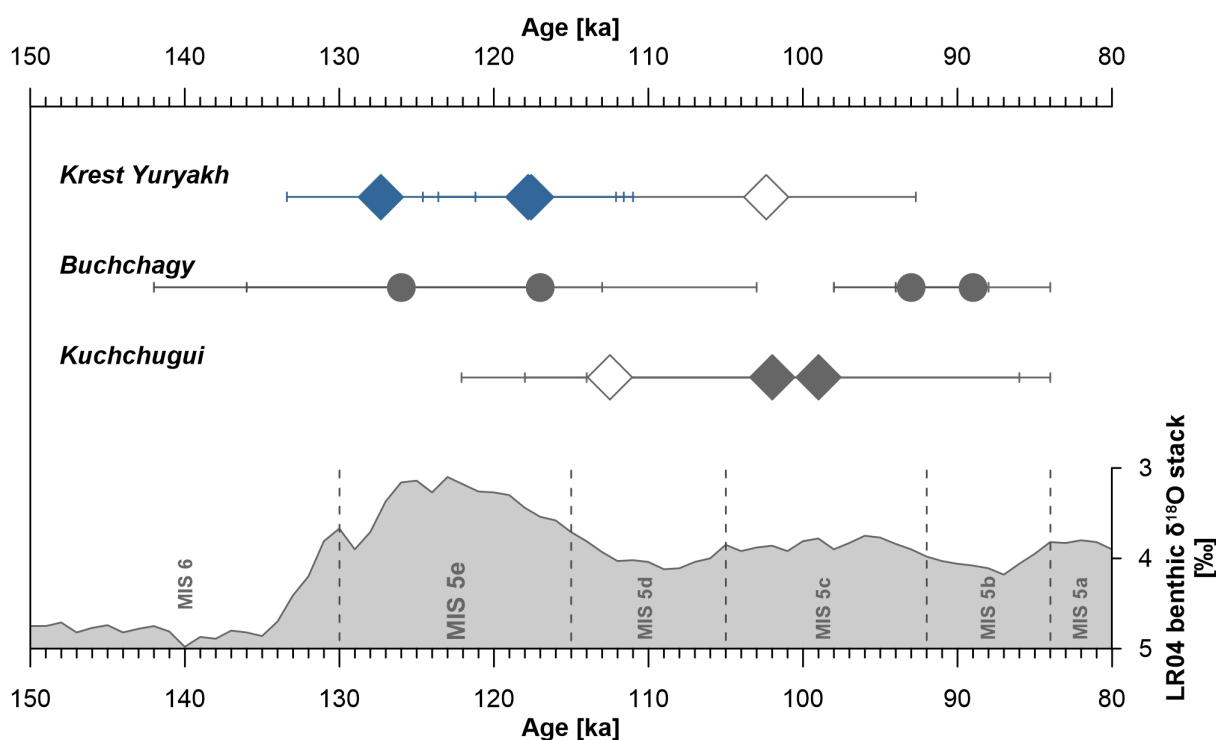
Figure 11. Age information obtained by IRSL (diamonds) and [230]Th/U dating (circles) of cryostratigraphic units exposed at both coasts of the Dmitry Laptev Strait and aligned with MIS 5. White symbols refer to samples from the Oyogos Yar mainland coast, and filled symbols to those from the southern coast of Bol'shoy Lyakhovsky Island – compared to the LR04 benthic stack (Lisiecki and Raymo, 2005). Age determinations of Krest-Yuryakh lake deposits are from this study (highlighted in blue; Bol'shoy Lyakhovsky) and Opel et al. (2017; Oyogos Yar), Buchchagy Ice Complex from Wetterich et al. (2016; Bol'shoy Lyakhovsky) and Kuchchugui floodplain deposits from Opel et al. (2017; Oyogos Yar) and Andreev et al. (2004; Bol'shoy Lyakhovsky).

5.3 Proxy-based quantitative paleoclimate reconstructions compared to PMIP model simulations

When we compare the proxy-based and modeled climate and environmental parameters, regional differences between Bol'shoy Lyakhovsky Island and the Oyogos Yar coast are obvious, as well as differences between different proxy reconstructions at the same site (Table 7). The general pattern, however, is that all proxy-based MTWA reconstructions indicate significantly warmer-than-today conditions.

For MTWA on Bol'shoy Lyakhovsky Island pollen, plant macrofossils, beetles, and chironomids overlap at 10.3-10.5 °C. The modeled temperatures (Plobs+(lig127k-PI)) are distinctly lower (Figure 12). BrGDGT-based AIR GST are lower (2.8±0.3 °C) but fit well with the MTWA estimates since they integrate the entire growing season of bacteria. At Oyogos Yar, the MTWA of pollen, beetles, and chironomids overlaps at 12-12.6 °C, while plant macrofossils indicate higher MTWA. The modeled temperatures for Oyogos Yar are again distinctly lower but are similar to those of Bol'shoy Lyakhovsky. The mean temperatures of the coldest month (MTCO) show joint overlaps between beetles and model data between –32.6 and –29.8 °C for Bol'shoy Lyakhovsky Island and –33.0 and –30.2 °C. For the mean annual precipitation (MAP), pollen and model data of PMIP concur between 228-327 mm for Bol'shoy Lyakhovsky Island (i.e., higher than at present, which is also implied by GDGTs) and 230-251 mm for Oyogos Yar. The WD of thermokarst lakes, which were reconstructed using chironomids, overlap between 1.7 and 3.3 m for both sites. The clumped-isotope-reconstructed water temperature of these lakes is 10.2±3.0 and 10.3±3.2 °C near the surface and 5.3 °C at the bottom.

The generic LandPoint data of PMIP overlap quite well for MTWA with most of the proxy data from Oyogos Yar, with chironomid data, and a bit with plant macrofossil data from Bol'shoy Lyakhovsky (Figure 12). For MTCO, a small overlap is visible with beetle data from Oyogos Yar. For MAP PaleoMIP reconstruction, the three points and pollen data from Bol'shoy Lyakhovsky overlap between 258 and 327 mm.

Part of the mismatch between model and proxy data can be reconciled by considering the potential seasonal bias of the proxy record and/or the uncertainties in the dating of the proxy records for the LIG thermal maximum (Pfeiffer and Lohmann, 2016). The differences among proxy reconstructions and between the two locations can have various causes. For example, pollen, plant macrofossils, beetles, and chironomids may have reached their detectable stage in the fossils at different times during the summer months. Thus, different conditions may have prevailed between early, peak, and late summer during MIS 5e. On the other hand, MIS 5e lasted about 9 ka between 125 and 116 ka (van Nieuwenhove et al., 2011). Unfortunately, the dating results available to us do not allow us to determine more precisely whether our records relate to early, middle, or late MIS 5e. Therefore, differences may also have stratigraphic and/or chronological causes.

Table 7: LIG proxy-based quantitative reconstructions and paleoclimate modeling results of Mean Air Temperature of the Warmest Months (MTWA), Mean Temperature of the Coldest Month (MTCO), Growing Season Temperature (Air GST, April to October), Mean Annual Precipitation (MAP), and Water Depth (WD) and Water Temperature (T$_{water}$) of thermokarst lakes on Bol'shoy Lyakhovsly Island and the Oyogos Yar mainland coast. Values in parentheses refer to the present-day reference from ERA5 (1990-2019) and the derived PIobs values from NOAA GlobTemp (1850-1900). n/a – not applicable. For model values, uncertainty values are given as ± one standard deviation. For proxy values, uncertainties are provided according to the methodology.

Climatic Information Source	MTWA [°C]	Air GST [°C]	MTCO [°C]	MAP [mm]	WD [m]	Open T$_{water}$ [°C]	Bottom T$_{water}$ [°C]
LandPoint							
(ERA5 reanalysis)	(11.0)		(−36.3)	(259)			
(PIobs)	(10.2)		(-37.9)				
PMIP Modeling				328±70			
PIobs+(lig127k-PI)	13.6±0.9		−38.7±1.0				
Bol'shoy Lyakhovsky Island							
(ERA5 reanalysis)	(2.7)		(−32.7)	(262)			
(PIobs)	(2.1)		(-31.2)				
PMIP Modeling				278±50			
PIobs+(lig127k-PI)	4.4±1.0		−31.1±1.4				
Air GST (GDGTs)		2.8 ± 0.3					
Chironomids	9.4 to 15.3				1.7 to 5.6		
Beetles	8.0 to 10.5		−34 to −26				
Plant macrofossils	10.3 to 12.9						
Pollen	9.0±3.0			271±56			
Oyogos Yar coast							
(ERA5 reanalysis)	(7.5)		(−34.1)	(243)			
(PIobs)	(1.9)		(-31.5)				
PMIP Modeling				285±55			
PIobs+(lig127k-PI)	4.5±1.2		−31.6±1.4				
Chironomids	12.0 to 13.8				1.1 to 3.3		
Beetles	8.0 to 14.0		−38.0 to −26.0				
Plant macrofossils	12.7 to 15.3						
Pollen	9.7±2.9			229±22			
Clumped isotopes (*Pisidium casertanum*)							5.3±1.5
Clumped isotopes (*Cytherissa lacustris*)						10.3±3.0	
Clumped isotopes (*Candona candida*)						10.2±3.2	

Present-day ERA5 data has a severe bias over sea ice, especially during periods with cold temperatures; temperatures are overestimated by up to 10°C when the air temperature is around –40°C (Wang et al., 2019, Batrak & Müller, 2019). The differences between the PaleoMIP model's land-sea mask and the actual coastline during the LIG, especially MAP and MTWA, might lead to underestimated MAP and MTWA. The MTWA for the generic LandPoint (13.6±0.9 °C, Table 6) is in the range of the reconstructed data sets between about 6 and 15 °C (Table 7). On the other hand, analog-based climate reconstruction methods applied to biotic proxies may overestimate temperatures in northern Siberia (Klemm et al., 2013). The sites are presently located at the lower temperature range of the training dataset, and as such, the taxa present in the observations are not covered with their full occurrence range, which typically results in biases toward higher temperature values.
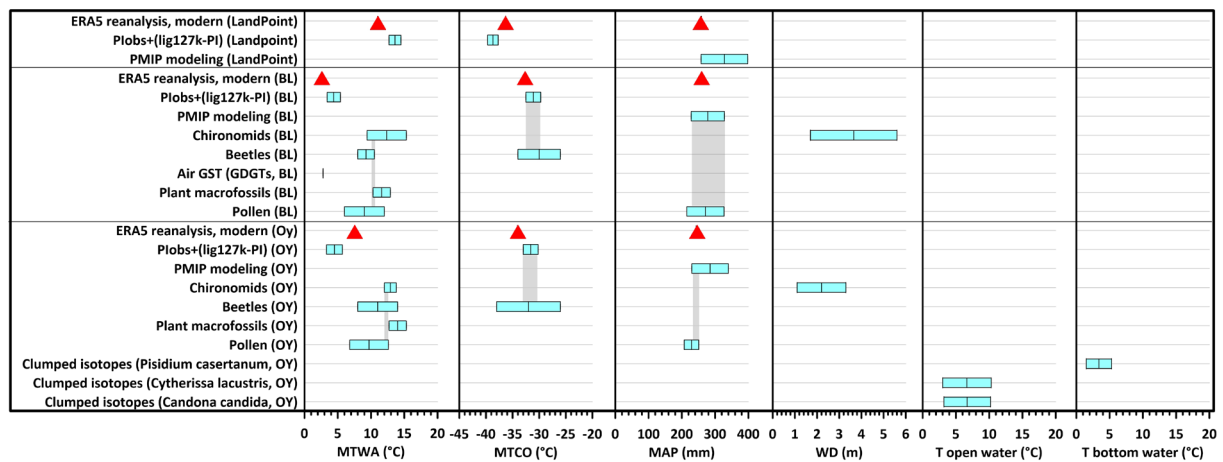
Figure 12. Boxplot of proxy-reconstructed and modeled climate and environmental data according to Table 7. BL – Bol'shoy Lyakhovsky, OY – Oyogos Yar, MTWA - mean temperature of the warmest month, MTCO – mean temperature of the coldest month, WD – water depth of thermokarst lakes, T open water – surface water temperature of lakes, T bottom water – bottom water temperature of lakes. Grey-shaded areas indicate ranges of overlap among paleoclimate indicators ; red triangles indicate the present-day reference.

5.4 Biogenic carbonate: Clumped and stable isotopes

All species analyzed (*Candona candida, Cytherissa lacustris, Pisidia casertanum*) require freshwater habitats and thus depend on the presence of open water bodies, which are present solely in summer in modern times. Thus, the derived temperatures are interpreted as reflecting the mean temperature of the warm season that integrates all ice-free periods, i.e., the growth window of ostracods and bivalves.

Ostracod-derived clumped isotope temperatures ($T\Delta_{47}$) are considerably warmer (10.2±3.2 and 10.3±3.0 °C) for *C. candida* and *Cy. lacustris*, respectively) than those of *P. casertanum* (+5.3±1.5 °C) (Table 5). This difference is attributed to differing habitation depths, with ostracods proliferating throughout the water column (Scharf, 1998; Decrouy et al., 2012), and therefore recording surface and upper water column temperatures, and *P. casertanum*, a benthic species that burrows continually into sediments (McMahon and Bogan, 2001) and thus records bottom water temperature. Monitoring data in a polygon pond at Oyogos Yar during August 2007 shows that mean air and surface water temperatures differed by only 0.3 °C, while bottom water at 0.6 m WD and only about 0.2 m above the permafrost table showed almost constant water temperature of 3.6 °C (Boike et al., 2008). Thus, we conclude that our reconstructed ostracod temperatures are likely similar to, or slightly below, warm

season mean surface air paleotemperature. Our summer surface $T\Delta_{47}$ reconstructions of ca. 10 °C are considerably warmer (ca. +2 °C) than modern and in good agreement with other air temperatures derived in this study.

Our measured *Cy. lacustris* $\delta^{18}O$ values show good agreement with those previously recorded from the LIG at Oyogos Yar in section Oy7-08 (−14.5 to −12.2 ‰, Wetterich et al., 2009). However, our *C. candida* values are ca. 2 to 3 ‰ more negative than those previously recorded in Oy7-08 (−12.6 to −11.3 ‰, Wetterich et al., 2009). Wetterich et al. (2008a) showed that offsets in $\delta^{18}O$ between single species in neighboring polygon ponds of 2 to 3 ‰ are common, and this likely could explain the discrepancies observed here.

Stable isotope compositions of ostracod calcite are driven by temperature and the isotopic composition of the surrounding precipitation waters, making them effective proxies for paleoenvironmental conditions (Xia et al., 1997; von Grafenstein et al., 1999). For comparison with our paleorecord, modern *C. candida* $\delta^{18}O$ has been measured at Samoylov Island (72.37 °N, 126.48 °E), in the Lena Delta, ranging between −17.7 and −10.4 ‰ (Wetterich et al., 2008a), the Moma region (NE Yakutia, 66 °N, 143 °E) where values between −15.2 and −11.9 ‰ were recorded, and in Central Yakutia (62 °N, 129 °E) with values between −11.0 and−8.9 ‰ (Wetterich et al., 2008b). The more continental location of the latter two records, compared to the Samoylov record, induces higher temperature amplitudes, warmer summers, and higher evaporation and is reflected in more enriched (less negative) modern carbonate $\delta^{18}O$. The similarity of Oya 5-1 data to Samoylov Island, compared with the more continental locations, suggests a precipitation and temperature regime closer to the former site in the modern day. Samoylov Island is at a similar latitude as Oyogos Yar but records mean July air temperatures between 4 to 8 °C, approximately 1 to 5 °C warmer due to its delta setting influenced by warm Lena River water (Boike et al., 2019).

Calculated $\delta^{18}O$ of carbonate precipitation waters between −18.5 and −16.6 ‰ are similar to modern summer rainfall values, which range from −20.2 to −11.7 ‰ (Opel et al., 2011). Small water bodies, such as those inhabited by ostracods, have been shown to be predominantly fed by precipitation in northern Siberia (Wetterich et al., 2008a). Thus, their $\delta^{18}O$ will largely reflect that of precipitation with a small shift towards more positive values (ca. +2 ‰), driven by evaporative processes (Wetterich et al., 2008b). The similarity of our reconstructed water $\delta^{18}O$ to modern precipitation would suggest a summer precipitation regime similar to the modern day.

5.5 Last Interglacial ecosystems

The paleobotanical and entomological data prove the presence of an open subarctic shrub tundra with restricted steppe areas in the area of Bol'shoy Lyakhovsky Island and the existence of an open forest tundra at Oyogos Yar during the LIG. The presence of the ant *Leptothorax acervorum* and the true bug *Sciocoris microphthalmos* in the Oyogos Yar records is notable as both species at present inhabit forested areas, while tundra-steppe indicators are rare and only represented by *Morychus viridis* and the meadow-steppe species *Protapalochrus arcticus* (former *Troglocollops arcticus*). True steppe insects are not present in Oyogos Yar, but two steppe weevils (*Stephanocleonus eruditu*s and *S. fossulatus*) were recorded in the Bol'shoy Lyakhovsky fauna. The presence of tall boreal shrubs and even trees during the LIG in an area that is covered with arctic tundra today is noteworthy. The only woody plants that are currently occurring at Oyogos Yar are the dwarf shrubs *Dryas octopetala* ssp. *punctata* and *Salix polaris*, the latter forming thin prostrate stems piercing through and protected by the moss cover. Ericaceae, Betulaceae, or other mainly boreal taxa do not occur in the study area today (Aleksandrova, 1980; Kienast et al., 2008) but were represented by many species during the LIG, e.g., *Betula pendula, B. divaricata, B. fruticosa, B. nana* s.l., *Arctostaphylos uva-ursi, Andromeda polifolia, Chamaedaphne calyculata, Rhododendron tomentosum,* and *Vaccinium vitis-idaea*. The majority of plant species recovered in LIG deposits

at both sides of the Dmitry Laptev Strait are extralimital, i.e., they do not occur in high arctic tundra today but considerably farther south. At Oyogos Yar, only ca. 80 km to the southeast of the Bol'shoy Lyakhovsky site, tree species like *Larix gmelinii, Betula pendula* s.l.*,* and *Alnus hirsuta* were already present during the LIG, indicating that the treeline was shifted about 270 km farther north than currently (Kienast et al., 2011). The nearest known modern occurrence of grey alder is located at the Sobolokh Mayan River, 910 km southwest of Oyogos Yar (Krasnoborov and Malyschev, 2003; GBIF, 2023).

Numerous coprophilous Sordariaceae fungi spores found in our LIG deposits point to the presence of grazing herds during this time. In West Beringia, forest-steppe-tundra provided grazing areas for large Pleistocene mammals so they could survive the Pleistocene interglaciations (Kuzmina, 2015b).

Plant-derived *sed*aDNA shows substantial overlap with the plant macrofossil record in recovering taxa that do not occur at Bol'shoy Lyakhovsky today, including *Betula*, several Ericaceae species, and *Potamogeton*. The taxonomic composition in profile L14-04 from Bol'shoy Lyakhovsky Island indicates that the interglacial vegetation was likely a mosaic of subarctic shrub-tundra and dry steppe communities with arctic-alpine and pioneer plants. The record shows many similarities in the sedaDNA plant record with the MIS 5e record from the Batagay megaslump (Courtin et al., 2022).

A major discrepancy to prior studies but also a highlight of our record is the detection of *Larix*, *Picea*, and *Populus* in the interglacial strata, suggesting that the treeline reached indeed as far north as Bol'shoy Lyakhovsky Island (73.3 °N). This is in line with MIS 5e pollen spectra at Lake Elgygytgyn (Lozhkin and Anderson, 2013) that indicate the extensive presence of forest in northern areas of the Russian Far East and the likely establishment of deciduous forest in the Chukchi Uplands. Similar MIS 5e pollen spectra are also known from the Yana Lowland, the Lower Indigirka Basin, and the Kolyma Lowland. (Lozkin and Anderson 1995).

Larix-DNA was detected in several samples, all of which showed at least 2 % *Larix* in the pollen assemblage (Zimmermann et al., 2017). The pollen records of *Larix* are usually underrepresented because pollen is produced in low quantities, and due to a high fall speed, the potential for long-distance dispersal is low (Sjögren et al., 2008; Jørgensen et al., 2012; Niemeyer et al., 2015). Hence, single pollen grains have been accepted as evidence for the local presence of *Larix* (Edwards et al., 2005). We verified the presence of *Larix*-DNA by re-amplification and re-sequencing with *Larix*-specific primer pairs, corroborating the authenticity of even low *Larix* sequence counts in the metabarcoding record. Beetle remains and plant macrofossils derived from profile R35, about a kilometer away from this site, indicate subarctic shrub tundra and the absence of trees at Bol'shoy Lyakhovsky Island. Hence, we conclude that *Larix* was heterogeneously distributed in the landscape of Bol'shoy Lyakhovsky Island, likely as individual trees or stands of trees within an open forest tundra, where trees were growing in more protected sites with a favorable microclimate. Evidence of the presence of *Larix* trees as far north as Kotelny Island during MIS 3 (van Geel et al., 2017) substantiates our assumptions.

In our LIG *sed*aDNA record, *Larix* was mostly accompanied by evergreen *Picea* and deciduous, broadleaved *Populus*, yet the absence of macrofossil and pollen evidence requires a critical evaluation. The genetic marker used in this study is located on the chloroplast genome, which in the genus *Picea* is inherited paternally via pollen (Sutton et al., 1991). As such, *Picea* pollen, susceptible to long-distance transport, could be a source of DNA in our record. Indeed, samples in which *Picea*-DNA was detected contained relatively high amounts of *Picea* pollen grains. However, not all samples in which pollen proportions were relatively high also contained *Picea*-DNA, rendering this explanation uncertain as well. Moreover, previous work implies that pollen likely be not the source of *Picea sed*aDNA (Sjögren et al., 2017; Niemeyer et al., 2017; Parducci et al., 2017) because the pollen

exine is very durable, making the pollen resistant to degradation but at the same time prevent the release of DNA during our gentle DNA extraction procedure. Moreover, the relatively low biomass contribution of pollen, combined with its limited endogenous chloroplast DNA content, likely results in the dilution or loss of any *sed*aDNA signal derived from pollen (Alsos et al., 2024). A similar discussion about the authenticity of *Picea abies* in a *sed*aDNA record from the Ural Mountains was led by Clarke et al. (2020), where findings of stomata were considered strong evidence for local occurrence. One of our samples indeed contained *Picea* cf. stomata, but identifying the species-specific source of stomata was difficult, and they cannot be considered as strong evidence. In contrast to *Picea*, the chloroplast genome of *Populus* is maternally inherited, and therefore, long-distance transported pollen as a source of *Populus*-DNA can be excluded (Rajora and Dancik, 1992). Today, *Populus suaveolens* populations occur relatively far north, with the northernmost documented individual in the Lena Delta (73.2 °N, 128.6 °E; Seregin, 2023). As modern woody taxa penetrate the subarctic tundra belt along rivers (Aleksandrova, 1980), it is possible that during the LIG, *P. suaveolens* could have progressed into our study area at riversides and floodplains. The map "Late Pleistocene (Riss-Würm), 120 000 Years" of Alekseev et al. (1991b) shows river valleys and temporary lakes on Bol'shoy Lyakhovsky Island and around Svyatoy Nos. In addition, most of the area is labeled as relict alluvial and lacustrine plains.

Unless macrofossil evidence confirms the presence of *Picea* or *Populus* in the area, the question of whether these taxa were truly part of the interglacial vegetation cannot be answered fully. However, given that (1) absence of evidence is not evidence of absence, (2) *Populus* has been detected more often in the DNA than in the macrofossil record (Kjær et al., 2022) or the surrounding vegetation (Alsos et al., 2018), (3) the findings of extralimital species in interglacial strata (Kienast et al., 2008), and (4) the uncertainty about alternative DNA sources, the possibility remains that *Picea* and *Populus* were growing that far north during the LIG.

Aquatic macrophytes such as *Potamogeton perfoliatus*, *Stuckenia filiformis*, *S. vaginata*, *Callitriche hermaphroditica*, and *Batrachium* sp. were abundant during the LIG but are completely absent today. These findings are another indication of warmer than present-day conditions (Kienast et al., 2008, 2011; Stoof-Leichsenring et al., 2022). The aquatic freshwater LIG habitats are further characterized by fossil chironomid, cladocera, ostracod, and mollusk communities. The presence of semi-terrestrial chironomid taxa at high abundances and low abundances of cold-stenotherm taxa can indicate a transition from the preceding colder MIS 6 conditions to a warmer MIS 5e setting and probably correspond to the lower part of the R35 section on Bol'shoy Lyakhovsky Island (Ilyashuk et al., 2006). Here, the subdominant taxa *Chironomus anthracinus*-type, *Cricotopus laricomalis*-type, *Tanytarsus pallidicornis*-type, and *Endochoronomus albipennis*-type prefer relatively warm and productive lakes (Nazarova et al., 2015, 2023), while *Tanytarsus lugens*-type and *Parakiefferiella triquetra*-type taxa are in contrast cold stenotherm and characteristic for oligotrophic cold subarctic lakes. *Limnophyes, Metriocnemus eurynotus*-type, and *Parametriocnemus- Paraphaenocladius* are typical for lake-level fluctuations (Massaferro and Brooks, 2002). *Smittia* might indicate shore erosion processes or unstable lake-level conditions (Brooks et al., 2008). The Oya 5-1 chironomid record from Oyogos Yar does not resolve lake development as R35 from Bol'shoy Lyakhovsky Island but instead aggregates different lake stages into one paleo-assemblage. The Oya5-1 cladoceran assemblages indicate habitats with a well-developed vegetated shallow littoral zone as well as pelagic open-water zones in the paleo-lake. The reconstructed WDs from chironomid data of 1.7±0.9 m to 5.6±1.0 m for Bol'shoy Lyakhovsky and 2.2±1.1 m for Oyogos Yar are within the range of measurements of modern thermokarst lakes of 1 to 6 m depth (e.g., Morgenstern et al., 2013, Kallistova e a., 2019; Wilcox et al., 2022 and references therein).

The LIG ostracod assemblages are characterized by species that tolerate considerable changes in temperature and salinity regimes that are comparable to modern conditions in the periglacial landscapes of East Siberia, where species such as *Candona candida*, *Fabaeformiscandona rawsoni*, and *Limnocytherina sanctipatricii* occur (Wetterich et al., 2008a, 2008b). Single findings of the thermophilous species *Cyclocypris ovum* – not present in modern environments of North Yakutia – indicate summer conditions distinctly warmer than today (Kienast et al., 2011). The presence of benthic ostracods in lacustrine LIG deposits further indicates a sufficiently high oxygen content in the water column of the host waters. Furthermore, the waters must have been ice-free for a certain period during summer to facilitate the ostracod larvae development. As ostracods in high latitudes are apparently adapted to a relatively short ice-free period, they conduct asexual reproduction (parthenogenesis), which explains relatively high shares of adult females and only rare males in the fossil assemblages (Meisch, 2000). The high number of juvenile shells indicates short summers in which the development of ostracods did not always reach its final stage. The often-complete preservation of the fragile ostracod shells points to stillwater habitats and deposition, as well as *in-situ* preservation. The shallow sublittoral zone of thermokarst lakes and ice-wedge casts formed by melting wedge ice are the most probable habitats for the fossil ostracod assemblage (Wetterich et al., 2009; Kienast et al., 2011).

The discrepancy in the species inventories of the last and the current interglacials is certainly the result of climatic differences, i.e., the recent phase – the late Holocene – is comparatively cold in comparison to earlier warm stages in Northern Siberia. This is even true for the MIS 3 Interstadial when larch trees existed as far north as Kotel'ny Island (van Geel et al., 2017). Larch and other woody plants probably spread northward during the LIG when Kotel'ny Island was still part of the mainland. The connection of the New Siberian Archipelago with the mainland during the LIG can be deduced from the highly continental climate character existing adjacent to today's Dmitry Laptev Strait. The persistence of this potential feeding base for herbivores during preceding warm stages helps explain why large cold-adapted grazers survived earlier interglacials in Beringian refugia, which became centers of their dispersal during subsequent cold stages.

6   Conclusions

New IRSL ages confirm the LIG (MIS 5e) origin of the Krest Yuryakh ice-wedge pseudomorphs and lake sediments that are exposed at both coasts of the Dmitry Laptev Strait. The present study results are consistent with previous work interpreting the MIS 5e as a key warm period during which extensive permafrost thawing and thermokarst development occurred in north-eastern Siberia. The cryolithological features observed in the LIG deposits bear striking similarities to those of Lateglacial and early Holocene refrozen thermokarst deposits, suggesting comparable processes of deposition that were characterized by ground ice melting, surface subsidence, and thermokarst formation driven by climate warming.

Paleoclimate data synthesized from a variety of proxies – including plant macrofossils, aquatic and terrestrial invertebrates, and lipid biomarkers – indicate that temperatures during the LIG were significantly warmer than today. Mean temperatures of the warmest month (MTWA) reconstructed from proxies show a range of 6.0 °C (pollen data of Bol'shoy Lyakhovsky) and 15.3 °C (plant macrofossils of Bol'shoy Lyakhovsky and chironomid of Oyogos Yar) and overlap of 10.3 °C and 10.7 °C for Bolshoy Lyakhovsky) and 12.0 and 12.6 °C for Oyogos Yar, demonstrating the pronounced warming of this period.

According to ERA5 (1990-2019) simulations, the present-day MTWA of Bol'shoy Lyakhovsky Island and the Oyogos Yar coast is 2.7 and 7.5 °C, respectively, and the MTCO is -32.7 and -34.1 °C. The PIobs+(lig127k-PI) MTWA for Bol'shoy Lyakhovsky and Oyogos Yar are very close to each other (4.4±1.0 and 4.5±1.2 °C). Also, the MTCO with –31.1±1.4 and –31.6±1.4 °C, respectively. This suggests summers warmer than today by 5.5 to 12.8°C for Bol'shoy Lyakhovsky Island and by 0.2 to 7.5 °C for Oyogos Yar coast, and winters warmer than today by up to 7.1 °C and 8.4 °C, respectively.

However, one of the critical challenges in predicting future ecosystem responses lies in the fact that the land-ocean distribution during the LIG was markedly different from today, affecting the degree of continentality, which played a major role in modulating climate and ecosystem dynamics.

Paleoclimate models generally agree well with the mean temperature of the coldest month (MTCO) proxy data but consistently underestimate the mean temperature of the warmest month (MTWA) across proxy records when using modern land-sea configurations. This mismatch is significantly reduced when models incorporate land-sea distributions that more closely reflect those of the LIG. This adjustment highlights the importance of considering past land-sea configurations in regional paleoclimate modeling when comparing proxy and model results, a critical step in refining our understanding of Arctic climate dynamics during MIS 5e.

The strong ecosystem response to the LIG warming, reflected in the high diversity of proxies, shows the sensitivity of permafrost regions to rising temperatures. In particular, the development of thermokarst landscapes created a mosaic of terrestrial, wetland, and aquatic habitats, fostering an increase in biodiversity. This biodiversity is evident in the wide variety of terrestrial insects, vegetation, and aquatic invertebrates preserved in these deposits. In addition, the treeline extended 270 km further north during the LIG than it does today, yet the cold-adapted mammoth fauna managed to persist in this region, probably finding refuge in the microclimates created by the thermokarst landscape. The LIG treeline shift is a transregional record that affected both Northeastern Siberia and the Chukchi Peninsula, as well as the Far East.

While the LIG is often used as an analog for future climate warming in the Arctic, there are important differences. Most notably, the LIG warming was driven primarily by increased summer insolation. In contrast, current Arctic warming so far is most pronounced in winter due to anthropogenic forcing and climate system feedback mechanisms. This seasonal distinction is crucial because many of the environmental changes relevant today, particularly those related to ecosystem processes and permafrost dynamics, occur during the transitional seasons (spring and fall) - for which we currently lack proxy data from MIS 5e.

Ultimately, our results highlight the complexity of Arctic climate responses and emphasize the sensitivity to seasonal factors, which are important aspects of future climate scenarios. Nevertheless, the lessons learned from MIS 5e, particularly regarding thermokarst development and ecosystem adaptation to warming, provide valuable insights into the potential future trajectory of permafrost regions in the context of ongoing climate change. Further research is essential, particularly to fill gaps in proxy data for transitional seasons and to refine model-proxy comparisons to improve our predictions of Arctic climate dynamics.

7   Appendices

Table A1: Overview of sample collections for cryolithological and fossil proxy studies of Krest Yuryakh deposits exposed at both coasts of the Dmitry Laptev Strait.

8   Code availability

not applicable

9   Data availability

Andreev, A.A., Grosse, G., Schirrmeister, L., Kuznetsova, T.V., Kuzmina, S.A., Bobrov, A.A., Tarasov, P.E., Novenko, E.Y., Meyer, H., Derevyagin, A.Yu., Kienast, F., Bryantseva, A., Kunitsky, V.V. (2010): Pollen records from Bol'shoy Lyakhovsky Island, Siberia. PANGAEA, https://doi.org/10.1594/PANGAEA.736069,

Andreev, A.A., Grosse, G., Schirrmeister, L., Kuznetsova, T.V., Kuzmina, S.A., Bobrov, A.A., Tarasov, P.E., Novenko, E.Y., Meyer, H., Derevyagin, A.Yu., Kienast, F., Bryantseva, A.,Kunitsky, V.V. (2010): Pollen record of profile L11. PANGAEA, https://doi.org/10.1594/PANGAEA.736068,

Kienast, F., Schirrmeister, L. (2017): Plant macrofossil records from permafrost deposits of the Bol'shoy Lyakhovsky Island (New Siberian Archipelago). PANGAEA, https://doi.org/10.1594/PANGAEA.882619

Kusch, S. (2021): GDGT data in Siberian permafrost deposits. PANGAEA, https://doi.org/10.1594/PANGAEA.934054

Schirrmeister, L., Grosse, G., Kunitsky, V.V., Siegert, C. (2017): Sedimentological, biogeochemical and geochronological data from permafrost exposures of the Bol'shoy Lyakhovsky Island (Expedition 1999), site R23+40. PANGAEA, https://doi.org/10.1594/PANGAEA.880949

Schirrmeister, L., Grosse, G., Kunitsky, V.V., Siegert, C. (2017): Sedimentological, biogeochemical and geochronological data from permafrost exposures of the Bol'shoy Lyakhovsky Island (Expedition 1999), site L14. PANGAEA, https://doi.org/10.1594/PANGAEA.880937

Schirrmeister, L., Grosse, G., Kunitsky, V.V., Siegert, C. (2017): Sedimentological, biogeochemical and geochronological data from permafrost exposures of the Bol'shoy Lyakhovsky Island (Expedition 1999), site R22+60. PANGAEA, https://doi.org/10.1594/PANGAEA.880948

Schirrmeister, L., Grosse, G., Kunitsky, V.V., Siegert, C. (2017): Sedimentological, biogeochemical and geochronological data from permafrost exposures of the Bol'shoy Lyakhovsky Island (Expedition 1999), site L11+40. PANGAEA, https://doi.org/10.1594/PANGAEA.880935

Schirrmeister, L., Grosse, G., Kunitsky, V.V., Siegert, C. (2017): Sedimentological, biogeochemical and geochronological data from permafrost exposures of the Bol'shoy Lyakhovsky Island (Expedition 1999), site L13+80. PANGAEA, https://doi.org/10.1594/PANGAEA.880936

Schirrmeister, L. (2009): Lithology, color and structural description of sediment profile L7-11, Appendix 6.1. PANGAEA, https://doi.org/10.1594/PANGAEA.727667

Schirrmeister, L. (2009): Documentation of ice wedge L7-11. PANGAEA, https://doi.org/10.1594/PANGAEA.727710

Schirrmeister, L. (2009): Lithology, color and structural description of sediment profile L7-16, Appendix 6.1. PANGAEA, https://doi.org/10.1594/PANGAEA.727671

Schirrmeister, L. (2009): Documentation of ice wedge L7-16. PANGAEA, https://doi.org/10.1594/PANGAEA.727714

Schirrmeister, L. (2009): Lithology, color and structural description of sediment profile L7-14, Appendix 6.1. PANGAEA, https://doi.org/10.1594/PANGAEA.727669

Schirrmeister, L. (2009): Documentation of ice wedge L7-14. PANGAEA, https://doi.org/10.1594/PANGAEA.727712

Schirrmeister, L. (2009): Lithology, color and structural description of sediment profile L7-08, Appendix 6.1. PANGAEA, https://doi.org/10.1594/PANGAEA.727666

Schirrmeister, L. (2009): Documentation of ice wedge Oy7-01. PANGAEA, https://doi.org/10.1594/PANGAEA.727717

Schirrmeister, L. (2009): Lithology, color and structural description of sediment profile Oy7-01, Appendix 6.1. PANGAEA, https://doi.org/10.1594/PANGAEA.727673

Schirrmeister, L. (2009): Documentation of ice wedge Oy7-07. PANGAEA, https://doi.org/10.1594/PANGAEA.727725

Schirrmeister, L. (2009): Lithology, color and structural description of sediment profile Oy7-07, Appendix 6.1. PANGAEA, https://doi.org/10.1594/PANGAEA.727676

Schirrmeister, L. (2009): Documentation of ice wedge Oy7-08. PANGAEA, https://doi.org/10.1594/PANGAEA.727734

Schirrmeister, L. (2009): Lithology, color and structural description of sediment profile Oy7-08-A/B, Appendix 6.1. PANGAEA, https://doi.org/10.1594/PANGAEA.727677

Strauss, J., Laboor, S, Schirrmeister, L., Grosse, G., Fortier, D., Hugelius, G., Knoblauch, C., Romanovsky, V.E., Schädel, C., Schneider von Deimling, T., Schuur, E.A.G., Shmelev, D., Ulrich, M., Veremeeva, A., (2020): Geochemical, lithological, and geochronological characteristics of sediment samples from thermokarst deposits in Siberia and Alaska 1998-2016. PANGAEA, https://doi.org/10.1594/PANGAEA.919062,

Schwamborn, G., Wetterich, S. (2016): Geochemistry and physical properties of permafrost core L14-04. PANGAEA, https://doi.org/10.1594/PANGAEA.868983

Schwamborn, G., Wetterich, S. (2016): Characteristics of samples obtained during the expedition to Bol'shoy Lyakhovsky Island in July/August 2014. PANGAEA, https://doi.org/10.1594/PANGAEA.859265

Schwamborn, G., Wetterich, S. (2016): Sample list and field descriptions of the L14 profiles studied in summer 2014. PANGAEA, https://doi.org/10.1594/PANGAEA.859305

Zimmermann, H.H., Raschke, E., Epp, L.S., Stoof-Leichsenring, K.R., Schirrmeister, L., Schwamborn, G., Herzschuh, U. (2017): Pollen profile of sediment hand-pieces L14-04B. PANGAEA, https://doi.org/10.1594/PANGAEA.878885,

Zimmermann, H.H., Raschke, E., Epp, L.S., Stoof-Leichsenring, K.R., Schirrmeister, L., Schwamborn, G., Herzschuh, U. (2017): Pollen profile of sediment hand-pieces L14-04C. PANGAEA, https://doi.org/10.1594/PANGAEA.878886,

Zimmermann, H.H., Raschke, E., Epp, L.S., Stoof-Leichsenring, K.R., Schirrmeister, L., Schwamborn, G., Herzschuh, U. (2017): Pollen profile of sediment core L14-04. PANGAEA, https://doi.org/10.1594/PANGAEA.878884,

Clumped isotope samples and normalization data will be uploaded to the EarthChem Library pending publication of this manuscript.

10   Executable research compendium (ERC)

not applicable

11   Sample availability

Original samples are available on request in the sample archives of the AWI Research Unit Potsdam.

12. Video supplement

not applicable

13   Supplement link

Supplement material_Figures

14   Team list

not applicable

15   Author contribution

LS designed the paper concept, compiled the various results, carried out the cryolithological studies and evaluations, organized the writing process, and wrote the first manuscript draft. LS, TO, FK, TK, SK, VT, GG, VK, HaMe, GS, SB, SW, and MCF participated in one or more of the five expeditions to Bol'shoy Lyakhovsky Island and the Oyogos Yar mainland coast between 1999 and 2014. MCF conducted the geochronological studies. HaMe was responsible for isotope chemistry studies. A number of co-authors were responsible for certain paleoproxies and environmental reconstructions based on them: AA - pollen, FK - plant macrofossils, mussels, AS - ostracods, plant macrofossils, LN - chironomids, LF - cladocerans, SK - insects, TK - mammals, UH, TB - pollen-based climate reconstructions, HHZ - *sed*aDNA, SB, SU, SM - clumped isotope analysis, SK - lipid biomarkers, SW - ostracods. AP contributed with data on marine MIS 5e deposits. HeMa and GL carried out paleoclimate modeling. All authors were involved in the data interpretation, took part in the scientific discussions, and helped with writing and editing the manuscript.

16   Competing interests

The authors declare that they have no conflict of interest.

19   Acknowledgements

We acknowledge funding from the following projects: BMBF project SYSTEM LAPTEV SEA 2000 (03G0134), INTAS project "Permafrost Dating" (INTAS 8133), IPY project 15 Past Permafrost "From the beginning of the Pliocene cooling to the modern warming – Past Periglacial Records in Arctic Siberia", DFG project "Late Quaternary warm stages in the Arctic" (SCHI 975/1-1), RFFI project № 06-05-64197, BMBF project CARBOPERM "Carbon in permafrost: formation, transformation, and release" (03 G 0836), Leverhulme Trust (Research Project Grant RPG-2020-334 for project "IsoPerm"). We would also like to thank the three reviewers and the editor of Climate of the Past for their very helpful and constructive comments and suggestions.

Labs and field parties

We want to thank all colleagues involved with sample processing in the various laboratories. We would also like to thank many AWI colleagues and local partners in Tiksi for their excellent and long-standing logistical support for fieldwork at these remote study sites. This includes the expeditions to Bol'shoy Lyakhovsky Island in the summer of 1999, 2007, and in the spring and summer of 2014, as well as the ship tour to the New Siberian Islands in the summer of 2002 and the expedition to the Oyogos Yar coast in the summer of 2007.

20 References Alekseev, M.N., Arkhangelov, A.A., Oolubeva, L.V., and Sulerzhitsky, L.D.: Paleoecological correlation of the Quaternary events on the shelf and intracontinental areas of Eastern Siberia Geological - Paleoecological situations for the Quaternary for the XIII Congress of INQUA, China, 1991 (in Russian), 1991a.

Alekseev, M.N., Arkhangelov, A.A., Ivanova, N.M., Paty-kara, N.G., Plakht, I.V., Sekretov, S.B., and Shkarubo, S.I.: Laptev Sea and East-Sibirian Cenozoic - Atlas of paleogeographic map of Eurasian shelf during the Mesozoic and Cenozoic. Volume 1 Moscow, Inst. of Geology, Russian Academy of Science: 1-20 (In Russian), 1991b.

Alekseev, M.N., and Drushchits, V.A.: Climatic events of the Kazantsevo Interglacial and Holocene of the Eastern part of the Russian shelf and Siberia, Bulletin of the Quaternary Commission, 64, 78–88 (in Russian), 2001.

Aleksandrova, V.D.: The Arctic and Antarctic, their division into geobotanical areas. Cambridge University Press, pp 247, 1980.

Alfimov, A.V., Berman, D.I., and Sher, A.V.: Tundra-steppe insect assemblages and reconstruction of Late Pleistocene climate in the lower reaches of the Kolyma River, Zoologicheskiy Zhurnal, 82(2), 281–300 (in Russian), 2003.

Allen, M.R., Dube, O.P., Solecki, W., Aragón-Durand, F., Cramer, W., Humphreys, S., Kainuma, M., Kala, J., Mahowald, N., Mulugetta, Y., Perez, R., Wairiu, M., and Zickfeld, K.: Framing and Context. In: Global Warming of 1.5°C. An IPCC Special Report on the impacts of global warming of 1.5°C above pre-industrial levels and related global greenhouse gas emission pathways, in the context of strengthening the global response to the threat of climate change, sustainable development, and efforts to eradicate poverty [Masson-Delmotte, V., Zhai, P., Pörtner, H.-O., Roberts, D., Skea, J., Shukla, P.R., Pirani, A., Moufouma-Okia, W., Péan, C., Pidcock, R., Connors, S., Matthews, J.B.R., Chen, Y., Zhou, X., Gomis, M.I., Lonnoy, E., Maycock, T., Tignor, M., and Waterfield, T. (eds.)]. Cambridge University Press, Cambridge, UK and New York, NY, USA, 49-92, https://doi.org/10.1017/9781009157940.003, 2018.

Alsos, I.G., Lammers, Y., Yoccoz, N.G., Jørgensen, T., Sjögren, P., Gielly, L., and Edwards, M.E.: Plant DNA metabarcoding of lake sediments: How does it represent the contemporary vegetation, PLOS One, 13(4), e0195403, https://doi.org/10.1371/journal.pone.0195403, 2018.

Alsos IG, Boussange V, Rijal DP, Beaulieu M, Brown AG, Herzschuh U, Svenning J-C, Pellissier L.: Using ancient sedimentary DNA to forecast ecosystem trajectories under climate change. Phil. Trans. R. Soc. B 379: 20230017. https://doi.org/10.1098/rstb.2023.0017, 2024.

Anderson, N.T., Kelson, J.R., Kele, S., Daëron, M., Bonifacie, M., Horita, J., Mackey, T.J., John, C.M., Kluge, T., Petschnig, P., Jost, A B., Huntington, K.W., Bernasconi, S.M., and Bergmann, K.D.: A Unified Clumped Isotope Thermometer Calibration (0.5–1,100°C) Using Carbonate-Based Standardization, Geophysical Research Letters, 48(7). https://doi.org/10.1029/2020GL092069, 2021.

Andreev, A.A., Schirrmeister, L., Tarasov, P.E., Ganopolski, A., Brovkin, V., Siegert, C., and Hubberten, H.-W.: Vegetation and climate history in the Laptev Sea region (arctic Siberia) during Late Quaternary inferred from pollen records, Quaternary Science Reviews. 30, 2182–2199 https://doi.org/10.1016/j.quascirev.2010.12.026, 2011.

Andreev, A., Grosse, G., Schirrmeister, L., Kuznetsova, T. V., Kuzmina, S. A., Bobrov, A. A., Tarasov, P. E., Novenko, E. Yu., Meyer, H., Derevyagin, A. Yu., Kienast, F., Bryantseva, A., and Kunitsky, V. V.: Weichselian

and Holocene palaeoenvironmental history of the Bol'shoy Lyakhovsky Island, New Siberian Archipelago, Arctic Siberia., Boreas 38(1), 72–110., https://doi.org/10.1111/j.1502-3885.2008.00039.x, 2009.

Andreev, A.A., Grosse, G., Schirrmeister, L., Kuzmina, S. A., Novenko, E.Yu., Bobrov, A.A., Tarasov, P.E., Kuznetsova, T.V., Krbetschek, M., Meyer, H., and Kunitsky, V.V.: Late Saalian and Eemian palaeoenvironmental history of the Bol'shoy Lyakhovsky Island (Laptev Sea region, Arctic Siberia), Boreas, 33(4), 319–348. https://doi.org/10.1111/j.1502-3885.2004.tb01244.x, 2004.

Ashastina, K., Schirrmeister, L., Fuchs, M., and Kienast, F.: Palaeoclimate characteristics in interior Siberia of MIS 6–2: first insights from the Batagay permafrost mega-thaw slump in the Yana Highlands, Clim. Past, 13, 795–818, https://doi.org/10.5194/cp-13-795-2017, 2017.

Artemov, I., and Egorova, A.: Locations of plants on dot distribution maps in the Flora of Siberia (Flora Sibiraea, 1987–1997). Version 1.2. Central Siberian Botanical Garden SB RAS, Occurrence dataset https://doi.org/10.15468/jb84wg accessed via GBIF.org on 2023-04-21, 2021.

Atkinson, T.C., Briffa, K.R., and Coope, G.R.: Seasonal temperature in Britain during the past 22 000 years, reconstructed using beetle remains, Nature, 325, 587–592. https://doi.org/10.1038/325587a0, 1987.

Batrak, Y. and Müller, M.: On the warm bias in atmospheric reanalyses induced by the missing snow over Arctic sea-ice. Nat Commun 10, 4170, https://doi.org/10.1038/s41467-019-11975-3, 2019.

Berman, D., Alfimov, A., Kuzmina, S.: Invertebrates of the relict steppe ecosystems of Beringia, and the reconstruction of Pleistocene landscapes, Quaternary Science Reviews 30, 17-18, 2200–2219, https://doi.org/10.1016/j.quascirev.2010.09.016, 2011.

Bernasconi, S. M., Daëron, M., Bergmann, K. D., Bonifacie, M., Meckler, A. N., Affek, H. P., Anderson, N., Bajnai, D., Dux, F., Eiler, J., … Ziegler, M.: InterCarb: A Community Effort to Improve Interlaboratory Standardization of the Carbonate Clumped Isotope Thermometer Using Carbonate Standards, Geochemistry, Geophysics, Geosystems, 22(5). https://doi.org/10.1029/2020GC009588, 2021.

Bernasconi, S. M., Müller, I. A., Bergmann, K. D., Breitenbach, S. F. M., Fernandez, A., Hodell, D. A., Jaggi, M., Meckler, A. N., Millan, I., and Ziegler, M.: Reducing Uncertainties in Carbonate Clumped Isotope Analysis Through Consistent Carbonate-Based Standardization, Geochemistry, Geophysics, Geosystems, 19(9), 2895–2914. https://doi.org/10.1029/2017GC007385, 2018.

Bledzki, L.A. and Rybak, J.I.: Freshwater Crustacean Zooplankton of Europe: Cladocera & Copepoda (Calanoida, Cyclopoida). Key to species identification, with notes on ecology, distribution, methods and introduction to data analysis, Springer International Publishing Switzerland, 918 pp., https://doi.org/10.1007/978-3-319-29871-9, 2016.

Blott, S.J. and Pye, K.: GRADISTAT: a grain size distribution and statistics package for the analysis of unconsolidated sediments, Earth Surf. Process. Landf. 26, 1237-1248, https://doi.org/10.1002/esp.261, 2001.

Boike, J., Bolshiyanov, D. Yu., Schirrmeister, L., Wetterich, S. (eds.): Russian-German Cooperation SYSTEM LAPTEV SEA: The Expedition Lena - New Siberian Islands 2007 during the International Polar Year (IPY) 2007/2008, Reports on Polar and Marine Research, 584, 265 pp., https://doi.org/10.2312/BzPM_0584_2008, 2008.

Boike, J., Nitzbon, J., Anders, K., Grigoriev, M.N., Bolshiyanov, D.Y., Langer, M., Lange, S., Bornemann, N.,

Morgenstern, A., Schreiber, P., Wille, C., Chadburn, S., Gouttevin, I., and Kutzbach, L.: Measurements in soil and air at Samoylov Station (2002-2018), version 201908. Alfred Wegener Institute, https://doi.org/10.1594/PANGAEA.905232, 2019.

Bochkov, D.A. and Seregin, A.P.: Local floras of Russia: records from literature. Version 1.71. Lomonosov Moscow State University. Occurrence dataset https://doi.org/10.15468/rxtjt2 accessed via GBIF.org on 2023-04-21, 2022.

Bøtter-Jensen, L., McKeever, S.W.S., and Wintle, A.G.: Optically Stimulated Luminescence Dosimetry. (1st edition) Elsevier Science, 374 pp., ISBN-13: 978-0444506849, 2003.

Bouchard, F., MacDonald, L.A., Turner, K.W., Thienpont, J.R, Medeiros, A.S., Biskaborn, B.K., Korosi, J., Hall, RI., Pienitz, R., and Wolfe, B.B. Paleolimnology of thermokarst lakes: a window into permafrost landscape evolution. Arctic Science, **3**(2): 91-117. https://doi.org/10.1139/as-2016-0022, 2017.

Brand, W.A., Assonov, S.S., and Coplen, T.B.: Correction for the 17O interference in δ(13C) measurements when analyzing CO2 with stable isotope mass spectrometry (IUPAC Technical Report), Pure and Applied Chemistry, 82(8), 1719–1733. https://doi.org/10.1351/PAC-REP-09-01-05, 2010.

Brooks, S.J., Langdon, P.G., and Heiri, O.: The Identification and Use of Palaearctic Chironomidae Larvae in Palaeoecology, QRA Technical Guide No. 10, Journal of Paleolimnology, 40(2), 751–753, https://doi.org/10.1007/s10933-007-9191-1, 2008.

Buckland, P.: The Bugs Coleopteran Ecology Package (BugsCEP) database: 1000 sites and half a million fossils later, Quaternary International, 341, 272–282, https://doi.org/10.1016/j.quaint.2014.01.030, 2014.

Buckland, P.: The development and implementation of software for palaeoenvironmental and palaeoclimatological research : the Bugs Coleopteran Ecology Package (BugsCEP) [Internet] [PhD dissertation]. [Umeå]: Arkeologi och samiska studier; (Archaeology and environment). Available from: http://urn.kb.se/resolve?urn=urn:nbn:se:umu:diva-1105, 2007.

Burke, K. D., Williams, J. W., Chandler, M. A., Haywood, A. M., Lunt, D. J., and Otto-Bliesner, L. B.: Pliocene and Eocene provide best analogs for near-future climates. Proceedings of the National Academy of Sciences, 115(52), 13288-13293. https://doi.org/10.1073/pnas.1809600115, 2018.

Cao, X., Herzschuh, U., Telford, R. J., and Ni, J.: A modern pollen–climate dataset from China and Mongolia: Assessing its potential for climate reconstruction, Review of Palaeobotany and Palynology, 211, 87–96, https://doi.org/10.1016/j.revpalbo.2014.08.007, 2014.

CAPE-LIG Project Members: LIG Arctic warmth confirms polar amplification of climate change, Quaternary Science Reviews, 25, 1383-1400, https://doi.org/10.1016/j.quascirev.2006.01.033, 2006.

Capron, E., Govin, A., Stone, E.J., Masson-Delmotte, V., Mulitza, S., Otto-Bliesner, B., Rasmussen, T.L., Sime, L.C., Waelbroeck, C., and Wolff, E. W.: Temporal and spatial structure of multi-millennial temperature changes at high latitudes during the LIG, Quaternary Science Reviews, 103, 116-133, https://doi.org/10.1016/j.quascirev.2014.08.018, 2014.

Carter, M. R. and E. G. Gregorich (eds.): Soil Sampling and Methods of Analysis, 2nd ed., 1224 pp., Taylor and Francis, London, 2008.

1   CAVM Team: Circumpolar Arctic Vegetation Map. (1:7,500,000 scale), Conservation of Arctic Flora and Fauna

2   (CAFF) Map No. 1. U.S. Fish and Wildlife Service, Anchorage, Alaska, 2003.

3   Chernov, Y.I. and Makarova, O.L.: Beetles (Coleoptera) in High Arctic. L. Penev, T. Erwin, and T. Assmann

4   (Eds.) Back to the Roots and Back to the Future. Towards a New Synthesis amongst Taxonomic, Ecological and

5   Biogeographical Approaches in Carabidology. Proceedings of the XIII European Carabidologists Meeting,

6   Blagoevgrad, August 20-24, 2007, pp. 207–240, 2008.

7   Clarke, C.L., Alsos, I.G., Edwards, M.E., Paus, A., Gielly, L., Haflidason, H., Mangerud, J., Regnéll, C., Hughes,

8   P.D.M., Svendsen, J.I., and Bjune, A.E.: A 24,000-year ancient DNA and pollen record from the Polar Urals

9   reveals temporal dynamics of arctic and boreal plant communities, Quaternary Science Reviews, 247, 106564,

10   https://doi.org/10.1016/j.quascirev.2020.106564, 2020.

11   Coplen, T.B.: Calibration of the calcite–water oxygen-isotope geothermometer at Devils Hole, Nevada, a natural

12   laboratory. Geochimica et Cosmochimica Acta, 71(16), 3948–3957, https://doi.org/10.1016/j.gca.2007.05.028,

13   2007.

14   Courtin, J., Perfumo, A., Andreev, A.A., Opel, T., Stoof-Leichsenring, K.R., Edwards, M.E, Murton, J.B., and

15   Herzschuh, U.: Pleistocene glacial and interglacial ecosystems inferred from ancient DNA analyses of permafrost

16   sediments from Batagay megaslump, East Siberia, Environmental DNA,   4 (6), 1199-1433,

17   https://doi.org/10.1002/edn3.336, 2022.

18   Crump, S. E., Fréchette, B., Power, M., Cutler, S., de Wet, G., Raynolds, M. K., Raberg, J. H., Briner, J. P.,

19   Thomas, E. K., Sepúlveda, J., Shapiro, B., Bunce, M., and Miller, G. H.: Ancient plant DNA reveals High Arctic

20   greening during the LIG, Proceedings of the National Academy of Sciences, 118, e2019069118,

21   https://doi.org/10.1073/pnas.2019069118, 2021.

22   Czudek, T. and Demek, J.: Thermokarst in Siberia and Its Influence on the Development of Lowland Relief,

23   Quaternary Research 1, 103–120, https://doi.org/10.1016/0033-5894(70)90013-X, 1970.

24   Daëron, M., Blamart, D., Peral, M., and Affek, H.P.: Absolute isotopic abundance ratios and the accuracy of Δ47

25   measurements, Chemical Geology, 442, 83–96, https://doi.org/10.1016/j.chemgeo.2016.08.014, 2016.

26   Decrouy, L., Vennemann, T.W., and Ariztegui, D.: Sediment penetration depths of epi- and infaunal ostracods

27   from Lake Geneva (Switzerland). Hydrobiologia, 688(1), 5–23, https://doi.org/10.1007/s10750-010-0561-8, 2012.

28   De Jonge, C., Guo, J., Hällberg, P., Griepentrog, M., Rifai, H., Richter, A., Ramirez, E., Zhang, X., Smittenberg,

29   R.H., Peterse, F., Boeckx, P., and Dercon, G.: The impact of soil chemistry, moisture and temperature on branched

30   and isoprenoid GDGTs in soils: A study using six globally distributed elevation transects, Organic Geochemistry

31   187, 104706, https://doi.org/10.1016/j.orggeochem.2023.104706, 2024.

32   Dennis, K.J., Affek, H.P., Passey, B.H., Schrag, D.P., and Eiler, J.M.: Defining an absolute reference frame for

33   'clumped' isotope studies of CO2, Geochimica et Cosmochimica Acta, 75(22), 7117–7131,

34   https://doi.org/10.1016/j.gca.2011.09.025, 2011.

35   Durcan, J.A., King, G.E., and Duller, G.A.T.: DRAC: Dose rate and age calculator for trapped charge dating,

36   Quaternary Geochronology, 28, 54-61, https://doi.org/10.1016/j.quageo.2015.03.012, 2015.

37   Edwards, M.E., Brubaker, L.B., Lozhkin, A.V., and Anderson, P.M.: Structurally Novel Biomes: A Response to

Past Warming in Beringia, Ecology, 86, 1696–1703, https://doi.org/10.1890/03-0787, 2005.

Edwards, M.E., Hamilton, T.D., Elias, S.A., Bigelow, N.H., and Krumhardt, A.P.: Interglacial Extension of the Boreal Forest Limit in the Noatak Valley, Northwest Alaska: Evidence from an Exhumed River-Cut Bluff and Debris Apron, Arctic Antarctic and Alpine Research, 35(4), 460–68, https://doi.org/10.1657/1523-0430(2003)035[0460:IEOTBF]2.0.CO;2, 2003.

Eiler, J.M.: "Clumped-isotope" geochemistry - he study of naturally-occurring, multiply-substituted isotopologues. Earth and Planetary Science Letters, 262(3–4), 309–327, https://doi.org/10.1016/j.epsl.2007.08.020, 2007.

Eiler, J.M. and Schauble, E.: $^{18}O^{13}C^{16}O$ in Earth's atmosphere, Geochimica et Cosmochimica Acta, 68(23), 4767–4777, https://doi.org/10.1016/j.gca.2004.05.035, 2004.

Elias, S.A.: Mutual climatic range reconstructions of seasonal temperatures based on late Pleistocene fossil beetle assemblages in Eastern Beringia, Quaternary Science Reviews, 20, 77–91, https://doi.org/10.1016/S0277-3791(00)00130-X, 2001.

Elias, S.A.: Climatic tolerances and zoogeography of the late Pleistocene beetle fauna of Beringia. Géographie physique et Quaternaire, 54(2), 143–155, https://doi.org/10.7202/004813ar, 2000.

Eyring, V., Bony, S., Meehl, G. A., Senior, C. A., Stevens, B., Stouffer, R. J., and Taylor, K. E.: Overview of the Coupled Model Intercomparison Project Phase 6 (CMIP6) experimental design and organization, Geosci. Model Dev., 9, 1937–1958, https://doi.org/10.5194/gmd-9-1937-2016, 2016.

Farquharson, L., Walter Anthony, K.M., Bigelow, N.H., Edwards, M.E., and Grosse, G.: Facies analysis of yedoma thermokarst lakes on the northern Seward Peninsula, Alaska. Sedimentary Geology, 340, 25-37. https://doi.org/10.1016/j.sedgeo.2016.01.002, 2016.

Fick, S.E. and Hijmans, R.J.: WorldClim 2: new 1-km spatial resolution climate surfaces for global land areas, Int. J. Climatol., 37, 4302–4315, https://doi.org/10.1002/joc.5086, 2017.

Fischer, H., Meissner, K.J., Mix, A.C. et al. Palaeoclimate constraints on the impact of 2 °C anthropogenic warming and beyond. Nature Geosci., 11, 474-485 (2018). https://doi.org/10.1038/s41561-018-0146-0.

Froese, D., Zazula, G., Westgate, J., Preece, S., Sanborn, P. A., Reyes, A., and Pearce, N.: The Klondike goldfields and Pleistocene environments of Beringia, GSA Today, 19, 4-10, https://doi.org/10.1130/GSATG54A.1, 2009.

Frolova L., Nazarova L., Pestryakova L., Herzschuh U.: Subfossil cladoceran remains from sediment in thermokarst lakes in northeastern Siberia, Russia, Journal of Paleolimnology, 52(1), 107-119, https://doi.org/10.1007/s10933-014-9781-7, 2014

Galbraith, R.F., Roberts, R.G., Laslett, G. M., Yoshida, H., and Olley, J. M.: Optical dating of single and multiple grains of quartz from Jinmium rock shelter, northern Australia: part I, experimental design and statistical models, Archaeometry 41(2), 339–364, https://doi.org/10.1111/j.1475-4754.1999.tb00987.x, 1999.

GBIF: The Global Biodiversity Information Facility: GBIF Home Page, https://www.gbif.org, Assessed 2023-04-21, 2023.

Grosse, G., Jones, B., and Arp, C.: Thermokarst Lakes, Drainage, and Drained Basins. In: Shroder JF (ed.): Treatise

on Geomorphology, Vol. 8, 325-353. San Diego: Academic Press. https://doi.org/10.1016/B978-0-12-374739-6.00216-5, 2013.

Guarino, M.-V., Sime, L. C., Schröeder, D., Malmierca-Vallet, I., Rosenblum, E., Ringer, M., Ridley, J., Feltham, D., Bitz, C., Steig, E. J., Wolff, E., Stroeve, J., and Sellar, A.: Sea-ice-free Arctic during the LIG supports fast future loss, Nat Clim Change, 10, 928-932, https://doi.org/10.1038/s41558-020-0865-2, 2020.

Günther, F., Overduin, P.P., Sandakov, A.V., Grosse, G., and Grigoriev, M.N.: Short- and long-term thermo-erosion of ice-rich permafrost coasts in the Laptev Sea region, Biogeosciences, 10, 4297–4318, https://doi.org/10.5194/bg-10-4297-2013, 2013.

Gulev, S.K., P.W. Thorne, J. Ahn, F.J. Dentener, C.M. Domingues, S. Gerland, D. Gong, D.S. Kaufman, H.C. Nnamchi, J. Quaas, J.A. Rivera, S. Sathyendranath, S.L. Smith, B. Trewin, K. von Schuckmann, and R.S. Vose,: Changing State of the Climate System. In Climate Change 2021: The Physical Science Basis. Contribution of Working Group I to the Sixth Assessment Report of the Intergovernmental Panel on Climate Change [Masson-Delmotte, V., P. Zhai, A. Pirani, S.L. Connors, C. Péan, S. Berger, N. Caud, Y. Chen, L. Goldfarb, M.I. Gomis, M. Huang, K. Leitzell, E. Lonnoy, J.B.R. Matthews, T.K. Maycock, T. Waterfield, O. Yelekçi, R. Yu, and B. Zhou (eds.)]. Cambridge University Press, Cambridge, United Kingdom and New York, NY, USA, pp. 287–422, doi:10.1017/9781009157896.004, .2021

Halffman, R., Lembrechts, J., Radujković, D., Gruyter, J.D., Nijs, I., and de Jonge, C.: Soil chemistry, temperature and bacterial community composition drive brGDGT distributions along a subarctic elevation gradient. Organic Geochemistry, 163, 104346,https://doi.org/10.1016/j.orggeochem.2021.104346, 2021.

Halamka, T.A., McFarlin, J.M., Younkin, A.D., Depoy, J., Dildar, N., and Kopf, S.H.: Oxygen limitation can trigger the production of branched GDGTs in culture. Geochemical Perspectives Letters 36–39,https://doi.org/10.7185/geochemlet.2132, 2021.

Halamka, T.A., Raberg, J.H., McFarlin, J.M., Younkin, A.D., Mulligan, C., Liu, X., and Kopf, S.H.: Production of diverse brGDGTs by Acidobacterium Solibacter usitatus in response to temperature, pH, and O2 provides a culturing perspective on brGDGT proxies and biosynthesis, Geobiology, 21, 102–118, https://doi.org/10.1111/gbi.12525, 2023.

Hamilton, T.D. and Brigham-Grette, J.: The last interglaciation in Alaska: Stratigraphy and paleoecology of potential sites. Quaternary International, 10–12, 49-71, https://doi.org/10.1016/1040-6182(91)90040-U, 1991.

Hersbach, H., Bell, B., Berrisford, P., Hirahara, S., et al.: The ERA5 global reanalysis, Q.J.R. Meteorol. Soc., 146, 1999–2049, https://doi.org/10.1002/qj.3803, 2020.

Herzschuh, U., Li, C., Böhmer, T., Postl, A. K., Heim, B., Andreev, A. A., Cao, X., Wieczorek, M., and Ni, J.: LegacyPollen 1.0: a taxonomically harmonized global late Quaternary pollen dataset of 2831 records with standardized chronologies, Earth Syst. Sci. Data, 14, 3213–3227, https://doi.org/10.5194/essd-14-3213-2022, 2022.

Herzschuh, U., Böhmer, T., Li, C., Chevalier, M., Hébert, R., Dallmeyer, A., Cao, X., Bigelow, N. H., Nazarova, L., Novenko, E. Y., Park, J., Peyron, O., Rudaya, N. A., Schlütz, F., Shumilovskikh, L. S., Tarasov, P. E., Wang, Y., Wen, R., Xu, Q., and Zheng, Z.: LegacyClimate 1.0: a dataset of pollen-based climate reconstructions from 2594 Northern Hemisphere sites covering the last 30 kyr and beyond, Earth Syst. Sci. Data, 15, 2235–2258,

https://doi.org/10.5194/essd-15-2235-2023, 2023.

Hopmans, E.C., Weijers, J.W.H., Schefuß, E., Herfort, L., Sinninghe Damsté, J.S. and Schouten, S.: A novel proxy for terrestrial organic matter in sediments based on branched and isoprenoid tetraether lipids, Earth and Planetary Science Letters, 224, 107–116, https://doi.org/10.1016/j.epsl.2004.05.012, 2004.

Huang, B., Yin, X., Menne, M.J., Vose, R., and Zhang, H.: NOAA Global Surface Temperature Dataset (NOAAGlobalTemp), Version 6.0.0. NOAA National Centers for Environmental Information. https://doi.org/10.25921/rzxg-p717, 2024.

Huntley, D.J. and Baril, M.R..: The K content of the K-feldspars being measured in optical dating or in thermoluminescence dating, Ancient TL 15(1), 11–13, URL: http://ancienttl.org/ATL_15-1_1997/ATL_15-1_Huntley_p11-13.pdf, 1997.

Ilyashuk, B.P., Andreev, A.A., Bobrov, A.A., Tumskoy, V.E., Ilyashuk, E.A.: Interglacial history of a palaeo-lake and regional environment: a multi-proxy study of a permafrost deposit from Bol'shoi Lyakhovsky Island, Arctic Siberia, Journal of Paleolimnology, 36, 855–872, https://doi.org/10.1007/s10933-005-5859-6, 2006.

iNaturalist: Observations of *Alnus hirsuta*, https://www.inaturalist.org/taxa/437257-Alnus-hirsuta. Accessed 2023-03-28, 2023.

Ivanenko, G.V.: State geological map of Russian Federation, New Siberian Islands, 1:1,00,000, map of Quaternary formations, Ministry of Natural Resources of Russian Federation, 1998.

Jensen, B.J.L., Reyes, A.V., Froese, D.G., Stone, D.B.: The Palisades is a key reference site for the middle Pleistocene of eastern Beringia: new evidence from paleomagnetics and regional tephrostratigraphy. Quaternary Science Reviews, 63, 91-108, https://doi.org/10.1016/j.quascirev.2012.11.035, 2013.

John, C.M. and Bowen, D.: Community software for challenging isotope analysis: First applications of 'Easotope' to clumped isotopes, Rapid Communications in Mass Spectrometry, 30(21), 2285–2300, https://doi.org/10.1002/rcm.7720, 2016.

Jones, M.C., Grosse, G., Treat, C., Tuetsky, M., Walter Anthony, K., and Brosius, L.: Past permafrost dynamics can inform future permafrost carbon-climate feedbacks. Commun Earth Environ 4, 272, https://doi.org/10.1038/s43247-023-00886-3, 2023.

Jones, B.M., Grosse, G., Farquharson, L.M. Roy-Leville, P., Veremeeva, A., Kanevskiy, M.Z., Gaglioti, B.V., Breen, A.L., Parsekian, A.D., Ulrich, M., and Hinkel, K.M.: Lake and drained lake basin systems in lowland permafrost regions. Nat Rev Earth Environ 3, 85–98, https://doi.org/10.1038/s43017-021-00238-9, 2022.

Jørgensen, T., Haile, J., Möller, P., Andreev, A., Boessenkool, S., Rasmussen, M., Kienast, F., Coissac, E., Taberlet, P., Brochmann, C., Bigelow, N.H., Andersen, K., Orlando, L., Gilbert, M.T.P., and Willerslev, E.: A comparative study of ancient sedimentary DNA, pollen and macrofossils from permafrost sediments of northern Siberia reveals long-term vegetational stability, Molecular Ecology, 21, 1989–2003. https://doi.org/10.1111/j.1365-294X.2011.05287.x, 2012.

Juggins, S.: C2 Version 1.5 User guide. Software for ecological and palaeoecological data analysis and visualization. Newcastle University, Newcastle upon Tyne, UK, 2007.

Juggins, S.: rioja: Analysis of Quaternary Science Data, R package version 0.9-21, https://cran.r-

project.org/web/packages/rioja, assessed 2021-11-22, 2019.

Kageyama, M., Sime, L. C., Sicard, M., Guarino, M.-V., de Vernal, A., Stein, R., Schroeder, D., Malmierca-Vallet, I., Abe-Ouchi, A., Bitz, C., Braconnot, P., Brady, E.C., Cao, J., Chamberlain, M. A., Feltham, D., Guo, C., LeGrande, A.N., Lohmann, G., Meissner, K. J., Menviel, L., Morozova, P., Nisancioglu, K. H., Otto-Bliesner, B.L., O'ishi, R., Ramos Buarque, S., Salas y Melia, D., Sherriff-Tadano, S., Stroeve, J., Shi, X., Sun, B., Tomas, R.A., Volodin, E., Yeung, N.K.H., Zhang, Q., Zhang, Z., Zheng, W., and Ziehn, T.: A multi-model CMIP6-PMIP4 study of Arctic sea ice at 127 ka: sea ice data compilation and model differences, Clim. Past, 17, 37–62, https://doi.org/10.5194/cp-17-37-2021, 2021.

Kageyama, M., Braconnot, P., Harrison, S.P., Haywood, A.M., Jungclaus, J., Otto-Bliesner, B.L., ... & Zhou, T.: PMIP4-CMIP6: the contribution of the Paleoclimate Modelling Intercomparison Project to CMIP6. Geoscientific Model Development Discussions, 11(3), 1033-1057.https://doi.org/10.5194/gmd-11-1033-2018, 2018.

Kallistova, A., Savvichev, A., Rusanov, I., and Pimenov, N.: Thermokarst Lakes, Ecosystems with Intense Microbial Processes of the Methane Cycle, Microbiology, 88, 649-661, https://doi.org/10.1134/S0026261719060043. 2019.

Kaplina, T.N.: Ancient alas complexes of northern Yakutia (Part 1), Kriosfera Zemli 15, 2, 3–13 (in Russian), 2011a.

Kaplina, T.N.: Ancient alas complexes of northern Yakutia (Part 2), Kriosfera Zemli 15, 3, 20–30 (in Russian), 2011b.

Kaplina T.N.: History of permafrost strata of northern Yakutia in the Late Cenozoic. In: History of the development of permafrost deposits of Eurasia. Moscow: Nauka, 153–181 (in Russian), 1981.

Kaplina, T.N., Sher, A.V., Giterman, R.E., Zazhigin, V.S., Kiselev, S.V., Lozhkin, A.V., and Nikitin, V.P.: Key section of Pleistocene deposits on the Allaikha river (lower reaches of the Indigirka). In: Bulletin of Commission on Quaternary Period research, USSR Academy of Sciences, 50, 73–95 (in Russian), 1980.

Kienast, F.: Plant macrofossil records – Arctic Eurasia, In: Encyclopedia of Quaternary Science. Elias, Scott A., Mock, Cary (Editors-in-Chief), Elsevier, 2nd Edition Vol. 3, 733–745, https://doi.org/10.1016/B978-0-444-53643-3.00213-2, 2013.

Kienast, F., Wetterich, S., Kuzmina, S., Schirrmeister, L., Andreev, A., Tarasov, P., Nazarova, L., Kossler, A., Frolova, A., and Kunitsky, V.V.: Paleontological records indicate the occurrence of open woodlands in a dry inland climate at the present-day Arctic coast in western Beringia during the LIG, Quaternary Science Reviews, 30, 2134–2159, https://doi.org/10.1016/j.quascirev.2010.11.024, 2011.

Kienast, F., Tarasov, P., Schirrmeister, L., Grosse, G., and Andreev, A.A.: Continental climate in the East Siberian Arctic during the LIG: implications from palaeobotanical records, Global and Planetary Change, 60(3/4), 535–562. https://doi.org/10.1016/j.gloplacha.2007.07.004, 2008.

Kiselev S.V. and Nazarov V.I.: Late Cenozoic Insects of Northern Eurasia., Ltd., Paleontological Journal Supplement, 43(7), 723-850, https://doi.org/10.1134/S0031030109070016. 2009. Kjær, K.H., Winther Pedersen, M., De Sanctis, B., De Cahsan, B., Korneliussen, T.S., Michelsen, C.S., Sand, K.K., Jelavić, S., Ruter, A.H., Schmidt, A.M.A., Kjeldsen, K.K., Tesakov, A.S., Snowball, I., Gosse, J.C., Alsos, I.G., Wang, Y., Dockter, C.,

Rasmussen, M., Jørgensen, M.E., … and Willerslev, E.: A 2-million-year-old ecosystem in Greenland uncovered by environmental DNA, Nature, 612, 7939. https://doi.org/10.1038/s41586-022-05453-y, 2022.

Klemm, J., Herzschuh, U., Pisaric, M.F.J., Telford, R.J., Heim, B., and Pestryakova, L.A.: A pollen-climate transfer function from the tundra and taiga vegetation in Arctic Siberia and its applicability to a Holocene record, Palaeogeography, Palaeoclimatology, Palaeoecology, 386, 702-713, https://doi.org/10.1016/j.palaeo.2013.06.033, 2013.

Krasnoborov, I..M. and Malyshev, L.I. (eds.): Flora of Siberia Vol. 5., Salicaceae - Amaranthaceae. Enfield (NH), USA: Science Publishers, Inc., 305 pp., ISBN: 9781578081042, 2003.

Krbetschek, M.R., Götze, I., Dietrich, A., and Trautmann, T.: Spectral information from minerals relevant for luminescence dating, Radiation Measurements, 27(5-6), 695–748, https://doi.org/10.1016/S1350-4487(97)00223-0, 1997.

Kreutzer, S., Schmidt, C., Fuchs, M., Dietze, M., Fischer, M., and Fuchs, M.; Introducing an R package for luminescence dating analysis. Ancient TL 3, 1–8, https://doi.org/10.26034/la.atl.2012.457, 2012.

Kusch, S., Winterfeld, M., Mollenhauer, G., Höfle, S.T., Schirrmeister, L., Schwamborn, G., Rethemeyer, J.: Glycerol dialkyl glycerol tetraethers (GDGTs) in high latitude Siberian permafrost: Diversity, environmental controls, and implications for proxy applications, Organic Geochemistry, 136, 103888, https://doi.org/10.1016/j.orggeochem.2019.06.009, 2019.

Kuzmina, S.A.: Quaternary Insects and Environment of the Northeastern Asia, Paleontological Journal, 49, 7, 679–867, https://doi.org/10.1134/S0031030115070011, 2015a.

Kuzmina, S.: Insect faunal response to environmental changes during the LIG in Western Beringia. Quaternary International, 379, 106–117, https://doi.org/10.1016/j.quaint.2015.04.036, 2015b.

Kuznetsova, T.V., Wetterich, S., Matthes, H., Tumskoy, V.E., and Schirrmeister, L.: Mammoth fauna remains from late Pleistocene deposits of the Dmitry Laptev Strait south coast (northern Yakutia, Russia), Frontiers in Earth Science, 10, 757629. https://doi.org/10.3389/feart.2022.757629, 2022.

Leemans, R. and Cramer, W.: The IIASA Climate Database for Mean Monthly Values of Temperature, Precipitation and Cloudiness on A Global Terrestrial Grid. International Institute of Applied Systems Analysis, Luxemburg (updated version), https://daac.ornl.gov/CLIMATE/guides/cramer_leemans.html, 1991.

Lenz, J., Jones, B.M., Wetterich, S., Tjallingii, R., Fritz, M., Arp, C.D., Rudaya, N., and Grosse, G.: Impacts of shore expansion and catchment characteristics on lacustrine thermokarst records in permafrost lowlands, Alaska Arctic Coastal Plain. arktos, 2, 25, https://doi.org/10.1007/s41063-016-0025-0, 2016.

Lisiecki, L.E. and Raymo, M.E.: A Pliocene–Pleistocene stack of 57 globally distributed benthic δ^{18}O records, Paleoceanography, 20, PA1003. https://doi.org/10.1029/2004PA001071, 2005.

Lozhkin A.V. and Anderson P.M.: Vegetation responses to interglacial warming in the Arctic: Examples from Lake El'gygytgyn, Far East Russian Arctic. Climate of the Past. 9. 1211-1219. 10.5194/cp-9-1211-2013. 2013.

Lozhkin A.V. and Anderson P.M.: The Last Interglaciation in Northeast Siberia. Quaternary Research. ;43(2):147-158. https://doi.org/10.1006/qres.1995.1016, 1995.

Luoto, T.P., Nevalainen, L., Kubischta, F., Kultti, S., Knudsen, K.L. and Salonen, V.-P.: Late Quaternary ecological turnover in high arctic Lake Einstaken, Nordaustlandet, Svalbard (80° N). Geografiska Annaler: Series A, Physical Geography, 93, 337–354, https://doi.org/10.1111/j.1468-0459.2011.00435.x, 2011

Marchegiano, M., Peral, M., Venderickx, J., Martens, K., García-Alix, A., Snoeck, C., Goderis, S., and Claeys, P.: The Ostracod Clumped-Isotope Thermometer: A Novel Tool to Accurately Quantify Continental Climate Changes, Geophysical Research Letters, 51(4), e2023GL107426. https://doi.org/10.1029/2023GL107426, 2024.

Maraun, D. and Widmann, M.: Statistical downscaling and bias correction for climate research, Cambridge University Press, Cambridge, UK, https://doi.org/10.1017/9781107588783, 2018.

Massaferro, J. and Brooks, S.J.: Response of chironomids to Late Quaternary environmental change in the Taitao Peninsula, southern Chile, Journal of Quaternary Science, 17, 101–111, https://doi.org/0.1002/jqs.671, 2002.

MacDonald, G.M., Kremenetski, K.V, and Beilman, D.W: Climate change and the northern Russian treeline zone, Phil. Trans. R. Soc. B, 363, 2285–2299, https://doi.org/10.1098/rstb.2007.220, 2008.

McMahon, R.F. and Bogan, A.E.: 11 - MOLLUSCA: BIVALVA. In: Thorp, J.H. and Covich, A.P. (eds.) Ecology and Classification of North American Freshwater Invertebrates, 2nd Edition, Academy Press, 331–429, https://doi.org/10.1016/B978-012690647-9/50012-0, 2001.

Meisch, C.: Freshwater Ostracoda of Western and Central Europe, Heidelberg, Berlin: Spektrum Akademischer Verlag, pp. 555, 2000.

Moller Pillot, H.K.M.: Chironomidae Larvae, Volume 2: Biology and ecology of the Chironomini, 270 pp. KNNV Publishing, https://doi.org/10.1163/9789004278042, 2009.

Morgenstern, A., Ulrich, M., Günther, F., Roessler, S., Fedorova, I.V., Rudaya, N.A., Wetterich, S., Boike, J. and Schirrmeister, L.: Evolution of thermokarst in East Siberian ice-rich permafrost: A case study, Geomorphology, 201, 363–379, https://doi.org/10.1016/j.geomorph.2013.07.011, 2013.

Murray, A.S. and Wintle, A.G.: Luminescence dating of quartz using an improved single-aliquot regenerative-dose protocol, Radiation Measurements, 32(1), 57–73, https://doi.org/10.1016/S1350-4487(99)00253-X, 2000.

Murray, A.S. and Wintle, A.G.: The single aliquot regenerative dose protocol: potential for improvements in reliability, Radiation Measurements, 37(4-5), 377–381, https://doi.org/10.1016/S1350-4487(03)00053-2, 2003,

Murton, J.B., Opel, T., Toms, P., Blinov, A., Fuchs, M., Wood, J., Gärtner, A., Merchel, S., Rugel, G., Savvinov, G., and Wetterich, S.: A multimethod dating study of ancient permafrost, Batagay megaslump, east Siberia, Quaternary Research, 105, 1–22, https://doi.org/10.1017/qua.2021.27, 2022.

Murton, J.B.: Thermokarst-lake-basin sediments, Tuktoyaktuk Coastlands, western arctic Canada. Sedimentology, 43, 737-760, https://doi.org/10.1111/j.1365-3091.1996.tb02023.x, 1996.

Nazarova, L., Syrykh, L., Grekov, I., Sapelko, T., Krasheninnikov, A.B., and Solovieva, N.: Chironomid-based modern summer temperature data set and inference model for the Northwest European part of Russia, Water, 15, 976, https://doi.org/10.3390/w15050976, 2023.

Nazarova, L.B., Self, A.E., Brooks, S.J., Solovieva, N., Syrykh, L.S., and Dauvalter, V.A.: Chironomid fauna of the lakes from the Pechora River Basin (East of European part of Russian Arctic): Ecology and reconstruction of

recent ecological changes in the region, Contemporary Problems of Ecology, 10, 350–362, https://doi.org/10.1134/S1995425517040059, 2017a.

Nazarova L., Bleibtreu A., Hoff U., Dirksen V., and Diekmann B.: Changes in temperature and water depth of a small mountain lake during the past 3000 years in Central Kamchatka reflected by chironomid record, Quaternary International, 447, 46–58, https://doi.org/10.1016/j.quaint.2016.10.008, 2017b.

Nazarova L., Self A., Brooks S.J., van Hardenbroek M., Herzschuh U., and Diekmann B.: Northern Russian chironomid-based modern summer temperature data set and inference models, Global and Planetary Change, 134, 10–25, https://doi.org/10.1016/j.gloplacha.2014.11.015, 2015.

Nazarova L., Herzschuh U., Wetterich S., Kumke T., and Pestjakova L.: Chironomid-based inference models for estimating mean July air temperature and water depth from lakes in Yakutia, northeastern Russia, Journal of Palaeolimnology. 45, 57–71, https://doi.org/10.1007/s10933-010-9479-4, 2011.

Nazarova, L., Pestryakova, L.A., Ushnitskaya, L.A., and Hubberten, H.-W.: Chironomids (Diptera: Chironomidae) in lakes of central Yakutia and their indicative potential for paleoclimatic research, Contemporary problems of ecology, 1, 335–345 https://doi.org/10.1134/S1995425508030089, 2008.Niemeyer, B., Klemm, J., Pestryakova, L.A., and Herzschuh, U.: Relative pollen productivity estimates for common taxa of the northern Siberian Arctic, Rev. Palaeobot. Palynol., 221, 71–82, https://doi.org/10.1016/j.revpalbo.2015.06.008, 2015.

Niemeyer, B., Epp, L.S., Stoof-Leichsenring, K.R., Pestryakova, L.A., and Herzschuh, U.: A comparison of sedimentary DNA and pollen from lake sediments in recording vegetation composition at the Siberian treeline, Mol Ecol Resour., 17, e46–e62. https://doi.org/10.1111/1755-0998.12689, 2017.

Niemeyer, B., Klemm, J., Herzschuh, U., and Pestryakova, L.: Relative pollen productivity estimates for common taxa of the northern Siberian Arctic, Review of Palaeobotany and Palynology, 221, 71-82, https://doi.org/10.1016/j.revpalbo.2015.06.008, 2015.

Nikolskiy P.A., Basilyan A.E., and Zazhigin V.S.: New Data on the Age of the Glaciation in the New Siberian Islands (Russian Eastern Arctic), Doklady Earth Sciences, 475(1), 748–752,, https://doi.org/10.1134/S1028334X17070194, 2017.

Opel, T., Bertran, P., Grosse, G., Jones, M., Luetscher, M., Schirrmeister, L., Stadelmaier, K. H., and Veremeeva, A.: Ancient permafrost and past permafrost in the Northern Hemisphere, in: Reference Module in Earth Systems and Environmental Sciences, Elsevier, https://doi.org/10.1016/B978-0-323-99931-1.00258-0, 2024.

Opel, T. Wetterich S., Meyer H., Dereviagin A.Yu., Fuchs M.C., and Schirrmeister L.: Ground-ice stable isotopes and cryostratigraphy reflect late Quaternary palaeoclimate in the Northeast Siberian Arctic (Oyogos Yar coast, Dmitry Laptev Strait), Clim Past, 13, 587–611, https://doi.org/10.5194/cp-13-587-2017, 2017.

Opel, T., Dereviagin, A. Y., Meyer, H., Schirrmeister, L., and Wetterich, S.: Palaeoclimatic information from stable water isotopes of Holocene ice wedges on the Dmitrii Laptev Strait, northeast Siberia, Russia, Permafrost and Periglacial Processes, 22(1), 84–100, https://doi.org/10.1002/ppp.667, 2011.

Otto-Bliesner, B.L., Brady, E.C., Zhao, A., Brierley, C.M., Axford, Y., Capron, E., Govin, A., Hoffman, J.S., Isaacs, E., Kageyama, M., Scussolini, P., Tzedakis, P.C., Williams, C.J.R., Wolff, E., Abe-Ouchi, A., Braconnot, P., Ramos Buarque, S., Cao, J., de Vernal, A., Guarino, M.V., Guo, C., LeGrande, A.N., Lohmann, G., Meissner,

K.J., Menviel, L., Morozova, P.A., Nisancioglu, K.H., O'ishi, R., Salas y Mélia, D., Shi, X., Sicard, M., Sime, L., Stepanek, C., Tomas, R., Volodin, E., Yeung, N.K.H., Zhang, Q., Zhang, Z., and Zheng, W.: Large-scale features of LIG climate: results from evaluating the lig127k simulations for the Coupled Model Intercomparison Project (CMIP6)–Paleoclimate Modeling Intercomparison Project (PMIP4), Clim. Past, 17, 63–94, https://doi.org/10.5194/cp-17-63-2021, 2021.

Otto-Bliesner, B. L., Braconnot, P., Harrison, S. P., Lunt, D. J., Abe-Ouchi, A., Albani, S., Bartlein, P. J., Capron, E., Carlson, A. E., Dutton, A., Fischer, H., Goelzer, H., Govin, A., Haywood, A., Joos, F., LeGrande, A. N., Lipscomb, W. H., Lohmann, G., Mahowald, N., Nehrbass-Ahles, C., Pausata, F. S. R., Peterschmitt, J.-Y., Phipps, S. J., Renssen, H., and Zhang, Q.: The PMIP4 contribution to CMIP6 – Part 2: Two interglacials, scientific objective and experimental design for Holocene and Last Interglacial simulations, Geosci. Model Dev., 10, 3979–4003, https://doi.org/10.5194/gmd-10-3979-2017, 2017.

Otto-Bliesner, B.L., Rosenbloom, N., Stone, E.J., McKay, N.P., Lunt, D.J., Brady, E.C., and Overpeck, J.T.: How Warm Was the Last Interglacial? New Model–Data Comparisons, Proceedings of the Royal Society A 371: 20130097, https://doi.org/10.1098/rsta.2013.0097, 2013. Overpeck, J.T., Webb, T., and Prentice, I.C.: Quantitative Interpretation of Fossil Pollen Spectra: Dissimilarity Coefficients and the Method of Modern Analogs, Quaternary Res., 23, 87–108, https://doi.org/10.1016/0033-5894(85)90074-2, 1985.

Parducci, L., Bennett, K.D., Ficetola, G.F., Alsos, I.G., Suyama, Y., Wood, J.R., and Pedersen, M.W.: Ancient plant DNA in lake sediments, New Phytol, 214, 924-942, https://doi.org/10.1111/nph.14470, 2017.

Past Interglacials Working Group of PAGES: Interglacials of the last 800,000 years, Rev. Geophys. 54, 162-219 (2016). https://doi.org/10.1002/2015RG000482.

Petersen, S.V., Winkelstern, I.Z., Lohmann, K.C., and Meyer, K.W.: The effects of Porapak(TM) trap temperature on $\delta^{18}O$, $\delta^{13}C$, and Δ_{47} values in preparing samples for clumped isotope analysis, Rapid Communications in Mass Spectrometry, 30, 199–208, https://doi.org/10.1002/rcm.7438, 2015.

Pfeiffer, M. and Lohmann, G.: Greenland Ice Sheet influence on LIG climate: global sensitivity studies performed with an atmosphere–ocean general circulation model, Clim. Past, 12, 1313–1338, https://doi.org/10.5194/cp-12-1313-2016, 2016.

R Core Team: R: A language and environment for statistical computing. R Foundation for Statistical Computing, Vienna, Austria, https://www.R-project.org, 2022.

R Core Team: R: A language and environment for statistical computing, R Foundation for Statistical Computing, Vienna, Austria, https://www.R-project.org/ (last access: 22 November 2021), https://www.r-project.org/, 2020.

Raberg, J.H., Miller, G.H., Geirsdóttir, Á., and Sepúlveda, J.: Near-universal trends in brGDGT lipid distributions in nature, Science Advances, 8, eabm7625, https://doi.org/10.1126/sciadv.abm7625, 2022.

Rajora, O.P. and Dancik, B.P.: Chloroplast DNA inheritance in *Populus*, Theor Appl Genet., 84(3-4), 280–285, https://doi.org/10.1007/BF00229483, 1992.

Reyes, A.V., Froese, D.G., and Jensen, B.J.L.: Permafrost response to LIG warming: field evidence from non-glaciated Yukon and Alaska. Quaternary Science Reviews, 29(23–24), 3256-3274, https://doi.org/10.1016/j.quascirev.2010.07.013, 2010.

Rovere, A., Raymo, M.E., Vacchi, M., Lorscheid, T., Stocchi, P., Gómez-Pujol, L., Harris, D.L., Casella, E., O'Leary, M.J., Hearty, P.J.: The analysis of LIG (MIS 5e) relative sea-level indicators: Reconstructing sea-level in a warmer world, Earth-Science Reviews, 159, 404-427, https://doi.org/10.1016/j.earscirev.2016.06.006. 2016.

Scharf, B.W.: Eutrophication history of Lake Arendsee (Germany), Palaeogeography, Palaeoclimatology, Palaeoecology, 140, 85–96, https://doi.org/10.1016/S0031-0182(98)00033-9, 1998.

Schirrmeister, L., Grosse, G., Kunitsky, V., Meyer, H., Derevyagin, A., and Kuznetsova, T.: 5.2.10 Oyogos Yar coast (30.08.), Reports on Polar and Marine Research, 466, 247–256, https://doi.org/10.2312/BzPM_0466_2003, 2003.

Schirrmeister, L. Grosse, G., Wetterich, S., Overduin, Paul, Strauss, J., Schuur E.A.G., and Hubberten, H.-W.: Fossil organic matter characteristics in permafrost deposits of the Northeast Siberian Arctic, Journal of Geophysical Research, 116, G00M02, https://doi.org/10.1029/2011JG001647, 2011a.

Schirrmeister, L., Kunitsky, V. V., Grosse, G., Wetterich, S., Meyer, H., Schwamborn, G., Babiy, O., Derevyagin, A. Y., and Siegert, C.: Sedimentary characteristics and origin of the Late Pleistocene Ice Complex on North-East Siberian Arctic coastal lowlands and islands - a review, Quaternary International 241, 3–25, https://doi.org/10.1016/j.quaint.2010.04.004, 2011b.

Schirrmeister, L., Kunitsky, V., Grosse, V., Meyer, H., Kuznetsova, T., Kuzmina, S., Tumskoy, V., Derevyagin, A., Akhmadeeva, I., and Syromyatnikov, I.: Quaternary deposits of Bol'shoy Lyakhovsky Island, Reports on Polar Research, 354, 113–168, https://doi.org/10.2312/BzP_0354_1_2000, 2000.

Schirrmeister, L. Oezen, D., and Geyh, M.A.: [230]Th/U dating of frozen peat, Bol'shoy Lyakhovsky Island (northern Siberia), Quaternary Research, 57, 253–258, https://doi.org/10.1016/j.margeo.2022.106802, 2002.

Schneider, A.: Characteristics of an Eemian thermokarst landscape based on fossil bioindicators from permafrost deposits at the Dimitri Laptev Strait, northeastern Siberia, Bachelor thesis, Geographical Institute of the Humboldt University of Berlin (in German), 2010.

Schwamborn, G. and Wetterich, S.: Russian-German Cooperation CARBOPERM: Field campaigns to Bol'shoy Lyakhovsky Island in 2014, Reports on Polar and Marine Research, 686, 11–19, https://doi.org/10.2312/BzPM_0686_2015, 2015.

Seregin, A.: Moscow University Herbarium (MW). Version 1.288. Lomonosov Moscow State University. Occurrence dataset. https://doi.org/10.15468/cpnhcc, accessed via GBIF.org on 2023-07-10. https://www.gbif.org/occurrence/1697205269, 2023.

Shackleton, N.J., Sánchez-Goñi, M.F., Pailler, D., and Lancelot, Y.: Marine Isotope Substage 5e and the Eemian Interglacial, Global and Planetary Change, 36(3), 151–155, https://doi.org/10.1016/S0921-8181(02)00181-9, 2003.

Shi, X., Werner, M., Krug, C., Brierley, C.M., Zhao, A., Igbinosa, E., Braconnot, P., Brady, E., Cao, J., D'Agostino, R., Jungclaus, J., Liu, X., Otto-Bliesner, B., Sidorenko, D., Tomas, R., Volodin, E.M., Yang, H., Zhang, Q., Zheng, W., and Lohmann, G.: Calendar effects on surface air temperature and precipitation based on model-ensemble equilibrium and transient simulations from PMIP4 and PACMEDY. Clim. Past, 18, 1047–1070, https://doi.org/10.5194/cp-18-1047-2022, 2022.

Shur, Y.L. and Jorgenson, M.T.: Patterns of permafrost formation and degradation in relation to climate and ecosystems. Permafrost Periglac. Process., 18, 7-19. https://doi.org/10.1002/ppp.582, 2007.

Sime, L. C., Sivankutty, R., Vallet-Malmierca, I., de Boer, A. M., and Sicard, M.: Summer surface air temperature proxies point to near-sea-ice-free conditions in the Arctic at 127 ka, Clim. Past, 19, 883-900, https://doi.org/10.5194/cp-19-883-2023, 2023.

Simpson, G.L.: Analogue Methods in Palaeolimnology, in: Tracking Environmental Change Using Lake Sediments: Data Handling and Numerical Techniques, edited by: Birks, H. J. B., Lotter, A. F., Juggins, S., and Smol, J. P., Springer Netherlands, Dordrecht, 495–522, https://doi.org/10.1007/978-94-007-2745-8_15, 2012.

Sinninghe Damsté, J.S.: Spatial heterogeneity of sources of branched tetraethers in shelf systems: The geochemistry of tetraethers in the Berau River delta (Kalimantan, Indonesia), Geochimica et Cosmochimica Acta, 186, 13–31, https://doi.org/10.1016/j.gca.2016.04.033, 2016.

Sjögren, P., van der Knaap, W.O., Huusko, A., and van Leeuwen, J.F.N.: Pollen productivity, dispersal, and correction factors for major tree taxa in the Swiss Alps based on pollen-trap results, Rev. Palaeobot. Palynol., 152, 200–210, https://doi.org/10.1016/j.revpalbo.2008.05.003, 2008.

Sjögren, P., Edwards, M.E., Gielly, L., Langdon, C.T., Croudace, I.W., Merkel, M.K.F., Fonville, T., and Alsos, I.G.: Lake sedimentary DNA accurately records 20th Century introductions of exotic conifers in Scotland, New Phytol, 213: 929–941, https://doi.org/10.1111/nph.14199, 2017.

Snyder, C. Evolution of global temperature over the past two million years. Nature 538, 226-228 (2016). https://doi.org/10.1038/nature19798.

Song, B., Zhang, K., Farnsworth, A., Ji, J., Algeo, T. J., Li, X., Xu, Y., and Yang, Y.: Application of ostracod-based carbonate clumped-isotope thermometry to paleo-elevation reconstruction in a hydrologically complex setting: A case study from the northern Tibetan Plateau, Gondwana Research, 107, 73–83, https://doi.org/10.1016/j.gr.2022.02.014, 2022.

Stoof-Leichsenring, K.R., Huang, S., Liu, S., Jia, W., Li, K., Liu, X., Pestryakova, L.A., and Herzschuh, U.: Sedimentary DNA identifies modern and past macrophyte diversity and its environmental drivers in high-latitude and high-elevation lakes in Siberia and China, Limnology and Oceanography, 67(5), 1007-1226, https://doi.org/10.1002/lno.12061, 2022.

Sutton, B.C., Flanagan, D.J., Gawley, J.R., Newton, C.H., Lester, D.T., and El-Kassaby, Y.A.: Inheritance of chloroplast and mitochondrial DNA in Picea and composition of hybrids from introgression zones, Theor Appl Genet, 82(2), 242–248, https://doi.org/10.1007/BF00226220, 1991.

Syrykh L.S., Nazarova L.B., Herzschuh U., Subetto D.A., and Grekov I..M.: Reconstruction of palaeoecological and palaeoclimatic conditions of the Holocene in the south of Taimyr according to the analysis of lake sediments, Contemporary Problems of Ecology 4, 363–369, https://doi.org/10.1134/S1995425517040114, 2017.

Tchebakova, N.M., Parfenova, E, and Soja, A.J.: The effects of climate, permafrost and fire on vegetation change in Siberia in a changing climate, Environ. Res. Lett. 4 045013DOI 10.1088/1748-9326/4/4/045013, 2009.

Tumskoy, V. and Kuznetsova, T.: Cryolithostratigraphy of the Middle Pleistocene to Holocene deposits in the Dmitry Laptev Strait, Northern Yakutia. Front, Earth Sci., 10, 789421. https://doi.org/10.3389/feart.2022.789421,

1   2022.

2   Tumskoy, V.: Peculiarities of cryolithogenesis in Northern Yakutia (middle Neopleistocene to Holocene),
3   Kriosfera Zemli 16(1), 12–21, (in Russian), 2012.

4   Vaks, A., Mason, A.J., Breitenbach, S.F.M., Kononov, A.M., Osinzev, A.V., Rosensaft, M., Borshevsky, A.,
5   Gutareva, O.S., and Henderson, G.M.: Palaeoclimate evidence of vulnerable permafrost during times of low sea
6   ice, Nature, 577, 221–225, https://doi.org/10.1038/s41586-019-1880-1, 2020.

7   Vaks, A., Gutareva, O.S., Breitenbach, S.F.M., Avirmed, E., Mason, A.J., Thomas, A.L., Osinzev, A.V., Kononov,
8   A.M., and Henderson, G.M.: Speleothems reveal 500,000-year history of Siberian permafrost, Science, 340, 6129,
9   183–186. https://doi.org/10.1126/science.1228729, 2013.

10   van Everdingen, R.O. (ed.). Multi-Language Glossary of Permafrost and Related Ground-Ice Terms, International
11   Permafrost Association (1998, revised 2005), The Arctic Institute of North America, The University of Calgary
12   Printing Services, Calgary, Canada, 159 pp., 2005.

13   van Nieuwenhove N., Bauch, H.A., Eynaud, F., Kandiano, E., Cortijo, E., and Turan, J.-L.: Evidence for delayed
14   poleward expansion of North Atlantic surface waters during the LIG (MIS 5e), Quaternary Science Reviews, 30,
15   934–946, https://doi.org/10.1016/j.quascirev.2011.01.013, 2011.

16   van Geel, B., Protopopov, A., Protopopova, V., Pavlov, I., van der Plicht, J., and van Reenen, G.B.A.: Larix during
17   the Mid-Pleniglacial (Greenland Interstadial 8) on Kotelny Island, northern Siberia, Boreas, 46, 338–345,
18   https://doi.org/10.1111/bor.12216, 2017.

19   Velichko, A.A., Borisova, O.K., and Zelikson, E.M.: Paradoxes of the LIG climate: reconstruction of the northern
20   Eurasia climate based on palaeofloristic data, Boreas, 37, 1-19. https://doi.org/10.1111/j.1502-3885.2007.00001.x,
21   2008.

22   Vermassen, F., O'Regan, M., de Boer, A., Schenk, F., Razmjooei, M., West, G., Cronin, T. M., Jakobsson, M.,
23   and Coxall, H. K.: A seasonally ice-free Arctic Ocean during the LIG, Nat. Geosci., 16, 723-729,
24   http://doi.org/10.1038/s41561-023-01227-x, 2023.

25   von Grafenstein, U., Erlenkeuser, H., and Trimborn, P.: Oxygen and carbon isotopes in modern fresh-water
26   ostracod valves: Assessing vital offsets and autecological effects of interest for palaeoclimate studies,
27   Palaeogeography Palaeoclimatology Palaeoecology, 148, 133–152, https://doi.org/10.1016/S0031-
28   0182(98)00180-1, 1999.

29   Walter Anthony, K., Zimov, S., Grosse, G., Jones, M.C., Anthony, P.M., Chapin III, F.S., Finlay, J.C., Mack,
30   M.C., Davydov, S., Frenzel, P., and Frolking, S.: A shift of thermokarst lakes from carbon sources to sinks during
31   the Holocene epoch. Nature 511, 452–456 (2014). https://doi.org/10.1038/nature13560, 2014.

32   Wang, C., Graham, R. M., Wang, K., Gerland, S., and Granskog, M.A.: Comparison of ERA5 and ERA-Interim
33   near-surface air temperature, snowfall and precipitation over Arctic sea ice: effects on sea ice thermodynamics and
34   evolution, The Cryosphere, 13, 1661–1679, https://doi.org/10.5194/tc-13-1661-2019, 2019.

35   Wetterich, S., Meyer, H., Fritz, M., Mollenhauer, G., Rethemeyer, J., Kizyakov, A., Schirrmeister, L., and Opel,
36   T.: Northeast Siberian permafrost ice-wedge stable isotopes depict pronounced Last Glacial Maximum winter
37   cooling, Geophysical Research Letters, 48, e2020GL092087, https://doi.org/10.1029/2020GL092087, 2021.

Wetterich, S., Rudaya, N., Kuznetsov, V., Maksimov, F., Opel, T., Meyer, H., Günther, F., Bobrov, A., Raschke, E., Zimmermann, H.H., Strauss, J., Starikova, A., Fuchs, M., Schirrmeister, L.: Ice Complex formation on Bol'shoy Lyakhovsky Island (New Siberian Archipelago, East Siberian Arctic) since about 200 ka, Quaternary Research, 92(2), 530–548. https://doi.org/10.1017/qua.2019.6, 2019.

Wetterich S., Schirrmeister L., Nazarova L., Palagushkina O., Bobrov A., Pogosyan L., Savelieva L., Syrykh L., Matthes H., Fritz M., Gunther F., and Opel T.: Holocene thermokarst and pingo development in the Kolyma Lowland 1 (NE Siberia), Permafrost and Periglacial Processes, 29(3), 182–198, https://doi.org/10.1002/ppp.1979, 2018.

Wetterich, S.; Tumskoy, V.E., Rudaya, N., Kuznetsov, V., Maksimov, F., Opel T., Meyer H., Andreev, A.A., and Schirrmeister, L.: Ice Complex permafrost of MIS5 age in the Dmitry Laptev Strait coastal region (East Siberian Arctic), Quaternary Science Reviews, 147, 298–311, https://doi.org/10.1016/j.quascirev.2015.11.016, 2016.

Wetterich, S., Rudaya, N., Andreev, A.A., Opel, T., Schirrmeister, L., Meyer, H., and Tumskoy, V.: Ice Complex formation in arctic East Siberia during the MIS3 Interstadial. Quaternary Science Reviews, 84, 39–55. https://doi.org/10.1016/j.quascirev.2013.11.009, 2014.

Wetterich, S., Schirrmeister, L., Andreev, A.A., Pudenz, M., Plessen, B., Meyer, H., and Kunitsky, V.V.: Eemian and Late Glacial/Holocene palaeoenvironmental records from permafrost sequences at the Dmitry Laptev Strait (NE Siberia, Russia), Palaeogeography, Palaeoclimatology, Palaeoecology, 279, 73–95 https://doi.org/10.1016/j.palaeo.2009.05.002, 2009.

Wetterich, S., Schirrmeister, L., Meyer, H., Viehberg, F.A., and Mackensen, A.: Arctic freshwater ostracods from modern periglacial environments in the Lena River Delta (Siberian Arctic, Russia): Geochemical applications for palaeoenvironmental reconstructions, Journal of Paleolimnology, 39(4), 427–449, https://doi.org/10.1007/s10933-007-9122-1, 2008a.

Wetterich, S., Herzschuh, U., Meyer, H., Pestryakova, L., Plessen, B., Lopez, C.M.L., and Schirrmeister, L.: Evaporation effects as reflected in freshwaters and ostracod calcite from modern environments in Central and Northeast Yakutia (East Siberia, Russia), Hydrobiologia, 614(1), 171–195, https://doi.org/10.1007/s10750-008-9505-y, 2008b.

Wickham, H.: ggplot2: Elegant Graphics for Data Analysis, Springer New York, 260 pp., 2016.

White, R.E.: Principles and Practice of Soil Science: The Soil as a Natural Resource, 4th Edition, 384 pp., Whiley-Blackwell, Malden, Mass., ISBN: 978-0-632-06455-7, 2005.

Wilcox, P.S., Honiat, C., Trüssel, M., Edwards, R.L., and Spötl, C.: Exceptional warmth and climate instability occurred in the European Alps during the Last Interglacial period. Commun Earth Environ 1, 57 (2020). https://doi.org/10.1038/s43247-020-00063-w

Wilcox, E.J., Wolfe, B.B., and Marsh, P.: Assessing the influence of lake and watershed attributes on snowmelt bypass at thermokarst lakes, Hydrology and Earth System Sciences, 26, 6185--6205, https://hess.copernicus.org/articles/26/6185/2022/, 2022.

Xia, J., Engstrom, D.R., and Ito, E.: Geochemistry of ostracode calcite 2: effects of the water chemistry and seasonal temperature variation on *Candona rawsoni*, Geochimica et Cosmochimica Acta, 61, 383–391, https://doi.org/10.1016/S0016-7037(96)00354-7, 1997.

Xu, S., Krebs-Kanzow, U., and Lohmann, G.: Arctic Amplification during the Last Glacial Inception due to a delayed response in sea ice and surface temperature. Geophys. Res. Lettters 51, e2023GL107927 https://doi.org/10.1029/2023GL107927, 2024.

Xie, J., Pancost, R.D., Chen, L., Evershed, R.P., Yang, H., Zhang, K., Huang, J., and Xu, Y.: Microbial lipid records of highly alkaline deposits and enhanced aridity associated with significant uplift of the Tibetan Plateau in the Late Miocene, Geology, 40, 291-294, https://doi.org/10.1130/G32570.1, 2012.

Yang, H., Lü, X., Ding, W., Lei, Y., Dang, X., and Xie, S.: The 6-methyl branched tetraethers significantly affect the performance of the methylation index (MBT′) in soils from an altitudinal transect at Mount Shennongjia, Organic Geochemistry, 82, 42-53, https://doi.org/10.1016/j.orggeochem.2015.02.003, 2015.

Zimmermann, H.H., Raschke, E., Epp, L.S., Stoof-Leichsenring, K.R., Schirrmeister, L., Schwamborn, G., and Herzschuh, U.: The history of tree and shrub taxa on Bol'shoy Lyakhovsky Island (New Siberian Archipelago) since the LIG uncovered by sedimentary ancient DNA and pollen data, Genes 8(10), E273, https://doi.org/10.3390/genes8100273, 2017.

1   **Appendix A**

2   Table A1 Overview of sample collections for cryolithological and fossil proxy studies of Krest Yuryakh deposits
3   exposed at both coasts of the Dmitry Laptev Strait

Profile	Location number in Table A1	Year	Coordinates °N, °E	Height [m asl]	Deposits type	cryo-lithology	Pollen,	*Sedal*DNA	Plant macro-fossils	Chironomids	Additional bioindicators, clumped isotopes, and IRSL-dated samples	Ostracods	References
Bol'shoy Lyakhovsky Island													
R22+60 (R22)	1	1999	73.339000 141.295100	1-4.8	pseudo-morph	x	R22+60 S-5, S-6, S-8, r2260s5_80, r22os54_200, r22os53_230		R22 OS-53, OS-54, OS-55		beetles and other small fossils, R22 B15 h=2.5-2.8 m (OS-53, OS-54); B16 h=4 m (OS-55); R22+30 BL-R-M2		Schirrmeister et al. (2000); Andreev et al. (2004); Kienast et al. (2008); https://doi.pangaea.de/10.1594/PANGAEA.880948
R23+40	2	1999	73.339400 141.292500	1.8-7.3	lake deposits	x	R23+40 S-1 to S-7				*Pisidium* sp. shell R23+40 –10	R23+40 -S1, -4, -9	Schirrmeister et al. (2000); Andreev et al. (2009); https://doi.pangaea.de/10.1594/PANGAEA.880949
R32		1999	73.344863 141.265733		lake deposits						R 32 mollusks BL-R-M4		Schirrmeister et al. (2000)
R35	3	1999	73.345898 141.261696	1-5.2	pseudo-morph		R35 S-1 to S-11		R35 S-9	R35 S-1 to S-11			Schirrmeister et al. (2000); Ilyashuk et al. (2006); Kienast et al. (2008)
L11+40	4	1999	73.32330 141.38650	0.5-4.3	lake deposits	x	L11+40 S-1 to S-10		OS-56,	OS-56, OS-57		L11-S-6	Schirrmeister et al. (2000); Andreev et al. (2009); https://doi.pangaea.de/10.1594/PANGAEA.880935

L12+30	5	1999	73.322792 141.389587	3.3-7.3	pseudo-morph	x	L12+30 OS-56 to OS-61		L12+30-OS-56, OS-57, OS-60	L12+30 OS-56, OS-57	beetles and other small fossils B-18 (OS-58, 59), B-17 (OS56, 57), B-19 (OS-60, OS-61)		Schirrmeister et al. (2000); Kienast et al. (2008)
L13+80	6	1999	73.322300 141.393200	5-6.3	lake deposits	x							Schirrmeister et al. (2000); https://doi.org/10.1594/PANGAEA.880936
L14	7	1999	73.322200 141.393800	3-5.4	pseudo-morph	x	L14 S-1, S-2						Schirrmeister et al. (2000); Andreev et al. (2004); https://doi.pangaea.de/10.1594/PANGAEA.880937
L7-11 A	8	2007	73.31672 141.42628	4-5.4	pseudo-morph	x			L7-11-07 to -12		Insects. daphnia, moss	L7-11-07 to -12	Boike et al. (2008); Schneider (2010); https://doi.pangaea.de/10.1594/PANGAEA.727667
L7-14 B-C	9	2007	73.2877 141.69097	2.5-5	pseudo-morph	x	L7-14-04 to -15					L7-14-04 to -15	Wetterich et al. (2009); Boike et al. (2008); https://doi.pangaea.de/10.1594/PANGAEA.727669
L7-16	10	2007	73.31385 141.4505	4.5-7	pseudo-morph	x							Boike et al. (2008); https://doi.pangaea.de/10.1594/PANGAEA.727669
L14-04	11	2014	73.34100 141.28586	3.9-12 core	lake deposits	x	L14-03 6.73 to 12.87, L14.04 6.15 to 8.03	L14.04 6.15 to 8.03			GDGT		Zimmermann et al. (2017); https://doi.pangaea.de/10.1594/PANGAEA.868983

													https://doi.pangaea.de/10.1594/PANGAEA.878884
L14-04 B	11	2014	73.34100 141.28586	0.6-5.0 outcrop	lake deposits	x		L14-04B 2.45, 3.45			GDGT		Zimmermann et al. (2017)
L14-04 C	11	2014	73.34100 141.28586	2.5-7.5 outcrop	lake deposits	x	L14-04C 2.55 to 4.45	L14-04C 2.55 to 4.45[LS3]			GDGT		Schwamborn and Wetterich (2015); Zimmermann et al. (2017)
L14-12	12	2014	73.34055 141.28498	3-7	lake deposits						IR-OSL: L14-12-OSL3, L14-12-OSL1		Schwamborn and Wetterich (2015); this study
Oyogos Yar coast													
Oya 3	13	2002	72.679317 143.551417	1-4	pseudo-morph	x							Grigoriev et al. (2003)
Oya 5-1	14	2002	72.68000 143.53000	3.5	pseudo-morph	x	Oya 5-1		Oya 5-1	Oya 5-1	beetles, cladocerans, molluscs, clumped isotopes	Oya 5-1	Grigoriev et al. (2003); Kienast et al. (2011)
Oy7-01 A-C	15	2007	72.67454 143.60981	1-2.5	lake deposits	x			Oy7-01-01 to 13		Insects. Daphnia, moss, mollusks	Oy7-01-01 to 13	Schneider (2010); https://doi.pangaea.de/10.1594/PANGAEA.727673
Oy7-07 B	16	2007	72.67865 143.55718	5-6	lake deposits	x							Boike et al. (2008); https://doi.pangaea.de/10.1594/PANGAEA.727676
Oy7-08 A-B	17	2007	72.68002 143.53181	2-6	pseudo-morph	x	Oy7-08-02 to 24					Oy7-08-02 to 24	Wetterich et al. (2009); Opel et al. (2017)